

APPROVAL SHEET

Title of Thesis: A lidar-based approach to measure channel incision in headwater streams in an urbanizing landscape

Name of Candidate: Marina Jean Metes
Master of Science, 2018

Thesis and Abstract Approved:



Andrew J. Miller
Professor
Geography and Environmental Systems

Date Approved: 11/29/2018

NOTE: *The Approval Sheet with the original signature must accompany the thesis or dissertation. No terminal punctuation is to be used.

ABSTRACT

Title of Document: A LIDAR-BASED APPROACH TO MEASURE CHANNEL INCISION IN HEADWATER STREAMS IN AN URBANIZING LANDSCAPE.

Marina Jean Metes, M.S., 2018

Directed By: Andrew J. Miller, Professor, Geography and Environmental Systems

Stream channel incision can occur following landscape disturbances commonly related to urbanization. A method was developed to map reach-scale incision from lidar-derived digital elevation models using topographic openness, a landscape metric measuring the enclosure of an area (i.e. channel bottoms) relative to the surrounding landscape (i.e. stream banks). The method was validated with field surveys and local photogrammetric models of stream banks. The method was then applied to watersheds undergoing urban development with lidar coverage for six time steps spanning an 11 year period. Channel incision was detected near the outlet of newly developed stormwater management facilities, but temporal analysis also identified areas already severely incised prior to urbanization, highlighting influence from previous agricultural land use, as well as areas that have resisted incision following urbanization. Although incision patterns varied across each watershed, there appeared to be no direct connection to the placement of SWM facilities beyond outlets.

A LIDAR-BASED APPROACH TO MEASURE CHANNEL INCISION IN
HEADWATER STREAMS IN AN URBANIZING LANDSCAPE

By

Marina Jean Metes

Thesis submitted to the Faculty of the Graduate School of the
University of Maryland, Baltimore County, in partial fulfillment
of the requirements for the degree of
Master of Science in
Geography and
Environmental Systems
2018

© Copyright by
Marina Jean Metes
2018

Acknowledgements

Lidar data for this research was provided by the Montgomery County Department of Environmental Protection, the US Geological Survey (USGS), UMBC, and the Environmental Protection Agency. Stormwater management data was provided by the USGS Eastern Geographic Science Center.

First, I would like to thank my graduate committee, Andrew Miller, Matthew Baker, and Dianna Hogan, for their extensive guidance, patience, and support from beginning to end. For field work, I would like to thank Alex Marcinkowski, Kristina Hopkins, Hilina Tarkegan, and Andrew Ellis. I would also like to thank Monica Palaseanu-Lovejoy, Daniel Jones, and Adam Benthem for GIS and structure from motion guidance. Finally, I want to thank all my colleagues at the USGS, fellow graduate students at UMBC, friends, and family for their continued support and encouragement.

Table of Contents

Acknowledgements.....	ii
Table of Contents.....	iii
List of Tables.....	v
List of Figures.....	vi
Chapter 1: Introduction.....	1
1.1. Background.....	1
1.1.1. Urban stream syndrome.....	1
1.1.2. Headwater streams significance.....	3
1.1.3. Monitoring change with remotely sensed data.....	4
1.2. Study Area.....	7
1.2.1. Previous research in the study area.....	12
1.3. Project Scope.....	15
Chapter 2: Remotely detecting stream channel incision using aerial lidar and topographic openness.....	17
2.1. Background.....	17
2.2. Methods.....	21
2.2.1. Channel incision field survey.....	21
2.2.2. Structure from motion field survey.....	23
2.2.3. Lidar data processing.....	27
2.2.3.a. Mask erroneous lidar.....	27
2.2.3.b. Positive topographic openness.....	29
2.2.4. Field vs. model comparison.....	31
2.3 Results.....	33
2.3.1. Structure from motion and field surveys.....	33
2.3.2. Using inter quartile ranges to select phi thresholds.....	40
2.3.3. Comparison of openness model vs. field incision.....	42
2.3.3.a. TR104 results.....	45
2.3.3.b. TR109 results.....	47
2.3.3.c. SB results.....	49
2.3.3.d. Combined results.....	50
2.4. Discussion.....	52
2.4.1. Method errors.....	52
2.4.2. Spatial variation of channel incision across reaches.....	60
2.4.3. Influence of DEM source, processing, and resolution.....	63
2.4.4. Applications and Future work.....	64
2.5. Conclusions.....	65
Chapter 3: Measuring changes in channel incision over time.....	67
3.1 Background.....	67
3.1.1. Geomorphic change.....	67
3.1.2. Infiltration-focused SWM.....	68
3.1.3. Seepage erosion.....	69
3.2. Methods.....	70
3.2.1. Lidar data processing.....	71

3.2.2. Classifying channel incision from 2002 to 2013	74
3.2.3. Comparing raw changes in phi	75
3.2.4. Groundwater seep survey.....	77
3.2.5. Thermal Infrared Camera Survey	79
3.3. Results.....	80
3.3.1. Change in incision class over time.....	80
3.3.2. Groundwater seeps.....	83
3.3.3. Raw phi differences and changes relative to IF-SWM and groundwater influx	89
3.3.4. Characterizing active seeps with a TIR camera	104
3.4. Discussion	107
3.4.1. Incision changes and management implications.....	107
3.4.2. Future work and data collection in the study area	109
3.5. Conclusions.....	110
Chapter 4: Conclusions.....	112
Appendices.....	116
Bibliography	128

List of Tables

Table 2.1: Examples of causes related to channel incision. Adapted from Galay (1983).....	18
Table 2.2: Results of accuracy and kappa values with various smoothing thresholds for each watershed	43
Table 2.3: Confusion matrix results for TR104 (A), TR109 (B), SB (C), and combined watersheds (D) showing results of the pixel by pixel comparison between the field survey and openness models for each class.....	44
Table 2.4: Statistics and indices calculated from the confusion matrix results. Sensitivity, precision, and F-score are broken down into results for each class, within each watershed.....	45
Table 2.5: Results of incision model using a coarser DEM. Results did not change significantly between the two resolutions.....	63
Table 2.6: Results of applying the Whitebox GAT De-Noise tool to the input DEM to test the sensitivity of the analysis to varying DEM pre-processing steps, compared with the original results.....	64
Table 3.1: Information on vendor, instruments, and accuracy for each year of lidar data reported by the vendor.....	72
Table 3.2: The number of active and inactive groundwater seeps surveyed within each watershed, grouped by incision classification based on the field survey	84
Table 3.3: Description and images for active groundwater seeps in TR104 and SB. In the TIR image, the warmest temperatures are shown in red and white, and the temperatures are relative	106

List of Figures

Figure 1.1: Example of positive (ϕ) and negative (ψ) topographic openness calculation for a pixel within a stream channel. Angles are constrained by inflection points along the topography within the specified search distance. Positive openness is constrained by stream banks and is therefore potentially able to detect incised channels.....	7
Figure 1.2: Study area located in Clarksburg, MD, within the Chesapeake Bay watershed. Soper Branch is primarily forested and flows to the north. Trib 104 and Trib 109 and primarily urban and flow to the south. All three watersheds eventually drain to the Potomac River. Streamflow in all three watersheds are continuously monitored by USGS stream gaging stations	8
Figure 1.3: Geologic map of Montgomery County, MD, and the location of the three study sites. All three sites are underlain by phyllite	9
Figure 1.4: Exposed bank in TR104 shows a stratigraphic profile similar to other piedmont streams resulting from an agricultural land use history	11
Figure 1.5: Pre- and Post-development stream network of TR104 showing where the development of artificial channels and loss of natural channels created an overall extension of the stream network. Adapted from Jones et al. (2014) ...	13
Figure 2.1: Severe channel incision in TR104. The depth and width of the channel have an approximate ratio of 1:1	18
Figure 2.2: Locations within each stream network that were surveyed for characteristics of channel incision. In TR104 and TR109 the entire main stem of the channel was surveyed. In areas where gaps exist, the delineated channel deviated from actual location of the channel (verified using aerial imagery) and these sections were removed from the analysis. In SB, sections of the main channel and tributaries were surveyed.....	22
Figure 2.3: Examples of photos collected in the field (A) that were used to derive a 3-dimensional point cloud of a stream reach (B). The blue squares are scale markers used to correctly scale the point cloud	24
Figure 2.4: Original 0.1 m DEM generated from the scaled, filtered point cloud (A). The overall elevation was adjusted to represent elevation above the local channel minimum (B). The degree slope was then calculated from the original DEM (C)	26
Figure 2.5: Workflow for processing SfM-derived DEMs of stream reaches to determine bank height and bank angle.....	26
Figure 2.6: Example of areas along the channel where there are low point counts, and ϕ values are > 84 (indicating a non-incised reach) even though this is an area with known severe incision (A). Two cross sections were extracted from the DEM. The channel is not detected along transect 1 but is detected in transect 2. (B). Additionally, the v-shape of Transect 2 isn't showing true channel form but is a result of using a coarser 1.8 m DEM, which is approximately the width of the channel.....	29
Figure 2.7: Results of original ϕ values reclassified into three different levels on incision, represented by red (level 2), orange (level 1), or blue (level 0) pixels	

	(A). The region group tool counts the number of contiguous pixels of the same value (B). The set null tool was set to remove groups under a value set by the user (C). The nibble tool was then used to fill in the gaps removed from set null with surrounding pixel values (D).....	31
Figure 2.8:	Example of TPs, TNs, FPs, and FNs for class 0. Metrics with TNs are not helpful in revealing anything about the success of the class because in this case, TNs could also include pixels classified incorrectly in groups 1 and 2...	32
Figure 2.9:	Results of SfM survey of bank height after elevation was adjusted to reflect height above channel rather than relative elevation	34
Figure 2.10:	Results of SfM survey of bank angle in degrees per pixel, to obtain bank slope information on each reach	35
Figure 2.11:	Decision tree for classifying reaches into incision classifications of severe, moderate, and none, based on channel observations and data extracted from the SfM-derived DEMs.....	37
Figure 2.12:	Results of incision field survey for TR104. Examples of reaches with moderate incision (A), severe incision (B), and no incision (C)	37
Figure 2.13:	Results of incision field survey for TR109. Examples of reaches with moderate incision (A), no incision (B), and severe incision (C)	39
Figure 2.14:	Results of incision field survey for SB. Examples of reaches with moderate incision (A), no incision (B), and severe incision (C)	40
Figure 2.15:	Boxplots displaying the distribution of positive openness values overlapping with each level of incision surveyed in the field. Notches show 95% confidence intervals of the median and suggest the median between groups differ when not overlapping.....	42
Figure 2.16:	Results of the openness model compared with the field survey for TR104	46
Figure 2.17:	Example of long continuous reach with no incision in TR109, likely driving the success of the overall model. The openness pixels within the stream are reclassified to the scale shown in the legend. The long stretch of blue pixels represent a section of the stream flowing through a wetland so the area is relatively flat and easy to identify as not being incised in the openness model.....	48
Figure 2.18:	Results of the openness model compared with the field survey for TR109	49
Figure 2.19:	Results of the openness model compared with the field survey for SB	50
Figure 2.20:	Large discrepancies between the field survey (A) and openness model (B) in main channel of SB. Reclassified openness pixels show some areas of the channel with a range of incision but the result of the openness model is based on where within the channel the network is delineated (C). High openness values within the incised channel are likely picking up bars within the channel (D). Here the channel is wider than much of the other survey locations, indicating adjustments may need to be made for higher order channels.....	54
Figure 2.21:	The 10 most common landforms classified with Geomorphon and an example of the typical form for each classification. Each of the 8 points	

	surrounding the focal pixel in each form indicate if the point is above (red), below (blue), or equal (green). Adapted from Jasiewicz & Stepinski (2013) .55	
Figure 2.22:	The output of the Geomorphon landform classification tool (A) was used to isolate pixels classified as valley or pits, indicative of stream channels (B). The valley and pits were used as a mask to isolate and then reclassify openness into incision levels. This method better displays channel complexity in wider channels (C). Cross section A shows how the side of the channel with severe incision corresponds to a steeper bank than the other side showing only moderate incision. Cross section B shows a severely incised channel, which corresponds to the incision classification56	
Figure 2.23:	Results from combining the focal range, reclassified openness, and field classification. The channel location is the same area shown in figure 2.20 where the channel has incised and then widened. The box highlights the area where the channel was misclassified and displayed complex incision and widening.....59	
Figure 2.24:	Longitudinal profile of a reach within Soper Branch that begins as an incised channel near the head, where the slope is steeper, and gradually transitions to moderately incised, and finally not incised, with slope of the bed becoming more gradual as incision severity declines.....62	
Figure 2.25:	Examples of various channel forms in SB extracted from Geomorphon and topographic openness, with the corresponding channel form described by Jain et al. (2008). Example 1 shows the channel in a confined valley setting, characterized by a relatively straight channel with steep banks. Example 2 shows a partially confined valley with evidence of meandering. The red pixels indicate some severe incision or steep slopes along cut banks but the orange pixels indicate more gradual banks throughout most of the channel as a result of channel widening and point bar development that creates discontinuous floodplains. Example 3 shows the lower portion of SB near the confluence with a larger channel within an unconfined valley. The blue pixels indicate small side channels suggesting there is a broad, continuous floodplain.....62	
Figure 3.1:	Example of lidar error resulting in stream network that deviates from actual location. Aerial imagery is from 2012 and the 2013 stream layer deviates outside the true channel, the 2013 stream is not an accurate representation in this area and this section would be removed from the analysis. Further upstream, the 2002 and 2013 stream layers accurately match the actual stream location.....74	
Figure 3.2:	Locations of IF-SWM facilities in TR104. The drywell recharge facilities on the lower west side of the watershed show an area where seeps would be expected to occur more frequently on the west side of the stream bank if there is a relationship between groundwater seeps and IF-SWM.....78	
Figure 3.3:	Indications of groundwater seeps in stream banks. The picture on the left shows iron in groundwater reacting with oxygen to form the rust color when seeping out. The picture in the middle shows water actively seeping from the bank. The picture on right does not have any indication of groundwater seepage other than the features formed in the bank.....79	

Figure 3.4: The percent of the stream network classified as not incised (0), moderately incised (1), and severely incised (2). Only areas of the stream network that overlap within a 2.7 m (9 ft) buffer in every year are considered	82
Figure 3.5: Areas of each network where the incision level has remained consistent in at least five of the six years. Gaps are areas where the stream network did not overlap within a 2.7 m buffer in every year	82
Figure 3.6: Example of a channel in TR109 that was added to the stream network as a direct result of urban development. This area was excluded from the portion of the analysis assessing overlapping stream networks but was included when incorporating Geomorphon to delineate the channel extent.	83
Figure 3.7: Results of the groundwater seep survey. Triangles indicate seeps were active. Circles indicate seeps were inactive but resembled characteristics of known groundwater seeps. Blue indicates the feature was on the left bank and red indicates the feature was on the right bank.....	84
Figure 3.8: The location of active seeps and nearby IF-SWM facilities in TR104....	85
Figure 3.9: TWI for two different locations in TR104 and one location in SB. The left panels show each location derived from 2002 lidar and the right panels show the same location derived from 2013 lidar	88
Figure 3.10: The range of phi value differences between 2002 and 2013 only within areas of consistent incision classes	91
Figure 3.11: The range of changes in phi between 2002 and 2013 near sites of active and potentially inactive groundwater seep locations. Similarities across all three watersheds indicate similar erosion patterns in the forested and urban watersheds with respect to groundwater seepage	92
Figure 3.12: The outlet of a SWM facility in TR104 where the phi difference is showing incision directly downstream from the outlet (top) and evidence of erosion observed in the field (bottom). Incision tapers to a small, non-incised channel in the floodplain.....	93
Figure 3.13: Transects 1 and 2 show channel instability and the pattern of bank retreat and downcutting resemble the patterns of change from the field surveyed cross sections in this area.....	96
Figure 3.14: This transect shows an area of headcut erosion at the beginning of a severely incised reach. There is also groundwater actively seeping into the banks just upstream from the heacut.....	97
Figure 3.15: Transect 1 and 2 both show areas that have never been moderately or severely incise during the study period, but appear to be flattening. This could potentially be a hot spot for sediment deposition	98
Figure 3.16: Transect 1 shows an area of stability which is also reflected in the phi difference. Transect 2 is an area that was already severely incised and continued to incise through 2013	99
Figure 3.17: Transects 1 shows an area that transitioned from moderately to severely incised. Transect 2 is an area that was already incised in 2002 and continued to incise through 2013.....	101
Figure 3.18: Two transects showing change over time in SB. Transect 1 shows an area where the channel has widened and has positive values of phi differences	

	because the channel became more open. Transect2 2 shows an area that has been eroding and becoming more enclosed	102
Figure 3.19:	Boxplots showing the difference in raw phi values for incremental time steps in each watershed. Negative values indicate areas becoming more enclosed, indicative of incision, and positive values indicate areas becoming more open, either through deposition or channel widening. Outliers have been removed from the plots	103
Figure 3.20:	Boxplots showing sediment export and runoff for SB (green plots) and TR104 (orange plots), along with a nearby watershed developed using older, centralized SWM (blue plots). Adapted from Hopkins et al. (2017).....	104
Figure 3.21:	An area with features formed from groundwater seeps and/or animal burrowing in November 2016 was observed with recent bank erosion two months later. These features create unstable banks that eventually leads to bank failure	110

Chapter 1: Introduction

1.1. Background

1.1.1. Urban stream syndrome

Stream change following urbanization is a well-documented phenomenon. Change can be indirect through response to altered amounts and delivery rates of sediment and water (Wolman 1967) or direct through channelization (Simon 1989). The primary driver of indirect change is the decrease in vegetation and increase of impervious surface from the addition of roads, sidewalks, parking lots, and buildings.

Impervious surfaces inhibit infiltration of precipitation, which increases the rate of stormwater runoff and creates a dramatic shift in the flow regime. To manage this excess runoff, stormwater management (SWM) was initially developed to evacuate runoff from streets as quickly as possible through an efficient storm drain system directly connected to nearby waterways (Dunne & Leopold 1978, Arnold & Gibbons 1996, Walsh et al. 2005). The combination of increased impervious surface cover and well-connected storm drain networks primarily contribute to the “flashy” nature of urban streams: greater stormflows that peak quickly (Leopold 1968, Arnold & Gibbons 1996). Such erosive flows typically cause stream enlargement, either through downcutting, i.e. incision, or by simultaneously deepening the bed and widening the banks (Hammer 1972, Booth 1990). In addition to physical changes, urban streams also experience chemical and biological changes as a result of increased water temperature, pollutants, and altered habitat (Paul & Meyer 2001,

Allen 2004, Roy et al. 2006, Kaushal et al. 2010). Collectively, these processes generate a condition known as the urban stream syndrome (Walsh et al. 2005).

As a result, many jurisdictions have implemented regulatory requirements intended to mitigate the environmental impacts of development. SWM evolved to include structural best management practices (BMPs) with the ability to store stormwater temporarily to control the volume and rate of runoff discharged to streams. Some structural BMPs are also designed to treat pollutants found in stormwater (Muthukrishnan et al. 2004). These structural BMPs were initially installed in a centralized manner adjacent to streams (Loperfido et al. 2014). However, these BMPs have not fully improved the hydrologic impacts of urban stormwater because they do not reduce stormwater runoff volume and may even extend the duration of erosive streamflows (Booth et al. 2002, Emerson et al. 2005, Loperfido et al. 2014, Bhaskar et al. 2016).

SWM has since developed further to mimic natural processing of storm precipitation by infiltrating stormwater at or near its source. This approach is commonly referred to by a number of names including low impact development, distributed SWM, green infrastructure SWM, stormwater control measures, or environmental site design (Tillinghast et al. 2012, Loperfido et al. 2014, Fletcher et al. 2015). This form of SWM is designed to reduce peak stormflows and runoff volume and to recharge groundwater, and it also allows some pollutants to filter through the subsurface (Tillinghast et al. 2012, Bhaskar et al. 2016). Although this is intended to mitigate the impacts of urbanization on local waterways, recent studies suggest that this type of SWM may still be contributing to symptoms of the urban

stream syndrome (Tillinghast et al. 2012, Hogan et al. 2014, Loperfido et al. 2014, Vietz et al. 2015).

1.1.2. Headwater streams significance

Although urbanization can alter rivers of all sizes, headwater streams are most vulnerable and are even eliminated altogether through diversion into subsurface pipes or infill (Elmore & Kaushal 2008, Napieralski et al. 2015). Headwater streams are crucial components of a river network (Gomi et al. 2002) yet they are still heavily impacted through development due to the fact that they are not adequately represented on maps and because the ecological importance of intermittently flowing channels is poorly recognized by society (Meyer & Wallace 2001). These small streams favor rapid uptake of nitrogen (Peterson et al. 2001), support diverse species (Meyer et al. 2007), and influence downstream water quality (Alexander et al. 2007, Freeman et al. 2007).

When restoration goals target water quality at the outlet of large watersheds like major tributaries to the Chesapeake Bay, efforts should focus especially on restoring or conserving headwaters to better promote healthy water downstream and successful restoration. There are ongoing efforts to protect headwater streams from urban development, but the most effective methods are still being researched and understood (Walsh et al. 2016, Fanelli et al. 2017). The motivation behind the research presented here was to investigate the geomorphic response of headwater streams in an area recently urbanized using green infrastructure SWM. This research utilizes high resolution spatial-temporal data to better understand if new protections

are helping to minimize the geomorphic impacts of urbanization on nearby headwater streams.

1.1.3. Monitoring change with remotely sensed data

Patterns of change should be monitored across the entire watershed to better understand how upland processes influence downstream responses. Detecting the spatial distribution of change along the entire stream network can help to clarify relationships between land use change or distributed SWM and the degree of geomorphic change. Insights gained from this type of monitoring can help guide future development projects to better help maintain pre-development channel processes and conditions.

Field-based measurements are highly accurate, but collection of these data are laborious and costly. Alternatively, data can be collected remotely via different types of sensors attached to platforms like satellites, aircraft, or unmanned aerial vehicles (UAVs). These types of data are collected over a large area and are necessary for a watershed-scale analysis that investigates the spatial component of change. Remotely sensed data collected at more than one time step can be used to better understand the temporal component of change.

High-resolution elevation information necessary for modeling geomorphic processes and topographic attributes is becoming more widely available. Aerial light detection and ranging (lidar) is a type of active remote sensing technique that records ground elevation information. Lidar data is collected with laser sensors mounted on an aerial vehicle such as an aircraft that flies over a specified flight track and collects ground elevation from surface reflectance of the laser pulse. With this data source,

continuous high-resolution bare-earth digital elevation models (DEMs) can be generated at resolutions as fine as 1 m. The U.S. Geological Survey (USGS) 3D Elevation Program is working to generate lidar coverage over the contiguous U.S. at Quality 2 or better (10 cm vertical error, 2 first return points per square meter) by 2022 (Sugarbaker et al. 2014).

Lidar-derived data has been used for many types of fluvial geomorphic analyses (James et al. 2007, Perroy et al. 2010, Jones et al. 2014, Cole et al. 2016, Cartwright & Diehl 2017). Repeat lidar is especially valuable for studying geomorphic change over time because it allows for a more complete spatial-temporal analysis (Jones 2013, Hogan et al. 2014, Jones et al. 2014, Obu et al. 2017, Le Mauff et al. 2018, Mora et al. 2018), especially in stream channels where data has previously been limited to sparsely spaced cross sections measured in the field (Gardina 2008). Where repeat lidar is available, the simplest method to detect change is with a DEM of difference (DoD). In a DoD, the raw elevation values in time 1 are subtracted from time 2 to identify areas of erosion (- change) and deposition (+ change) between the two time periods. This method can be informative in areas that experienced significant change (Hogan et al. 2014), but smaller scale erosion and deposition may not be accurately detected using DoDs due to the presence of multiple sources of error (Gardina 2008, Jones et al. 2014). For example, thick riparian vegetation has been shown to cause erroneous surface elevation values along streams (James et al. 2007, Jarnagin 2010). The aircraft's flight characteristics (e.g. altitude, forward speed), sensor, navigation equipment, and lidar point processing methods also contribute to overall lidar accuracy (Hodgson et al. 2005). Therefore, direct elevation

change from repeat lidar is not always the best method to quantify in-channel geomorphic change, especially in headwater channels, and additional topographic attributes should be considered.

Topographic openness is an angular measure of the degree of dominance or enclosure of a topographic feature relative to its surroundings (Yokoyama et al. 2002). This method takes a viewshed (line of sight) approach to measure the zenith (ϕ , positive openness) and nadir (ψ , negative openness) angles in eight azimuth directions from a central point of interest (i.e. each DEM pixel). These 8 values are then averaged to give the mean angle for each pixel (Figure 1.1). A flat surface would be represented as 90 in both measurements, but in positive openness (hereafter referred to as ϕ), values less than 90 represent depressions since the mean zenith angle is constrained by neighboring topography of higher elevation, as depicted in the hypothetical stream transect in Figure 1.1.

First developed as a visualization technique for terrain modeling, topographic openness has been applied to various aspects of geomorphic mapping such as landslide detection (Kasai et al. 2009) and stream network delineation (Jones et al. 2014, Metes et al. *in preparation*). This study investigated the ability for ϕ to detect channel incision and monitor channel change over time.

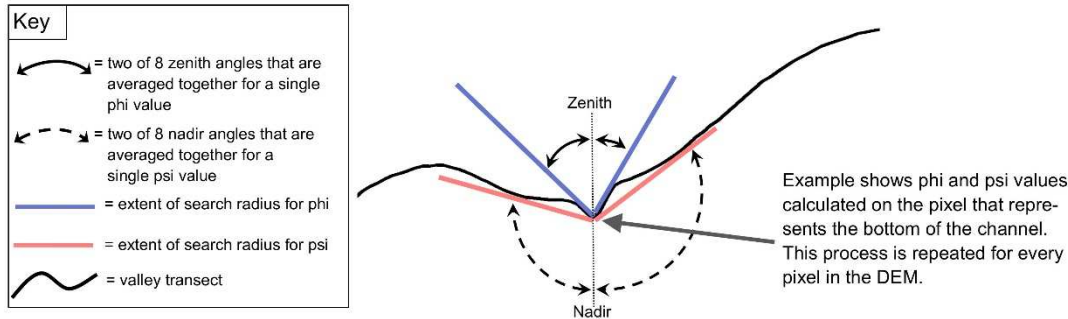


Figure 1.1: Example of positive (phi) and negative (psi) topographic openness calculation for a pixel within a stream channel. Angles are constrained by inflection points along the topography within the specified search distance. Positive openness is constrained by stream banks and is therefore potentially able to detect incised channels.

1.2. Study Area

The study area is located in the Clarksburg Special Protection Area (CSPA) in Clarksburg, MD (Figure 1.2) and is recognized as an area with sensitive, high-quality resources that are threatened by land use change unless extraordinary protective measures are taken to mitigate the effects of these changes (MCDEP, 2011). The area underwent urban development beginning in 2003. Since the area is within the CSPA boundary, developers were required to utilize the best available soil erosion control practices during construction and SWM BMPs following completion of development (Hogan et al. 2014).

This study focused on two small urbanized headwater watersheds and one forested reference watershed. The two urbanized watersheds include Tributary 104 (TR104) with a 1.2 km² drainage area at USGS stream gage 01644371 and Tributary 109 (TR109) with a 0.9 km² drainage area at USGS stream gage 01644372. Both watersheds drain into Seneca Creek, a tributary to the Potomac River. The forested watershed, Soper Branch (SB) is located to the northwest of the two study sites and has a 3.3 km² drainage area at USGS stream gage 01643395. This watershed serves as

the reference because it underwent little change during the study period and is protected from future development. This watershed drains to the Monocacy River, which eventually joins the Potomac River a few miles upstream from Seneca Creek. The watersheds are all located within the Piedmont physiographic province and are all underlain by phyllite/slate bedrock (Jones et al. 2014) (Figure 1.3). Soils are composed primarily of loam and silt loam, classified as potentially highly erodible by the Natural Resources Conservation Service (Hogan et al. 2014).

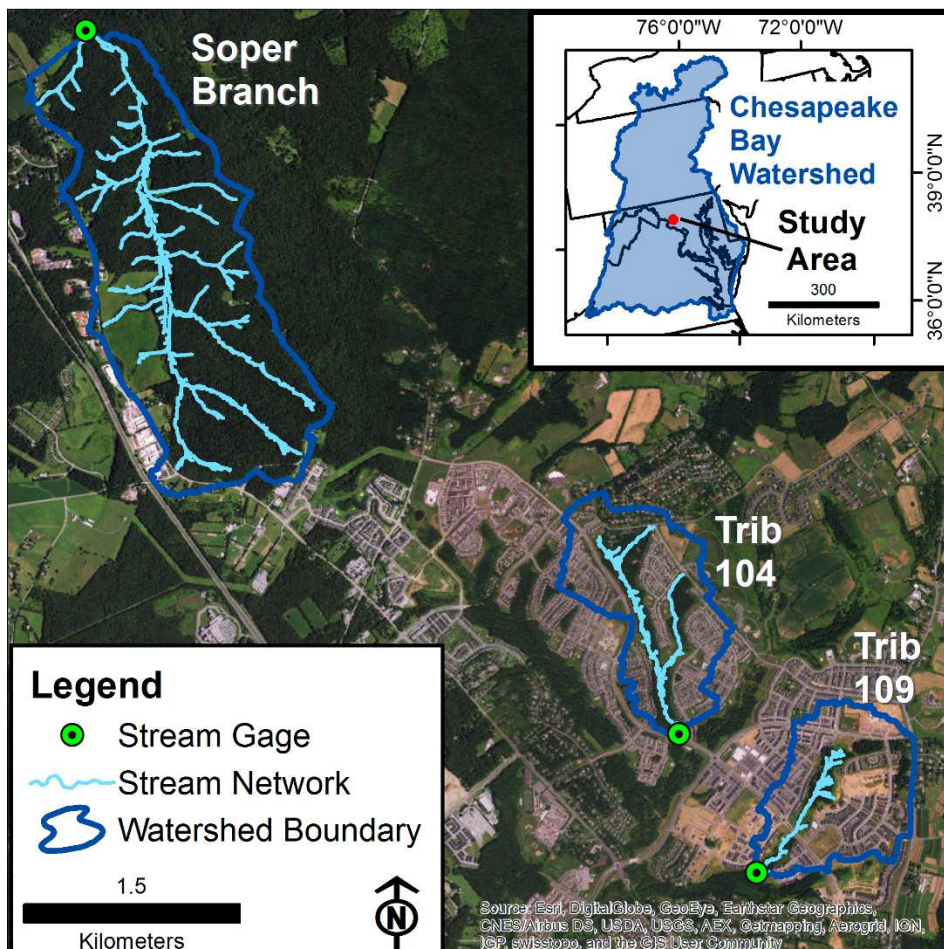


Figure 1.2: The study area is located in Clarksburg, MD, within the Chesapeake Bay watershed. Soper Branch is primarily forested and flows to the north. Trib 104 and Trib 109 are primarily urban and flow to the south. All three watersheds eventually drain to the Potomac River. Streamflow in all three watersheds are continuously monitored by USGS stream gaging stations.

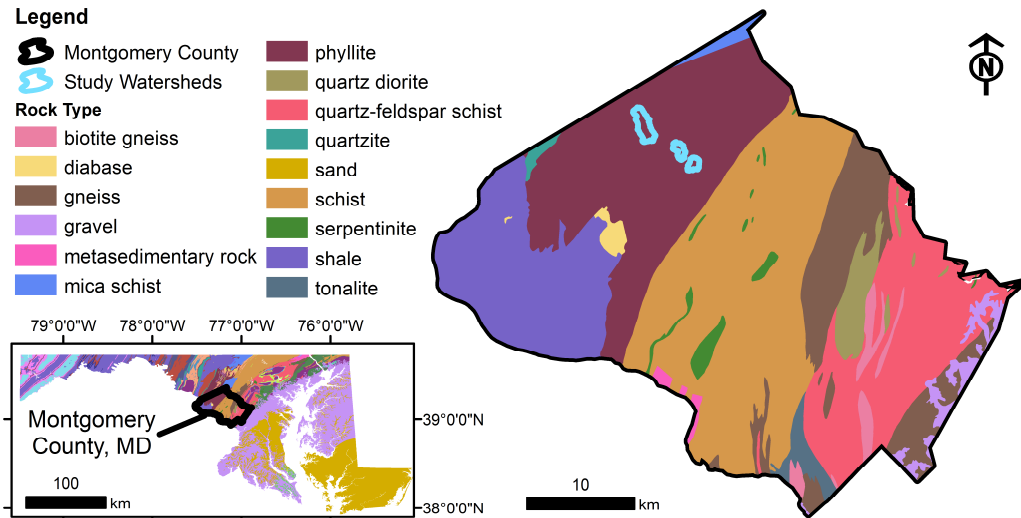


Figure 1.3: Geological map of Montgomery County, MD, and the location of the three study sites. All three sites are underlain by phyllite.

Before development began, all three watersheds had remnants of disturbance from an agricultural land use history due to settlement across the Piedmont beginning in the 1700s. During this time, forest clearing led to upland soil erosion and sediment deposition along streams (Costa 1975). Eventually mobilization of upland sediment declined due in part to the introduction of soil conservation practices. This decrease in sediment supply caused streams to further adjust by incising into legacy deposits (Costa 1975, Jacobson & Coleman 1986). The exposed banks in the study sites share characteristics similar to other streams across the Piedmont with exposed legacy sediment overlaying gravel deposits (Jacobson & Coleman 1986, Walter & Merritts 2008, Hupp et al. 2013). Some profiles within the study area contain a thin organic deposit, presumably buried wetlands (Groffman et al. 2003, Walter & Merritts 2008) (Figure 1.4). The extent and thickness of sediment interpreted as legacy deposits vary both within and across all three watersheds.

The detailed agricultural history in the study area is unknown, but historical aerial imagery provided by Montgomery County, MD (Historical Image Viewer n.d.) shows all three watersheds being used for agriculture in 1951. The north and west portions of SB were reforested beginning in the 1970s with about 10% of current land use/land cover in SB presently active agriculture (Hogan et al. 2014). TR104 and TR109 land use/land cover was converted from forested and agricultural to urban beginning in 2003 and currently has about 30% impervious surface cover (Hogan et al. 2014). While TR104 and TR109 may be adjusting to recent urban development, all three watersheds may also still be adjusting to land use that occurred prior to development. Since SB does not have the added influence of urbanization, its comparison to TR104 and TR109 is not intended to be as a pristine forested watershed but rather as a way to differentiate agricultural from urban geomorphic adjustments.

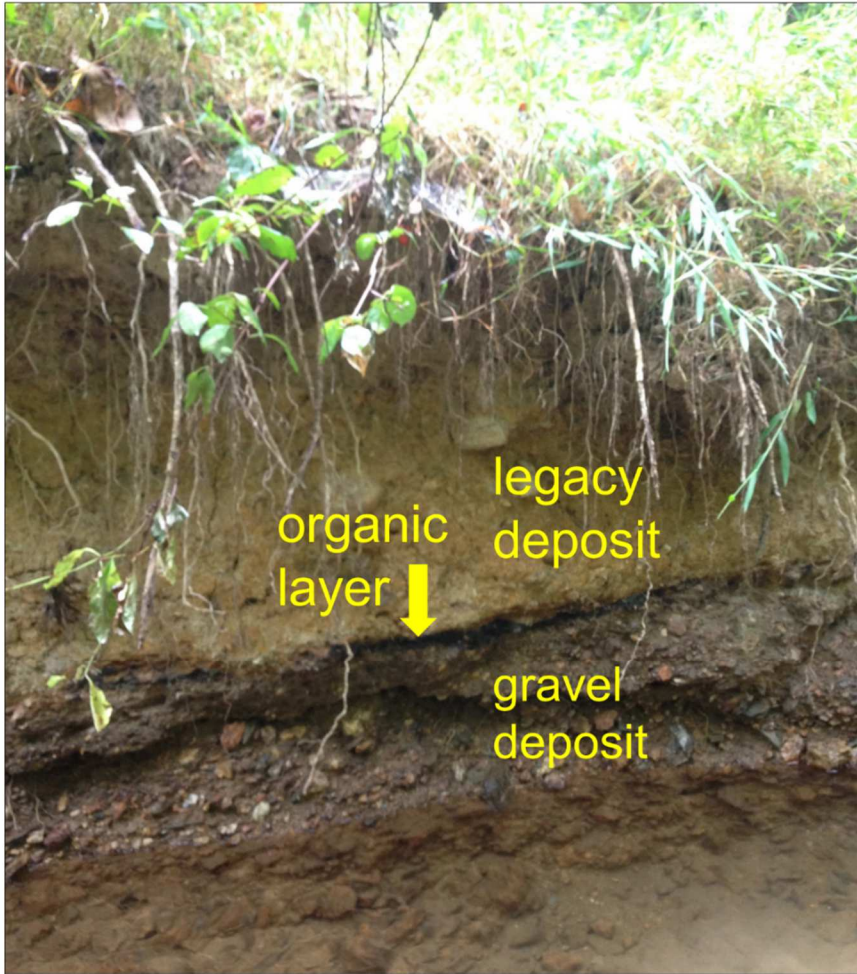


Figure 1.4: Exposed bank in TR104 shows a stratigraphic profile similar to other piedmont streams resulting from an agricultural land use history.

In the urbanized watersheds, distributed green infrastructure SWM facilities were implemented to infiltrate stormwater into the subsurface to mimic a more natural system. Though this type of SWM has many names, here it is referred to as infiltration-focused-SWM (IF-SWM). Although the term “low impact development” could also describe this type of SWM, the name implies impact lower than normal practice (Fletcher et al. 2015). Because the urbanized study area contains high-density urban development with 30% impervious surface cover (Hogan et al. 2014, Loperfido et al. 2014, Hopkins et al. 2017), it does not represent true low impact development.

When the area of Clarksburg, MD was urbanized, there was an effort to monitor changes associated with development to help inform future development decisions. Since 2004, USGS gaging stations have been recording continuous streamflow data for all three watersheds. Airborne lidar data were collected in 2002, 2004, 2006, 2007, 2008, and 2013, and can be used to track the watersheds as they underwent land use change (Hogan et al. 2014, Jones et al. 2014). This reduces the need to substitute space effects for time effects, a method that assumes to some extent that the spatial and temporal variations are equivalent (Pickett, 1989). This study area has been heavily monitored in the field by the Montgomery County Department of Environmental Protection, the Environmental Protection Agency and the US Geological Survey. Very few studies have robust datasets of repeat remotely sensed elevation data and field measurements collected before, during and after urban development to track changes in the physical landscape associated with the transition period (Jones et al. 2014).

1.2.1. Previous research in the study area

Hogan et al. (2014) studied TR104, TR109, SB, and an urban control watershed, Crystal Rock (CR), to assess the effectiveness of soil and erosion control BMPs intended to control sediment and erosion during construction. Changes in total stream discharge, channel geometry, and benthic macroinvertebrate communities were observed in the developing watersheds relative to the urban and forested controls. This suggests that the BMPs could not entirely mitigate the effects from urbanization and landscape grading (Hogan et al. 2014). A finer look at topographic change across the landscape revealed intense slope and elevation change in the

urbanized watersheds relative to the forested control watershed (Jones et al. 2014). As a result, there was a net gain in stream network length in the urbanized channels as artificial channels from engineered facilities added to the network, despite burial of a pre-development channel (Jones et al. 2014)(Figure 1.5). These observed stream network and upslope changes lead to further questions about physical response in the stream channels across time, which this study addresses.

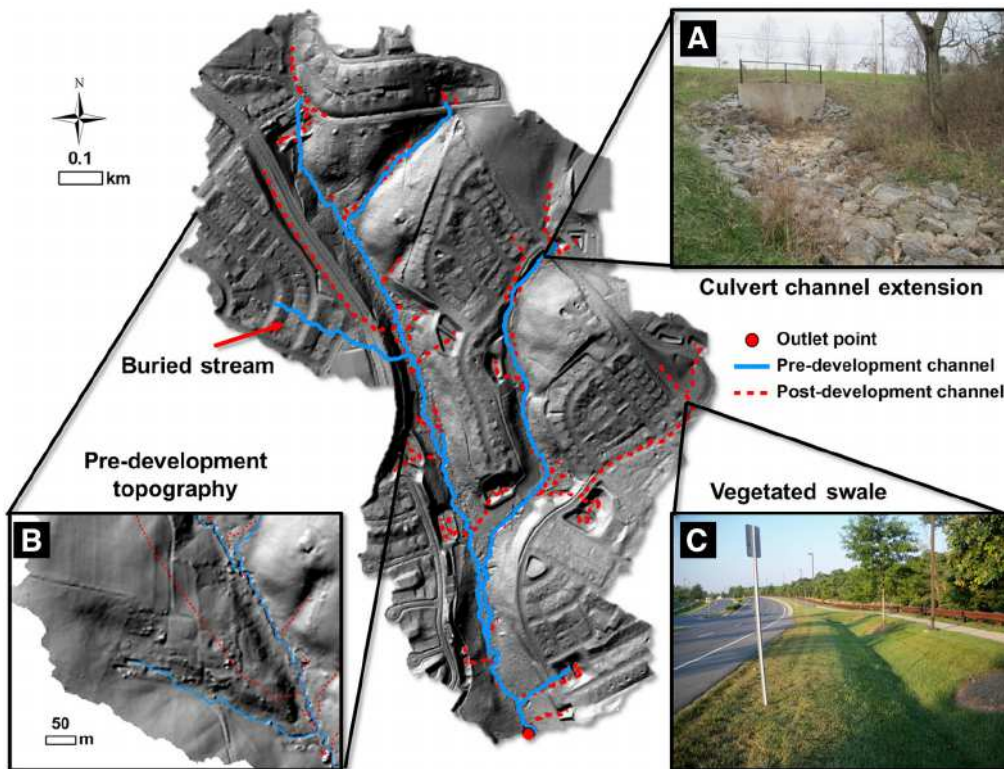


Figure 1.5: Pre- and Post-development stream network of TR104 showing where the development of artificial channels and loss of natural channels created an overall extension of the stream network. Adapted from Jones et al. (2014).

Continuous streamflow data collected at USGS stream gaging stations have also been investigated to better understand flow regime changes associated with urban development and IF-SWM. Loperfido et al. (2014) compared streamflow in TR104 with the urban control, CR, which contains older centralized SWM, and with SB, the forested control, to assess the effectiveness of distributed IF-SWM. There were noticeable differences in hydrologic response between the centralized SWM and distributed IF-SWM. In the watersheds with IF-SWM, stormflow decreased slightly and baseflow increased. Bhaskar et al. (2016) further investigated the characteristics of baseflow in TR104 during and after urban development and compared these changes with the same forested and urban control watersheds. They found that TR104 had a significant increase in baseflow during development (2004 – 2010) and no continued significant increase after development was completed (2010 – 2014). Bhaskar et al. (2016) also found that baseflow showed a strong pattern of seasonality similar to the forested control during development, but after development was completed TR104 did not show a seasonality pattern, reflecting patterns more similar to the urban control. Hopkins et al. (2017) further investigated stormflow in TR104. They split storm events into low (<1.3 cm precipitation), medium (1.3 – 3 cm precipitation), and high intensity (3 – 7 cm precipitation) and found that beyond low intensity events, stormflow in TR104 responded more similarly to the watershed with centralized SWM rather than the forested watershed.

Although the IF-SWM in TR104 was built to manage up to a 2.54 cm event (Hopkins et al. 2017), the distributed BMPs are not effectively managing even medium size events, which raises questions about how effective the BMPs are at

maintaining channel stability in streams. In medium events in TR104, sediment export is more similar to the urban control than the forested control (Hopkins et al. 2017). A large portion of sediment in the channel can be transported by moderate events since they occur more frequently than highly erosive high intensity storms (Wolman & Miller 1960). If the BMPs are only effectively managing low intensity events, it is unclear if these BMPs are mitigating physical symptoms of the urban stream syndrome such as channel widening, incision, and increased sedimentation. It is also unclear where within the watershed sediment is being mobilized or whether increased infiltration is accelerating bank erosion. The use of multi-temporal lidar allows for in-depth analysis over time to begin to clarify some of these uncertainties.

1.3. Project Scope

The research in this study builds on previous work in the study area by conducting a spatial-temporal analysis of channel characteristics and change to determine channel stability during and after completion of urban development. The goal was to develop a method to better assess geomorphic patterns in streams using lidar and then apply this method to multitemporal lidar capturing the two urbanizing watersheds and a forested control watershed through time to answer the following research questions:

- 1) Can topographic openness remotely detect channel incision? If so, are there limitations to the scale at which incision can be characterized?**
- 2) What does topographic openness reveal about the spatial pattern of incision at the watershed scale?**

3) To what extent can incision over time be measured using topographic openness with multitemporal lidar; are there observed differences in the magnitude of change between the forested and urban watersheds?

Results can illustrate limitations and methods to remotely detect channel incision for both a spatial and temporal analysis to assist with describing and predicting sediment dynamics and channel evolution. Results can also lead to a more precise understanding about the geomorphic consequences of urban development using IF-SWM and may help guide considerations for future development designs.

Chapter 2: Remotely detecting stream channel incision using aerial lidar and topographic openness

2.1. Background

Stream incision, caused by disproportional erosion of the bed vs. banks, is one of the most obvious signs of an unstable channel and steep vertical banks that form are more susceptible to erosion (Figure 2.1). A variety of factors can contribute to channel incision but they are generally grouped into two categories based on the progression of incision over time: those that cause incision to progress either downstream or upstream (Galay 1983) (Table 1). The primary driver of incision in urbanized watersheds is land use change, which alters sediment supply and the flow regime. Urban channels typically incise by rapid downcutting after the implementation of impervious surfaces and efficient storm drain networks rapidly deliver runoff from streets into adjacent streams (Hammer 1972, Booth 1990, Cole et al. 2016). Incised channels may perpetuate a positive feedback loop of erosion by confining higher magnitude flows within the steep banks that would have otherwise been able to overtop the banks and disperse energy by spilling onto the floodplain. Eventually, oversteepened banks may collapse and through subsequent removal, return the channel to a more stable form (Schumm et al. 1984). If impervious surfaces and/or stormwater outlets direct runoff to steep hillslopes, channels can also incise directly into upland surfaces where floodplains do not exist.



Figure 2.1: Severe channel incision in TR104. The depth and width of the channel have an approximate ratio of 1:1.

Causes of channel incision		
Type of incision	Primary cause	Type of change causing incision
Downstream progression	decrease in bed material discharge	<ul style="list-style-type: none"> • dam construction • excavation, diversion, or storage of bed material • land use change
	increase in water discharge	<ul style="list-style-type: none"> • flow diversion • flood
	decrease in bed material size	<ul style="list-style-type: none"> • river processes
Upstream progression	lowering of base level	<ul style="list-style-type: none"> • drop in lake/sea level or higher order river at confluence • excavation of bed material
	decrease in river length	<ul style="list-style-type: none"> • meander cutoff • channelization • stream capture
	removal of control point	<ul style="list-style-type: none"> • natural erosion • dam removal

Table 2.1: Examples of causes related to channel incision. Adapted from Galay (1983).

Incised channels are linked to numerous negative ecological and biological consequences. Incised channels tend to carry higher sediment loads and pollutants from eroding banks that degrade stream habitat (Shields et al. 1994, Shields et al. 2010). Incised channels can also influence riparian ecology by downcutting into the floodplain and lowering the water table beyond the point where riparian species can access the groundwater (Groffman et al. 2003). This hydrologic drought in the riparian zone causes upland soil types and vegetation species to migrate in. Riparian zones experiencing hydrologic drought may then become sources rather than sinks of nitrogen because they are no longer functioning in the same way (Groffman et al. 2003).

With a clear link between incision and resulting chemical and biological impacts, it is imperative to understand the spatial extent of channel incision in a watershed if restoration goals aim to improve habitat and water quality and limit total maximum daily loads (TMDLs) of sediment and nutrients. A very incised channel is relatively easy to identify in the field (Figure 2.1). However, surveying an entire watershed is time-consuming and labor is costly. Commonly, a series of cross sections representative of the reach are collected and used to infer stream characteristics in other areas of the watershed without field data. Typically, width-to-depth ratios are calculated from these cross section to classify the degree of incision or channel type (Rosgen 1994). However, width-to-depth ratios do not account for variations in bank slope or other geomorphic features in the channel that can be used to better describe the type and degree of incision or other dominate geomorphic processes. Although cross section data is important for ground-truthing and

monitoring channel change in a specific area, this method does not accurately represent the spatial variation in the degree and extent of channel incision across an entire watershed. Therefore, a need exists to rapidly map channel incision across an entire river network using remotely sensed datasets.

Although previous studies have explored new methods to map incision, there are a limited number of approaches to rapidly map incision at scales less than 10 m using solely DEM data for input. Heine & Lant (2009) developed a raster-based model at the scale of 30 m to calculate the spatial extent of incision upstream from known base-level lowering in the loess region of the Missouri River, which requires input on depth of base-level lowering. Cole et al. (2016) developed a vector-based approach to extract transects along a delineated channel from a 1 m lidar-derived DEM. They developed two automated methods to select the top of the bank from each transect and thus identify trends of channel width, depth, and longitudinal profile across a reach. This method relies on correct identification of the top of bank and is limited to areas where transects are extracted. This method cannot be fully automated without also including erroneous cross sections such as those generated along areas with gaps in lidar points, not oriented perpendicular to the channel, or crossing infrastructure such as bridges (Cole et al. 2016). Raster-based methods using high resolution DEMs derived from lidar have been successfully applied to map incision. Bigelow et al. (2016) developed a method combining slope and planform curvature to describe the degree of incision and identify the erosion potential by combining these topographic indices with a measured sediment yield. This can output a spatially explicit model at the pixel, reach, or watershed scale for estimated sediment yield

with more incised areas contributing more sediment. These are all valuable methods to describe channel incision but may be limited in function and applicability by requiring field data input or limiting measurements to cross sections.

Described here is a semi-automated raster-based method to identify channel incision in headwater streams using topographic attributes generated entirely from high-resolution aerial lidar-derived DEMs. The output is a map showing the degree and extent of channel incision on a continuous reach or pixel scale. With multitemporal high-resolution datasets, this method could also be used to estimate channel change over time, which is explored in chapter 3. This chapter introduces the method and documents the results when directly compared against field surveys of channel incision.

2.2. Methods

2.2.1. Channel incision field survey

Field surveys were conducted to obtain ground-truth information about the level and extent of channel incision in each watershed. The locations of transition areas between more and less incised channels were collected using a Trimble Juno 5 series with 2 - 4 m accuracy. Qualitative data on bank angle, bank height, and channel width were noted. In areas with a transition between dominant characteristics, GPS points were collected to identify the transition location. Field notes and photos were collected at each location where a GPS point was collected to thoroughly document changes in channel characteristics. The entire extent of the main channel in TR104 and TR109 was surveyed. In SB a field survey was conducted only in sections of the

main channel and major tributaries (Figure 2.2). The goal of the field surveys was to document the bank and channel characteristics and map the locations of transition between varying characteristics. The goal of the field surveys was only to collect data relevant to incision but not classify reaches into various levels of incision in the field.

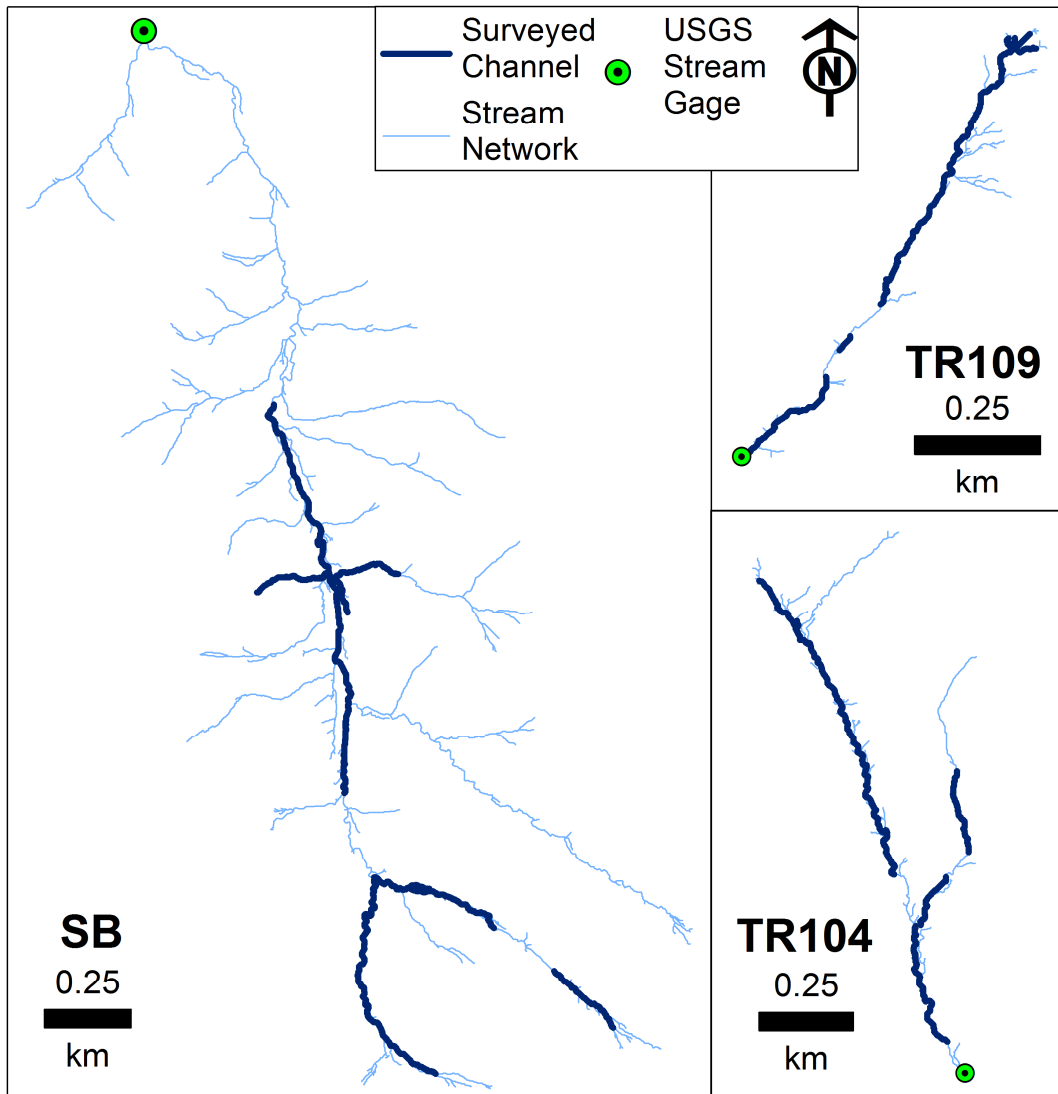


Figure 2.2: Locations within each stream network that were surveyed for characteristics of channel incision. In TR104 and TR109 the entire main stem of the channel was surveyed. In areas where gaps exist, the delineated channel deviated from actual location of the channel (verified using aerial imagery) and these sections were removed from the analysis. In SB, sections of the main channel and tributaries were surveyed.

2.2.2. Structure from motion field survey

Following field surveys, five reaches from TR104 and three reaches from TR109 ranging from 20 – 40 m long and representing a variety of channel characteristics documented from the initial field survey were selected for a structure from motion (SfM) analysis to quantify bank characteristics related to channel incision. SfM is a method for modeling fine-scale topography by extracting high-resolution 3-dimensional point clouds using 2-dimensional imagery (Westoby et al. 2012). A handheld Olympus SZ-10 14-megapixel digital camera was used to collect overlapping still images, taken at multiple angles along the banks. Four scale markers with known dimensions were placed along the banks in each reach to scale the point cloud into known units. The GPS coordinates were collected at the upstream and downstream extent of each reach using a Trimble Juno 5 series with 2 - 4 m accuracy to match the location of the SfM-derived DEM with the lidar-derived DEM. Since the SfM-derived point clouds were not georeferenced with the lidar-derived point clouds, an accuracy of 2 – 4 m was sufficient.

Images were processed for SfM using Agisoft Photoscan® 1.3.2. Images were aligned with high accuracy to find and match common points among images and locate camera positions. Once images were aligned, dense point clouds were created based on the estimated locations of the camera positions (Agisoft 2017). Scale bars were created using the scale makers that were visible in the photos to accurately measure distance in the final elevation model. This produced a point cloud where one unit was equal to 1 m. The scaled point clouds were then exported to Cloud

Compare® to filter out large sections of vegetation and other non-ground points (Figure 2.3).

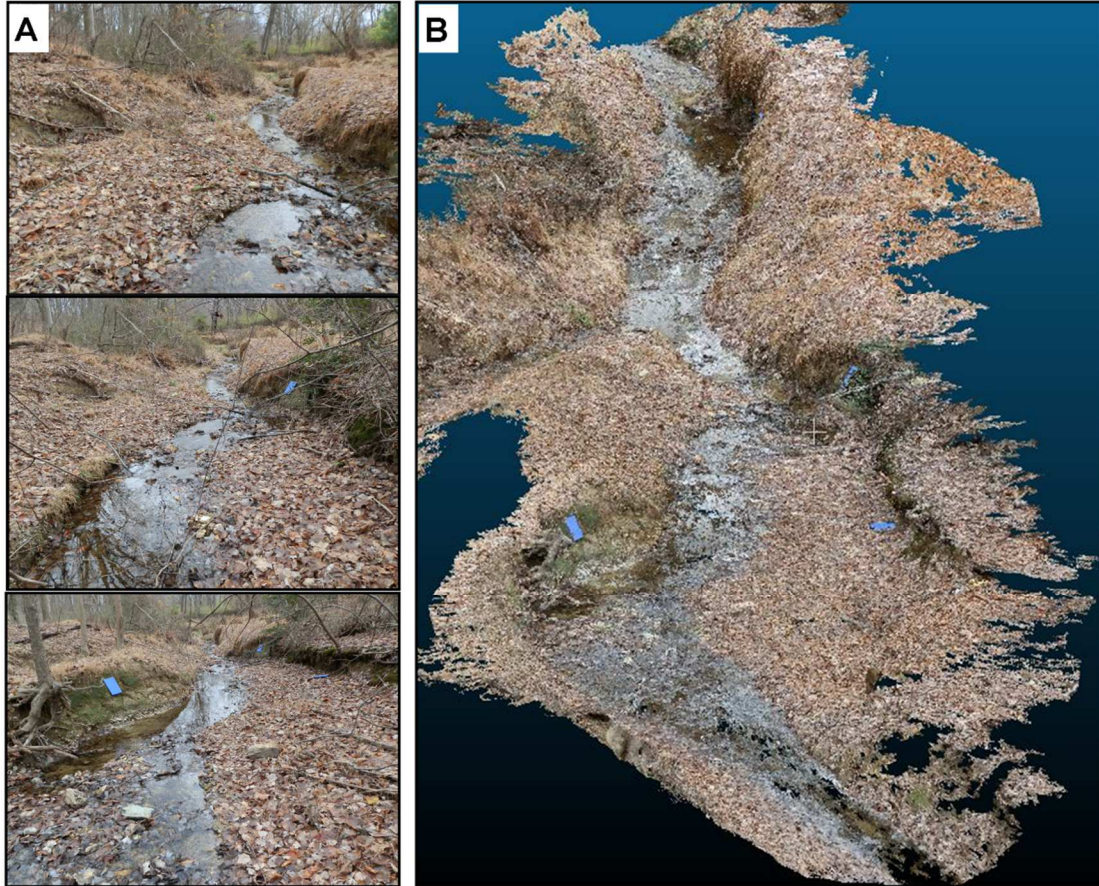


Figure 2.3: Examples of photos collected in the field (A) that were used to derive a 3-dimensional point cloud of a stream reach (B). The blue squares are scale markers used to correctly scale the point cloud.

The scaled, filtered point clouds were exported in las format to ArcGIS 10.3 to create DEMs with a resolution of 0.1 m. The elevation values of the channel bed, which typically decrease along a downstream gradient (Figure 2.4a), were detrended to reflect height above the channel, similar to the height above nearest drainage (HAND) terrain model (Nobre et al. 2011). To assign an elevation of 0 m across the bottom of the channel, the orientation of the raster was rotated so that the channel followed an East-West direction. The focal minimum was calculated in 0.1 m wide by

15 m long transects oriented perpendicular to the channel. The width of 0.1 m equaled one pixel and 15 m long was sufficient to extend beyond the maximum channel width. This method assumed that the lowest point along the transect fell within the channel. The resulting focal minimum DEM was then subtracted from the original elevation DEM, creating the final DEM representing height above the bottom of the channel (Figure 2.4b). The slope of the banks were also extracted from the original DEM (Figure 2.4c). The entire workflow is summarized in figure 2.5.

Because incised channels are characterized as having steep banks but can include a range of bank heights, the degree of incision along each SfM-derived DEM was determined by using a combination of slope and bank height. This allowed for a way to quantify the variation of stream bank characteristics in all the SfM study sites and less subjectively organize reaches into different levels of incision ranging from no incision to severe incision. Reaches were assigned a value of 0 for no incision, 1 for moderate incision, or 2 for severe incision; the specific details of separating reaches into various classes are further discussed in section 2.3.1.

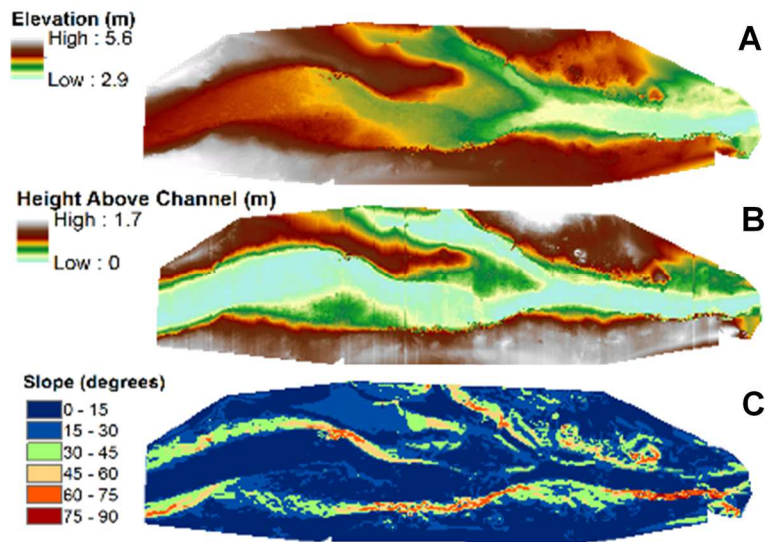


Figure 2.4: Original 0.1 m DEM generated from the scaled, filtered point cloud (A). The overall elevation was adjusted to represent elevation above the local channel minimum (B). The degree slope was then calculated from the original DEM (C).

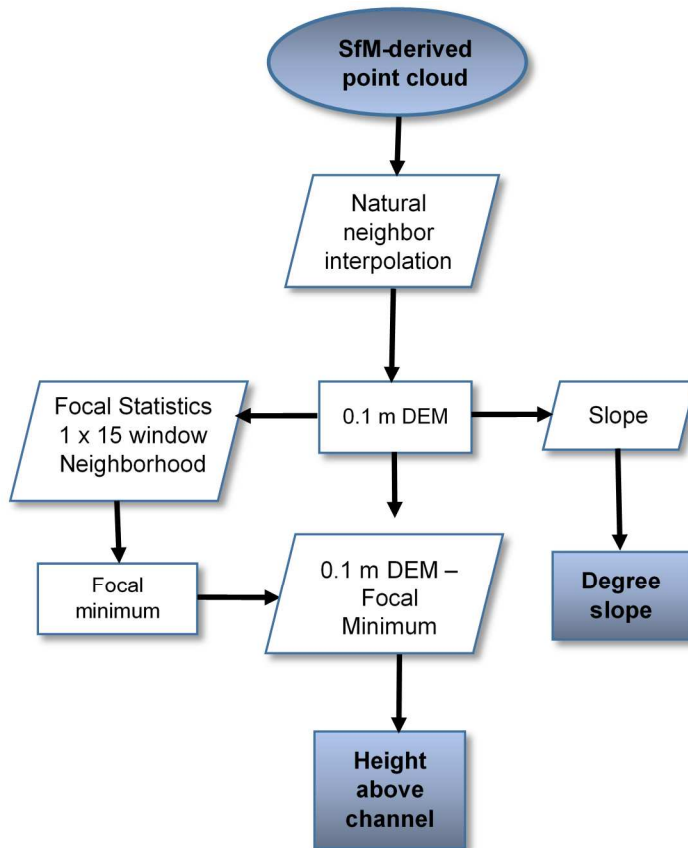


Figure 2.5: Workflow for processing SfM-derived DEMs of stream reaches to determine bank height and bank angle.

2.2.3. Lidar data processing

Airborne Lidar was collected over the study area on December 28, 2013 as part of the 2013 Montgomery County, MD lidar data collection effort. Lidar was flown by Kucera International Inc. and captured using a Leica ALS60, with a vertical accuracy of 0.052 m and a horizontal accuracy of 1 m. The data are referenced to the North American Datum of 1983/81, and projected in the Maryland State Plane Coordinate System in feet. After points were processed and classified by the vendor, 0.9 m (3 ft) resolution DEMs were interpolated from bare-earth point clouds using the natural neighbor interpolation algorithm (Sibson & Barnett 1981) in ArcGIS 10.3 (ESRI, Redlands CA). The DEMs were then aggregated to 1.8 m horizontal resolution to smooth and reduce noise in the interpolated topography (Jones et al. 2014, Metes et al. *in preparation*).

A stream network delineating the perennial portion of the channels was created from the 2013 lidar-derived DEM using the ESRI hydrology tools (ESRI, Redlands, CA). The GPS locations were used to identify areas of the channel that were surveyed, and all sections of the delineated stream network that were not included in the field survey were removed. This network was then converted into a raster to conduct a direct pixel overlap analysis with the openness incision results.

2.2.3.a. Mask erroneous lidar

Individual lidar ground points are typically spaced at sub-meter distances, but it is common for larger gaps in point spacing to occur, particularly in densely vegetated areas where lidar is blocked from reaching ground level (Jarnagin 2010). When gaps exist, the interpolation algorithms for converting raw points into a

continuous surface DEM use the surrounding elevation to fill in gaps. When voids are present over stream channels and breaklines are unavailable, valuable elevation information is lost and stream channels appear as flat surfaces (Figure 2.6). This is problematic when using lidar-derived DEMs to focus specifically on channel geometry.

To reduce errors from inadequate point cloud coverage, a “no data” mask was created to exclude clusters of pixels with gaps in points. The number of bare earth las points per each 1.8 m pixel were counted using las statistics (ESRI, Redlands, CA). Clusters of low point counts were identified using a 3 x 3 window to calculate the focal median for each cell. All cells with a median value of 0 were extracted to a no data mask. The no data mask was applied to the field-surveyed stream raster to exclude all pixels that overlapped with this mask from the analysis.

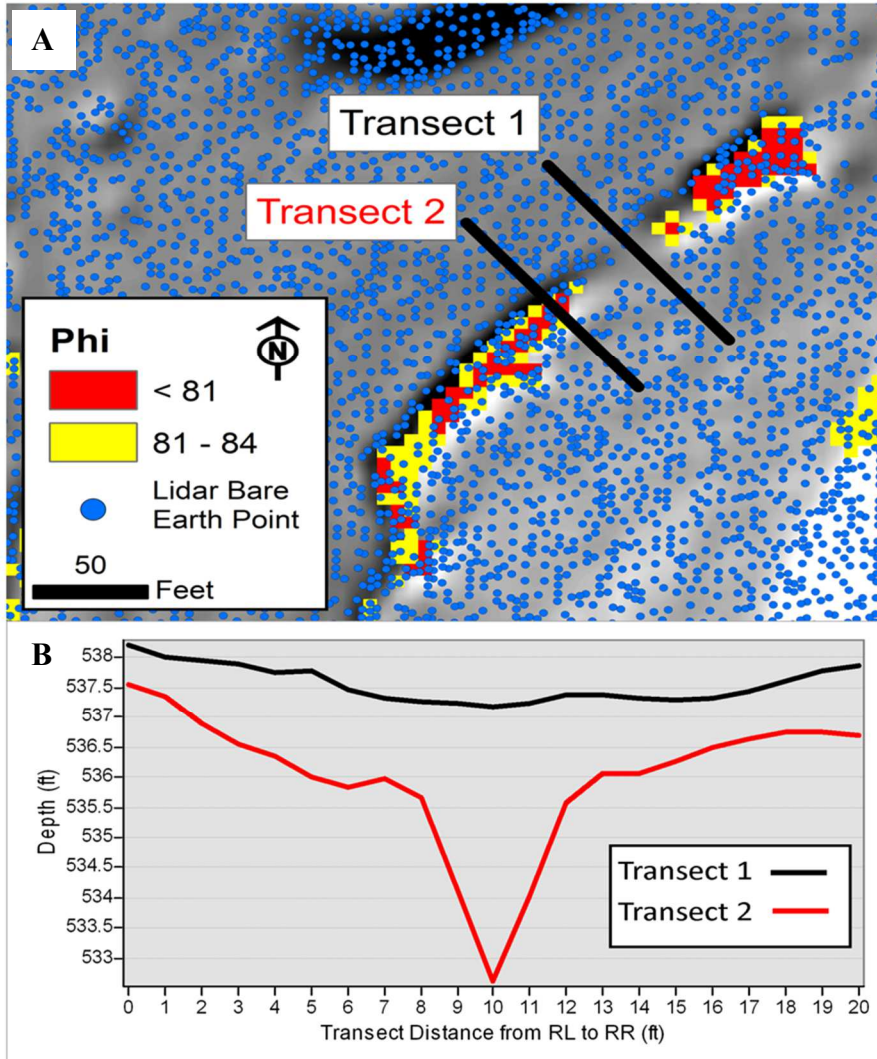


Figure 2.6: Example of areas along the channel where there are low point counts, and phi values are > 84 (indicating a non-incised reach) even though this is an area with known severe incision (A). Two cross sections were extracted from the DEM. The channel is not detected along transect 1 but is detected in transect 2. (B). Additionally, the v-shape of Transect 2 isn't showing true channel form but is a result of using a coarser 1.8 m DEM, which is approximately the width of the channel.

2.2.3.b. Positive topographic openness

Positive topographic openness (phi), the attribute used to detect stream channel incision from the lidar-derived DEMs, was extracted from each pixel in the 1.8 m lidar-derived DEM using a python script based on Yokoyama (2002) (Peters 2015) and applying a search radius of 36.6 m (120 ft). Stream channel pixels were

used to mask the phi grid, resulting in a phi layer including only pixels that also contained field information on channel incision.

The angular measure of positive openness in each stream channel pixel is constrained by stream banks (Figure 1.1) so it was hypothesized that phi values close to 90 indicate flat or non-incised channels and phi values less than 90 indicate more defined channels with the degree of incision increasing as phi values declined further. Each phi value was grouped into one of three incision classes that was determined from the field survey results. The phi values were grouped by overlapping incision class and the interquartile ranges were used to set empirical thresholds to reclassify phi values into incision classes.

Since changes were delineated in the field at a scale coarser than the resolution (1.8 m) of the DEM, the classified reaches were then aggregated to a scale more representative of shifts in incision detected in the field. The *Generalization* toolset within the Spatial Analyst extension of ArcGIS contains tools intended to clean up small erroneous areas within a raster dataset or remove small details (ESRI, Redlands, CA). The *region group* and *nibble* tools within this toolset were combined with the *set null* tool, also within the Spatial Analyst extension, to smooth classified reaches. A series of thresholds for smoothing the classified phi pixels were explored for optimal results. The *region group* tool was used to group connected pixels of the same incision value and count the number of connected pixels within each region. The *set null* tool was then used to remove groups under a selected pixel count, and gaps were filled with neighboring values using the *nibble* tool (Figure 2.7).

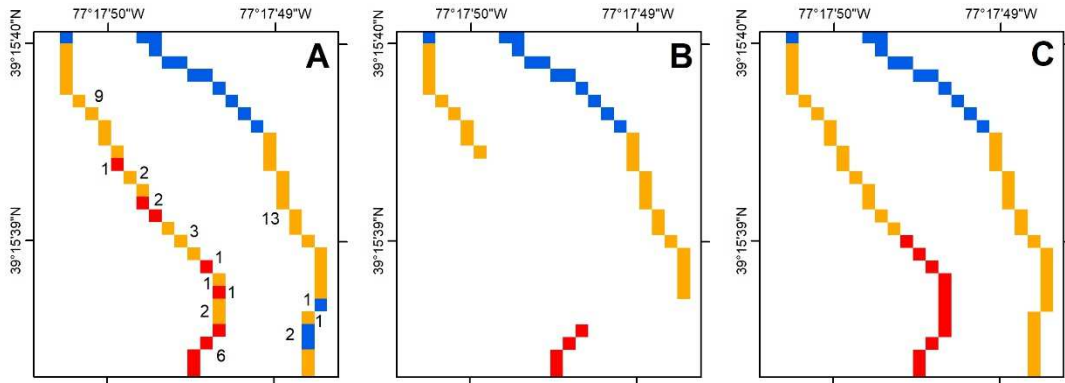


Figure 2.7: Result of original phi values reclassified into three different levels of incision, represented by red (level 2), orange (level 1), or blue (level 0) pixels. The region group tool counts the number of contiguous pixels of the same value (A). The set null tool was set to remove groups under a value set by the user (B). The nibble tool was then used to fill in the gaps removed from set null with surrounding pixel values (C).

2.2.4. Field vs. model comparison

The accuracy of the openness method was directly tested against the field data for both individual and combined watersheds by generating confusion matrices using the caret package in R (Kuhn 2008, R core team 2015). Overall percent accuracy of each model was calculated as:

$$\# \text{ correctly classified pixels} / \text{total pixels} * 100 \quad (1)$$

The kappa statistic was also calculated and generates a more robust measurement of accuracy by accounting for agreement due to chance (Cohen 1960, Viera and Garrett 2005). For each individual group in the model (i.e. pixels classified as 0, 1, or 2), the number of correctly and incorrectly classified pixels were counted as true positives or false positives and false negatives. True positives (TP) refer to the number of correctly classified pixels in a group. False positives (FP) refer to the

number of pixels classified in a given group when they should not have been, and false negatives (FN) refer to the pixels missed from being classified in a given group. True negatives (TN) refer to the number of pixels correctly excluded from a group and is only useful for binary classifications, but with 3 or more classes, TN does not reveal anything about the success of the class in question (Figure 2.8). Therefore, only TPs, FPs, and FNs were used to evaluate the success of each individual classification by calculating the following metrics:

$$\text{Sensitivity} = TP / (TP + FN) \tag{2}$$

$$\text{Precision} = TP / (TP + FP) \tag{3}$$

$$\text{F-Score} = 2(\text{Sensitivity} * \text{Precision}) / (\text{Sensitivity} + \text{Precision}) \tag{4}$$

Sensitivity measures the extent to which the model wrongfully excludes pixels that should have been classified in the group in question and precision measures the extent to which the model wrongfully includes pixels from another classification (Altman & Bland 1994, van Stralen et al. 2009). The F-score is the harmonic mean of these two metrics and can be used to evaluate the balance between FNs and FPs. A perfect model would result in a value of 1 for all metrics.

		Reference		
		0	1	2
Predicted	0	TP	FP	
	1	FN		TN
	2			

Figure 2.8: example of TPs, TNs, FPs, and FNs for class 0. Metrics with TNs are not helpful in revealing anything about the success of the class because in this case, TNs could also include pixels classified incorrectly in groups 1 and 2.

2.3 Results

2.3.1. Structure from motion and field surveys

A total of 123 locations of incision characteristics and transitions were collected with the GPS with at least one field photo and detailed field notes at each location, making it possible to reassess field sites after completion of site visits since reaches were not assigned an incision class in the field.

Detailed streambank information along eight 20 – 40 m long reaches was collected using SfM. About 100 to 200 photos were collected at each site. The survey focused on reaches with a variety of bank characteristics identified from the initial field survey and areas of transition between reaches with different levels of incision. Scaled, filtered DEMs at one-tenth meter resolution were used to calculate slope and bank height (Figures 2.9 - 2.10).

The SfM survey demonstrated that even in small reaches, slope and bank heights were variable. Reaches with no incision tended to have gradually sloping banks on both sides with angles less than about 45°. Severely incised channels tended to have nearly vertical banks and a range of bank heights. However, these characteristics were not always consistent across a study reach. At site 3 in TR104 the channel displayed characteristics of severe incision on one side of the bank and no incision on the opposite side (Figures 2.9 & 2.10). The criteria for grouping these types of reaches into moderately or severely incised channels depended on both bank height and angle. If the side of the steepest bank was near vertical and the opposite bank was not, the reach was considered severely incised if the steeper bank was about 1 m or taller, and moderately incised if the steeper bank was less than 1 m tall. If the

side of the steepest bank was sloping between about 40 – 70 degrees, the reach was considered moderately incised if the opposite bank was also sloping between about 40 – 70 degrees and not incised if the opposite bank was gently sloping. A full decision tree is explained in Figure 2.11. The bank height and slope criteria were developed using SfM data from sites with drainage areas less than 1 km² and channel widths less than 5 m, limiting the application of the decision tree to sites with similar characteristics.

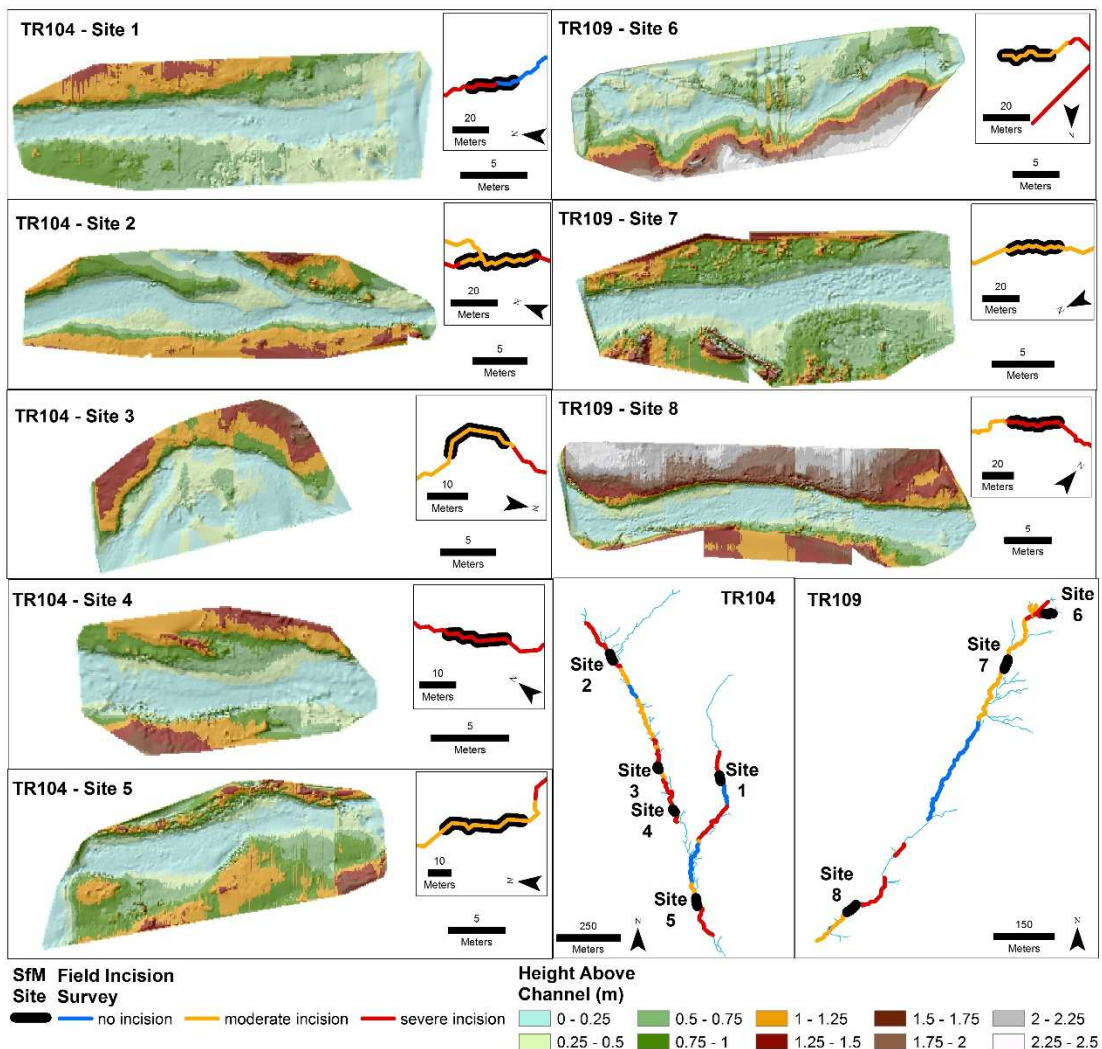


Figure 2.9: Results of SfM survey of bank height after elevation was adjusted to reflect height above the channel rather than relative elevation.

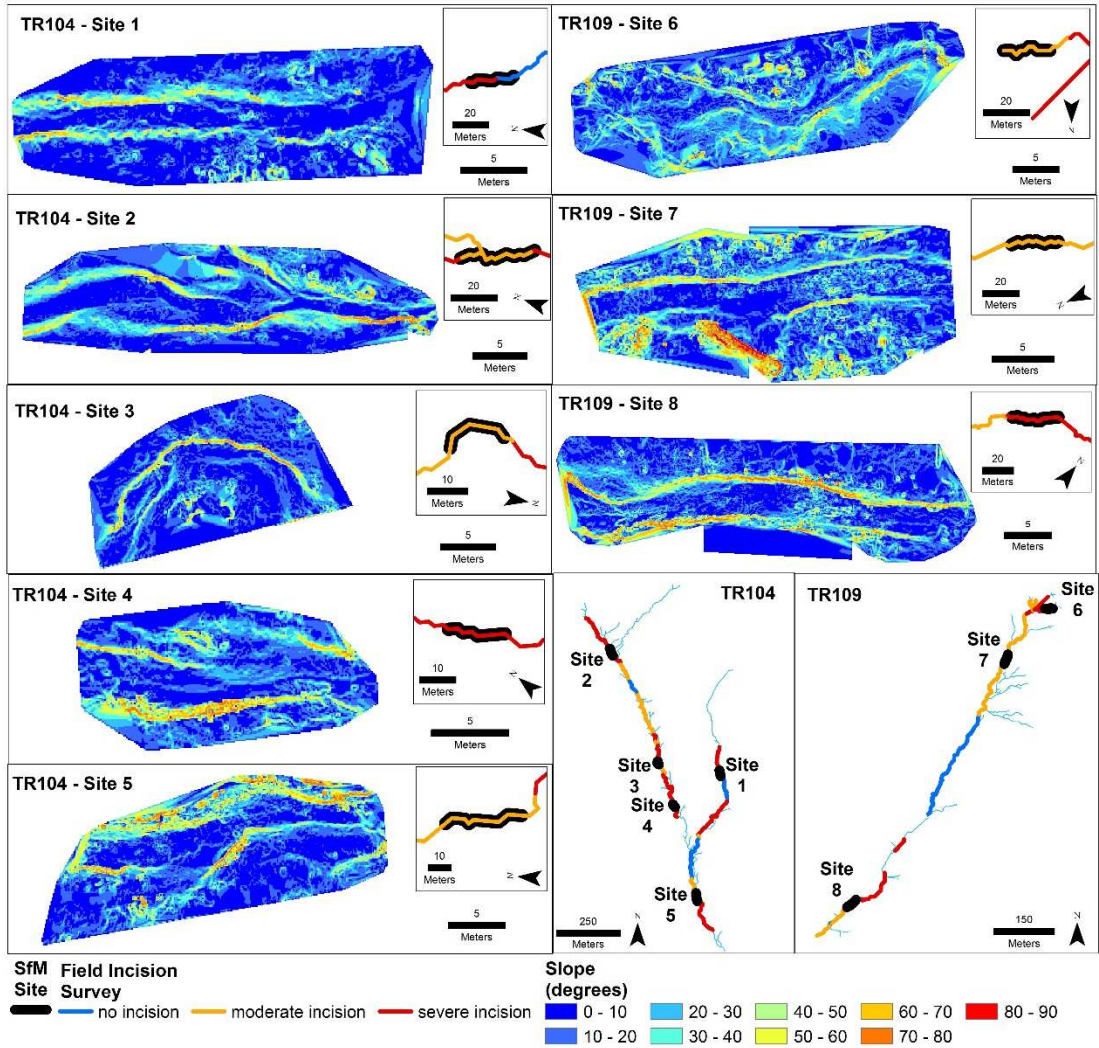


Figure 2.10: Results of SfM survey of bank angle in degrees per pixel, to obtain bank slope information on each reach.

To classify the remaining reaches that were surveyed initially but not surveyed using SfM, field notes on estimated bank height and angle along with corresponding field photos were compared to the decision tree (Figure 2.11) developed using the SfM surveys to assign an incision classification to these reaches. Reaches with moderate incision contained various characteristics consistent with observations from the SfM sites. Some reaches had small bank heights, but the banks were nearly vertical or moderately sloping (Figure 2.12a). Other moderately incised

reaches had stable banks on one side and unstable banks on the other side (Figures 2.13a & 2.14a). Reaches with no incision were characterized by gradually sloping banks (Figures 2.12c, 2.13b, and 2.14b). Reaches with severe incision were characterized by steep, nearly vertical banks on both sides of the channel and/or vertical banks above 1 m (Figures 2.12b, 2.13c & 2.14c). Some reaches that were in between moderate to severe incision were difficult to assign into a single group. For example, in Figure 2.13c the banks were not disproportionately tall for the width of the channel but the bank angles were nearly vertical on both sides of the channel, indicating rapid downcutting and erosion, so these reaches were included in the severely incised classification. The entire extent of classified field surveys for each watershed are displayed in Figures 2.12 – 2.14.

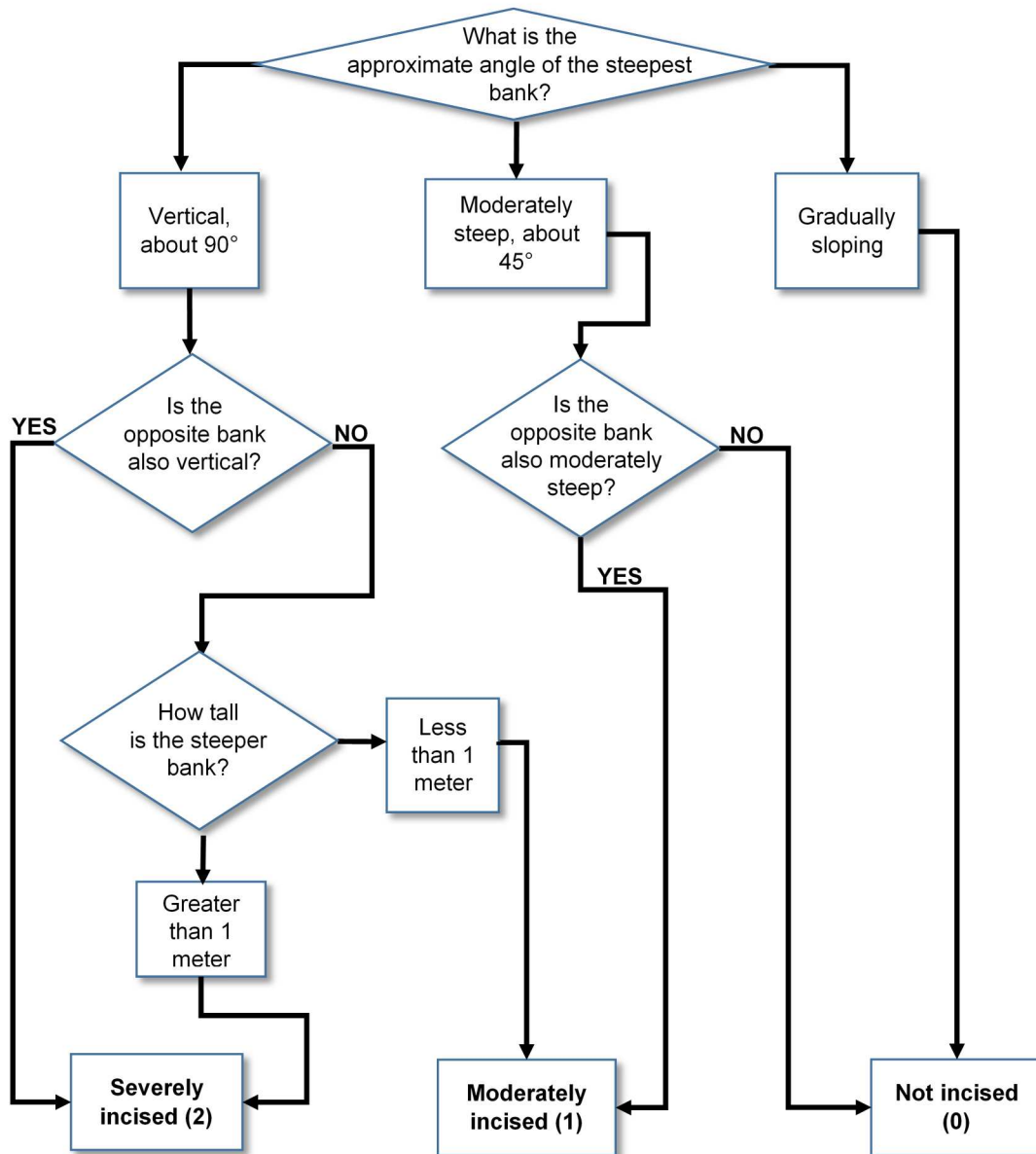


Figure 2.11: Decision tree for classifying reaches into incision classifications of severe, moderate, and none, based on channel observations and data extracted from the SfM-derived DEMs.

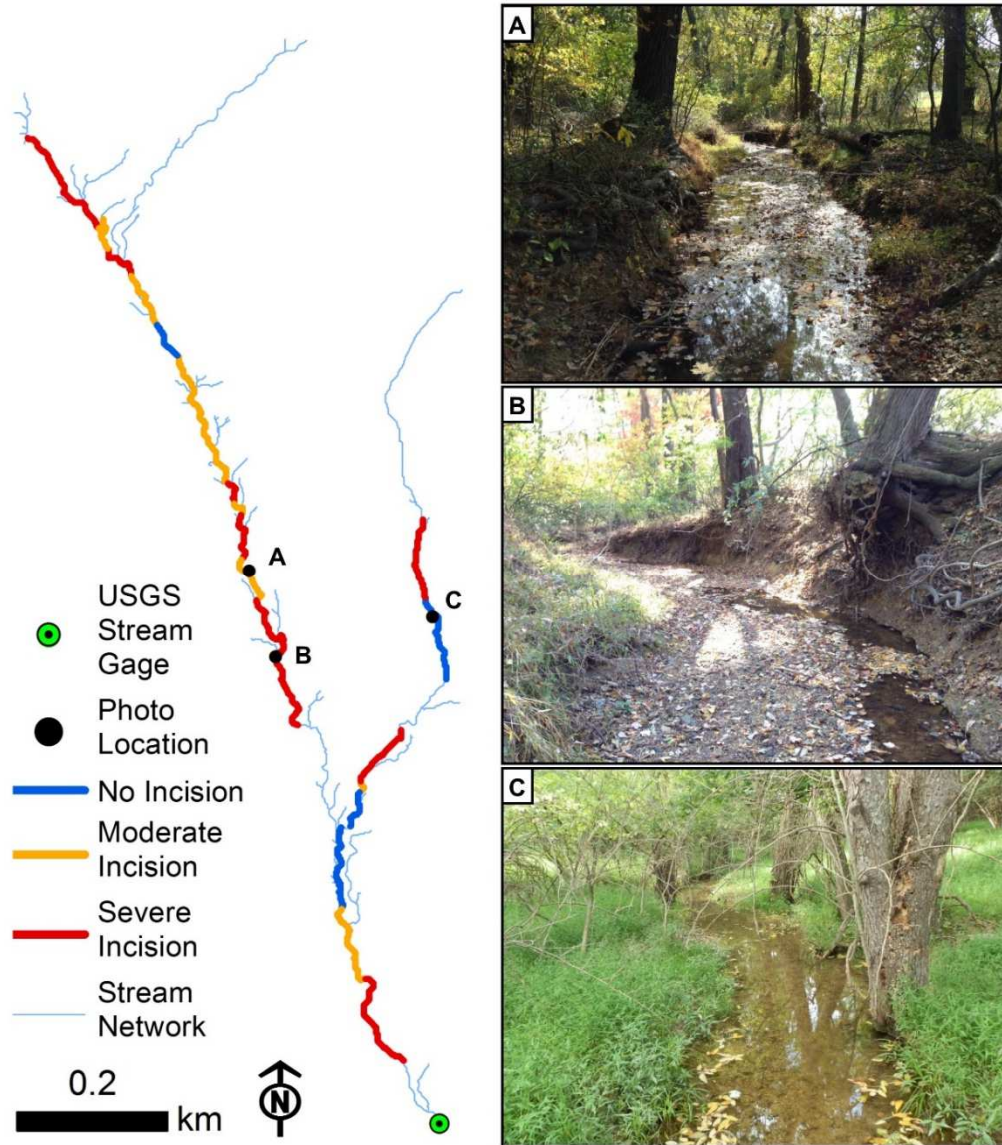


Figure 2.12: Results of incision field survey for TR104. Examples of reaches with moderate incision (A), severe incision (B), and no incision (C).

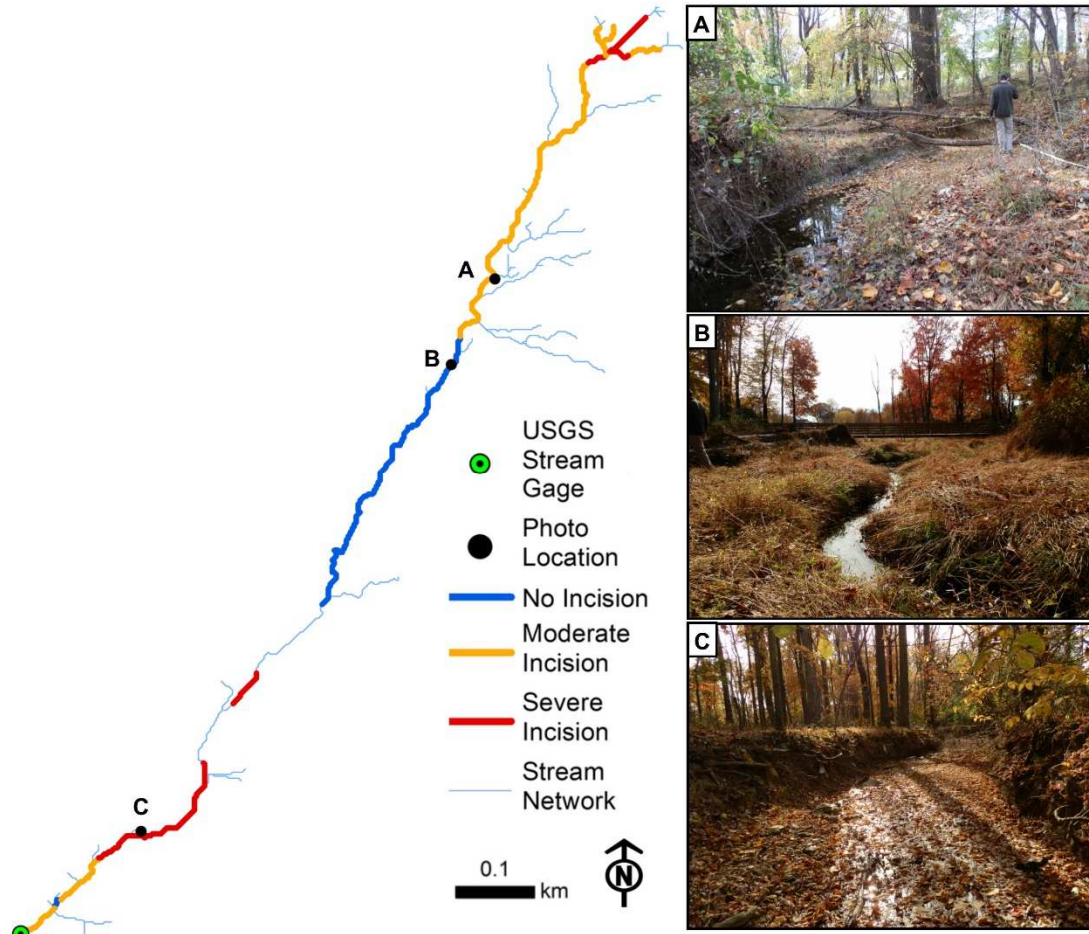


Figure 2.13: Results of incision field survey for TR109. Examples of reaches with moderate incision (A), no incision (B), and severe incision (C).

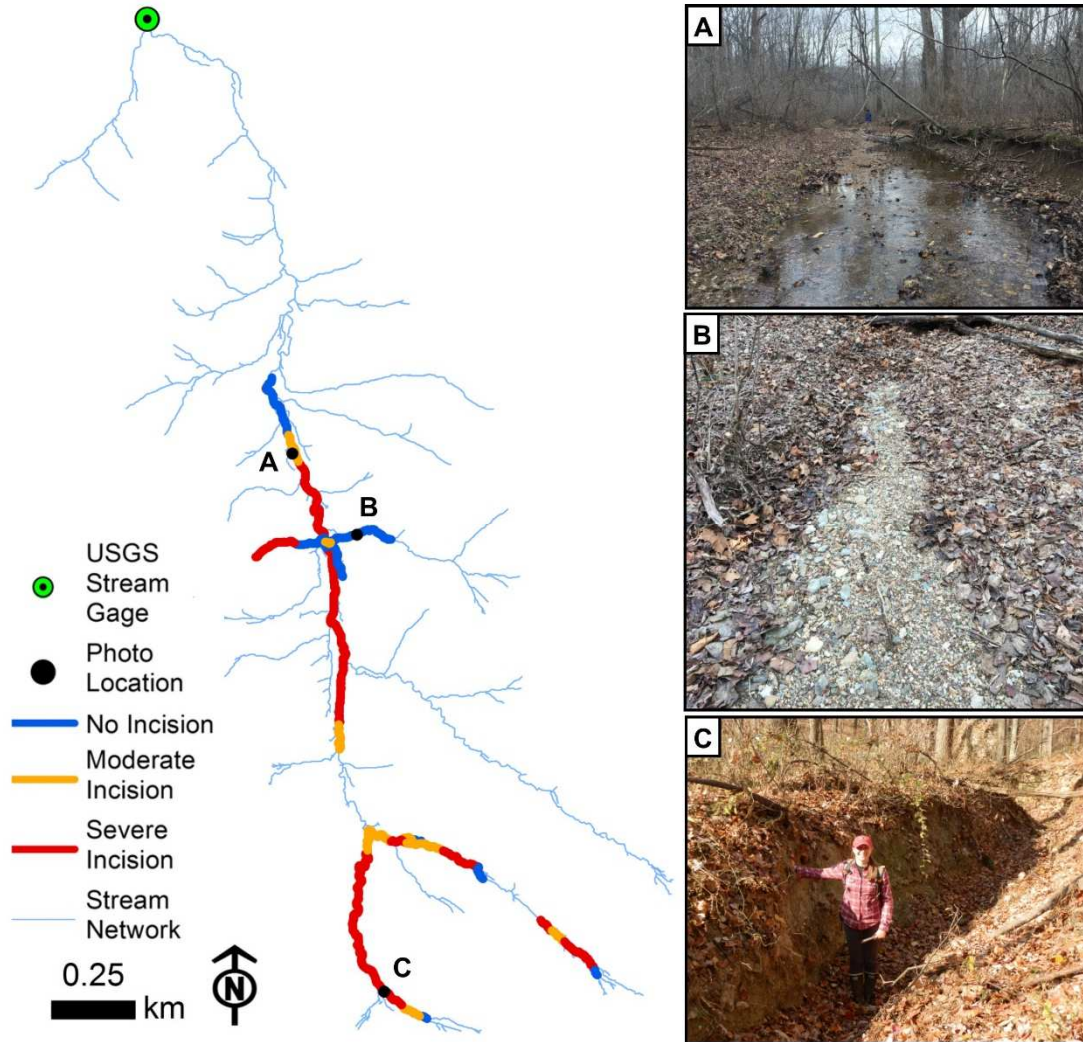


Figure 2.14: Results of incision field survey for SB. Examples of reaches with moderate incision (A), no incision (B), and severe incision (C).

2.3.2. Using inter quartile ranges to select phi thresholds

The inter quartile-ranges (IQR) for phi values within each incision class were relatively distinct between classes 0 and 1 in all watersheds but TR104 and TR109 exhibited some overlap with classes 1 and 2 (Figure 2.15). Almost 60% of SB was classified as severely incised compared with only 24% in TR109, which may contribute to a more robust range of phi values for class 2 in SB. The IQR in class 0 and 2 varied slightly in all three watersheds. In TR109 class 0 was higher than the

other groups and in SB class 2 was lower than the other groups. All three watersheds shared similar IQR values for class 1 and when these values were rounded to the nearest whole number, each group shared the same range (81 – 84). Therefore, the thresholds of 81 and 84 were selected to split phi pixels into the three classifications. Phi values > 84 were used to classify pixels as 0 for no incision, values between 81 - 84 were used to classify pixels as 1 for moderate incision, and values < 81 were used to classify pixels as 2 for severe incision.

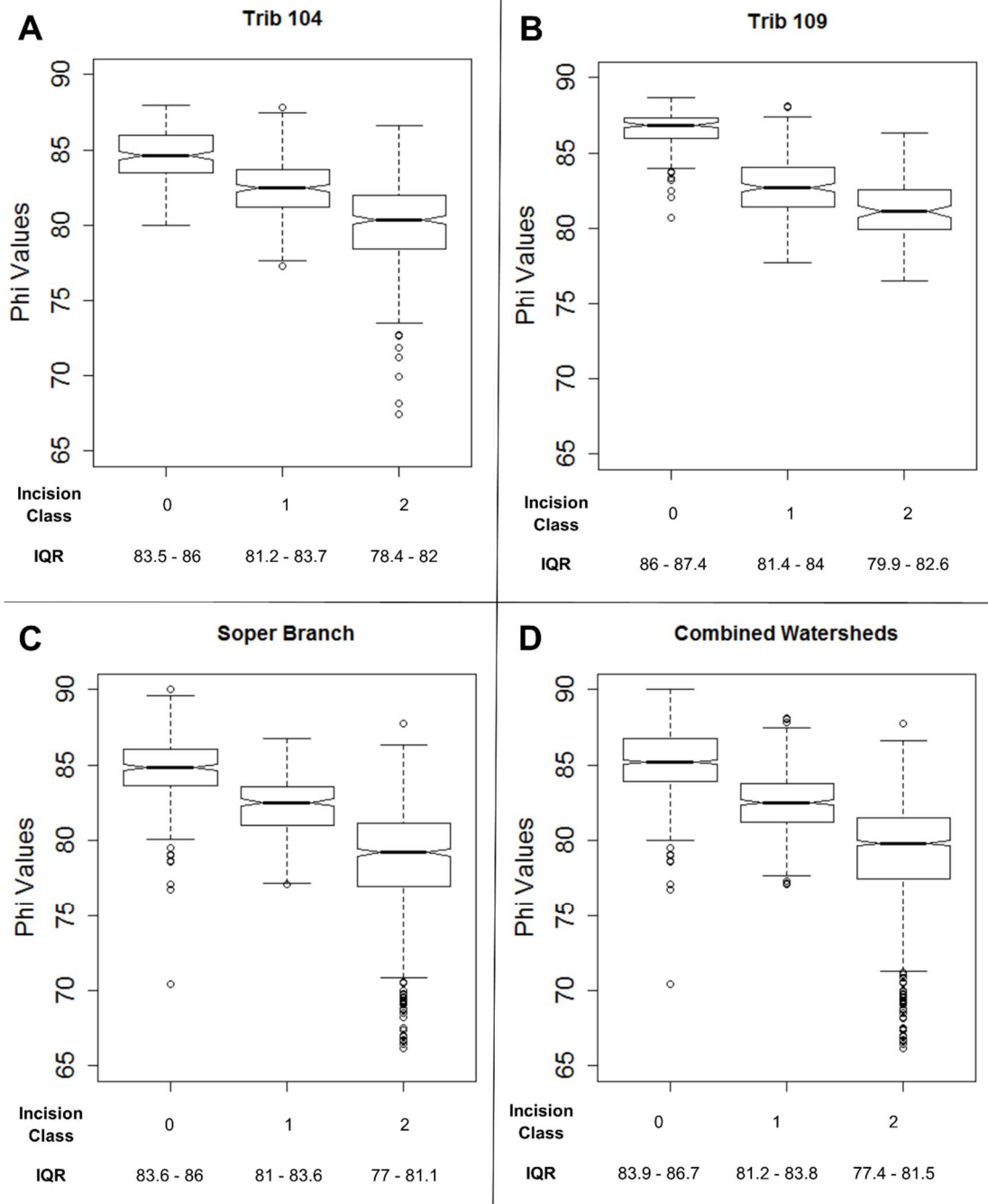


Figure 2.15: Boxplots displaying the distribution of positive openness values overlapping with each level of incision surveyed in the field. Notches show 95% confidence intervals of the median and suggest the median between groups differ when not overlapping.

2.3.3. Comparison of openness model vs. field incision

Once openness pixels overlapping with the stream raster were masked and reclassified into incision classes, the reaches were smoothed to reduce erroneous pixel

classifications and represent incision at a scale closer to what was typically detected in the field (Figure 2.7). All three watersheds had an improved accuracy and kappa statistic when single pixels different than the adjacent pixels were smoother over. The most improvement in TR109 and Soper Branch was observed using a threshold of smoothing areas with less than 4 (7 m) contiguous pixels of the same value (Table 2.2), with TR104 resulting in a slightly higher improvement with a threshold of 5 pixels (9 m). Since the incision method introduced here was also applied to lidar collected prior to 2013 to understand incision changes through time, the optimal threshold of 5 pixels was selected for all analyses in TR104, rather than the threshold of 4 pixels selected for all analyses in SB and TR109. This 7 – 9 m threshold is closer to the scale at which transitions in incision were observed in the field. In the absence of field data to support a more objective smoothing threshold, a threshold of 4 pixels, which improved the accuracy in all three watersheds tested here, would likely result in improved accuracy in similar settings.

Watershed	Smoothing Threshold	Accuracy (%)	Kappa
TR104	original	60.3	0.389
	< 3 pixels	66.6	0.483
	< 4 pixels	69.5	0.525
	< 5 pixels	70.7	0.539
TR109	original	66	0.475
	< 3 pixels	73.4	0.584
	< 4 pixels	75.1	0.604
	< 5 pixels	72.5	0.557
SB	original	69.3	0.497
	< 3 pixels	72	0.537
	< 4 pixels	73	0.556
	< 5 pixels	72.5	0.541

Table 2.2: Results of accuracy and kappa values with various smoothing thresholds for each watershed.

The results from the confusion matrix comparisons are summarized in tables 2.3-2.4. The accuracy for each watershed ranged from 70.7 – 75.1% and the kappa statistic ranged from 0.54 to 0.60, indicating moderate agreement between the model and field survey. The kappa statistic indicates substantial agreement beginning at 0.61 (Landis & Koch 1977). Sensitivity, precision, and F-score show that the openness method did not tend to consistently favor a specific incision class for each watershed, but overall group 1 resulted in the lowest performance.

TR104 A				TR109 B					
Field Survey				Field Survey					
	0	1	2		0	1	2		
Openness	0	111	23	0	Openness	0	134	42	0
	1	49	180	111		1	10	166	49
	2	0	50	270		2	0	18	58
SB C				Combined D					
Field Survey				Field Survey					
	0	1	2		0	1	2		
Openness	0	261	52	74	Openness	0	509	117	82
	1	98	189	142		1	154	539	310
	2	4	62	719		2	4	126	1031

Table 2.3: Confusion matrix results for TR104 (A), TR109 (B), SB (C), and combined watersheds (D) showing results of the pixel by pixel comparison between the field survey and openness models for each class.

Watershed	Accuracy (%)	95% CI	p-value	Kappa	Incision			
					class	Sensitivity	Precision	F-Score
TR104	70.7	67.4 - 73.8	2.20E-16	0.539	0	0.694	0.828	0.755
					1	0.712	0.529	0.607
					2	0.709	0.844	0.77
TR109	75.1	70.9 - 78.9	2.20E-16	0.604	0	0.931	0.761	0.838
					1	0.735	0.738	0.736
					2	0.542	0.763	0.634
SB	73	70.7 - 75.2	< 2.2e-16	0.556	0	0.712	0.674	0.696
					1	0.624	0.441	0.516
					2	0.769	0.916	0.836
Combined	72.4	70.7 - 74	< 2.2e-16	0.574	0	0.763	0.719	0.74
					1	0.689	0.537	0.604
					2	0.725	0.888	0.798

Table 2.4: Statistics and indices calculated from the confusion matrix results. Sensitivity, precision, and F-score are broken down into results for each class, within each watershed.

2.3.3.a. TR104 results

Of the individual watersheds, TR104 resulted in the lowest accuracy and kappa values. The F-score was strongest in classes 0 and 2. This may have been driven by precision, which had values above 0.8 for class 0 and 2 because no areas mapped as “severe incision” were classified as “no incision” and no areas mapped as “no incision” were classified as “severe incision.”. However, precision resulted in 0.529 for class 1 because almost half of the pixels classified as 1 in the openness method were FPs, with most of the FPs being areas identified as 2 in the field but classified as 1. Almost 30% of the pixels identified as 1 were also classified 2 or 0 (Table 2.3). This is partly due to the overlap in IQRs of phi values representing incision classes 1 and 2 (Figure 2.15). TR104 had an even balance of sensitivity, meaning the proportion of FNs was consistent across each group. There were many incision level transitions measured in the field in TR104 (Figure 2.16) and some of these areas may not have been distinct enough to be classified accurately in the

openness method. In the eastern branch of TR104 there are two distinct areas of transition moving downstream from areas of severe to no incision that were well represented with openness (Figure 2.16).

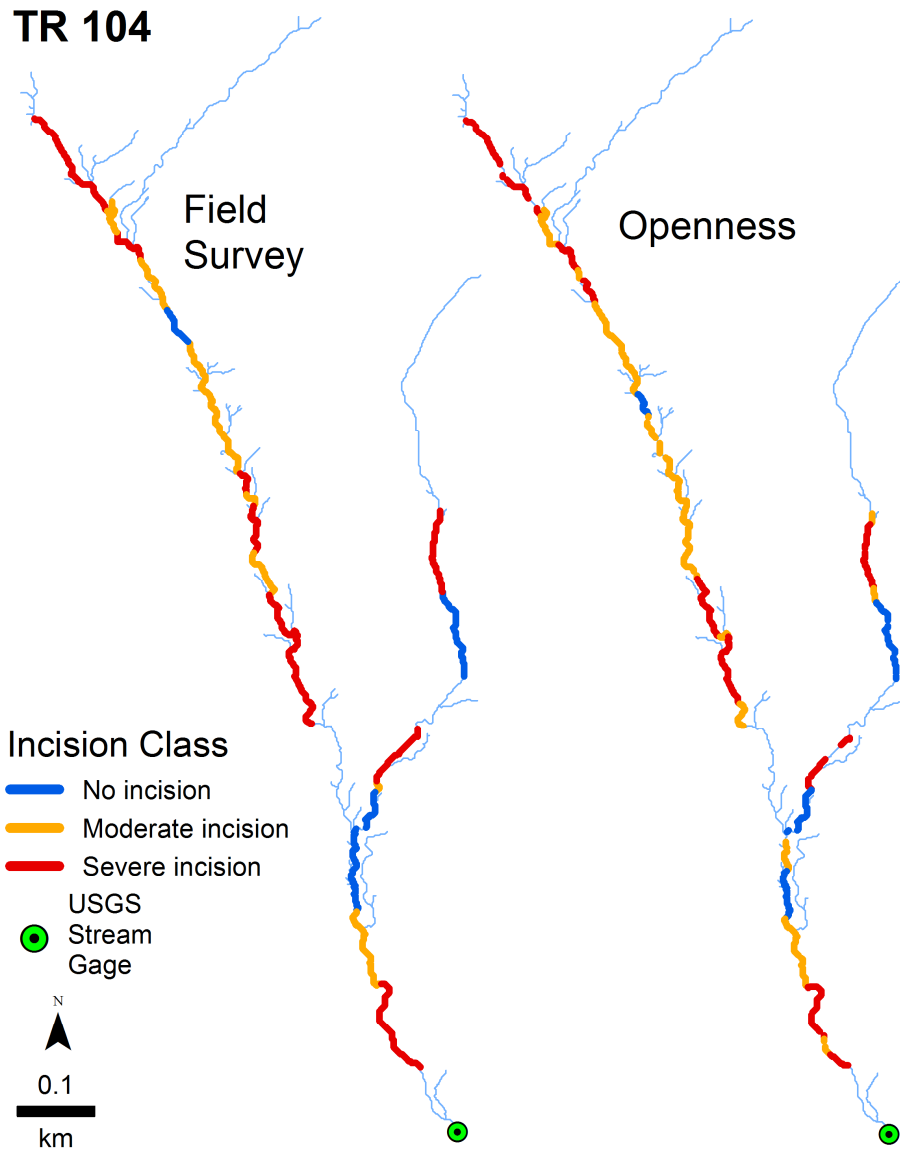


Figure 2.16: Results of the openness model, after smoothing, compared with the field survey for TR104.

2.3.3.b. TR109 results

Of the individual watersheds, TR109 had the highest kappa and accuracy. The high kappa in TR109 is likely driven by the high level of sensitivity for class 0 since the F-scores of class 1 and 2 are only average. This is due to a long non-incised reach that was very distinct both in the field and in the topographic openness layer. The reclassified phi pixels in Figure 2.19 show a continuous stretch of pixels greater than 84, which depicts an area flowing through a small, flat wetland.

Precision was similar across each incision group in TR109 but there were stronger differences in sensitivity and as a result the F-score. Incision group 0 had the highest sensitivity as there were only 10 FN pixels that were surveyed as 0 but classified as 1. This was due to a small reach about 8 pixels long surveyed as 0 but classified as 1 near the stream gage (Figure 2.17). Group 2 had the lowest sensitivity at 0.542: of the 107 pixels that were surveyed as 2, almost half (49) were classified as 1, mostly near the downstream end of the watershed (Figure 2.17). This high rate of misclassification is expected since group 1 and 2 contained the most overlapping IQRs in TR109. In addition, the entire distribution of phi values grouped into class 1 are similar to the distribution of class 2 and there are fewer outliers on the lower end of the distribution of group 2 than there are in TR104, which could be another reason for low sensitivity of group 2 in TR109, compared with the sensitivity of group 2 in TR104.

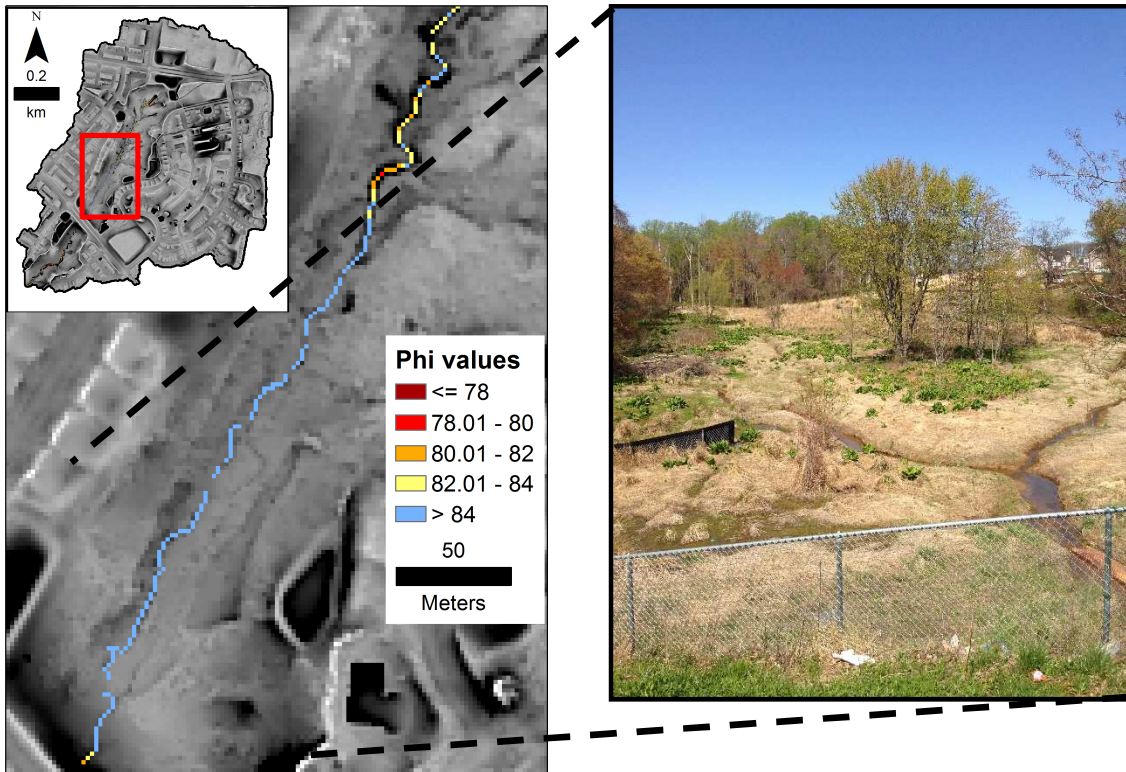


Figure 2.17: Example of long continuous reach with no incision in TR109, likely driving the success of the overall model. The openness pixels within the stream are reclassified to the scale shown in the legend. The long stretch of blue pixels represent a section of the stream flowing through a wetland so the area is relatively flat and easy to identify as not being incised in the openness model.

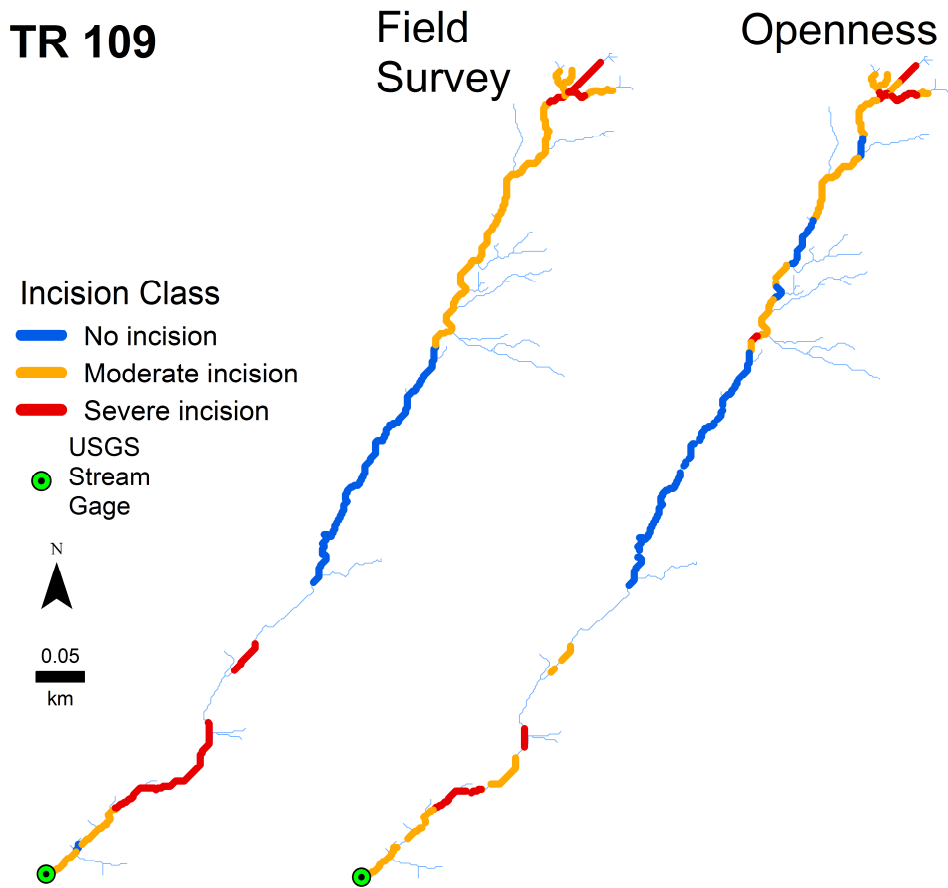


Figure 2.18: Results of the openness model, after smoothing, compared with the field survey for TR109.

2.3.3.c. SB results

The lowest scoring incision class in SB was group 1 for sensitivity, precision, and F-score. Precision in group 1 was less than 0.5 because there were more pixels incorrectly classified as 1 (FPs) than TPs. The majority of FPs were pixels that should have been classified as a 2 (142) but the number of FPs that should have been classified as 0 was also high (98) compared to the number of FPs in groups 1 and 2. FNs in group 1 were evenly distributed between class 2 and 0. Although the incised reaches were correctly classified in the upper portion of the watershed, the main stem

contained a significant portion that was surveyed 2 but classified as a mix between 0 and 1 (Figure 2.19). The cause of this is further explored in the discussion section.

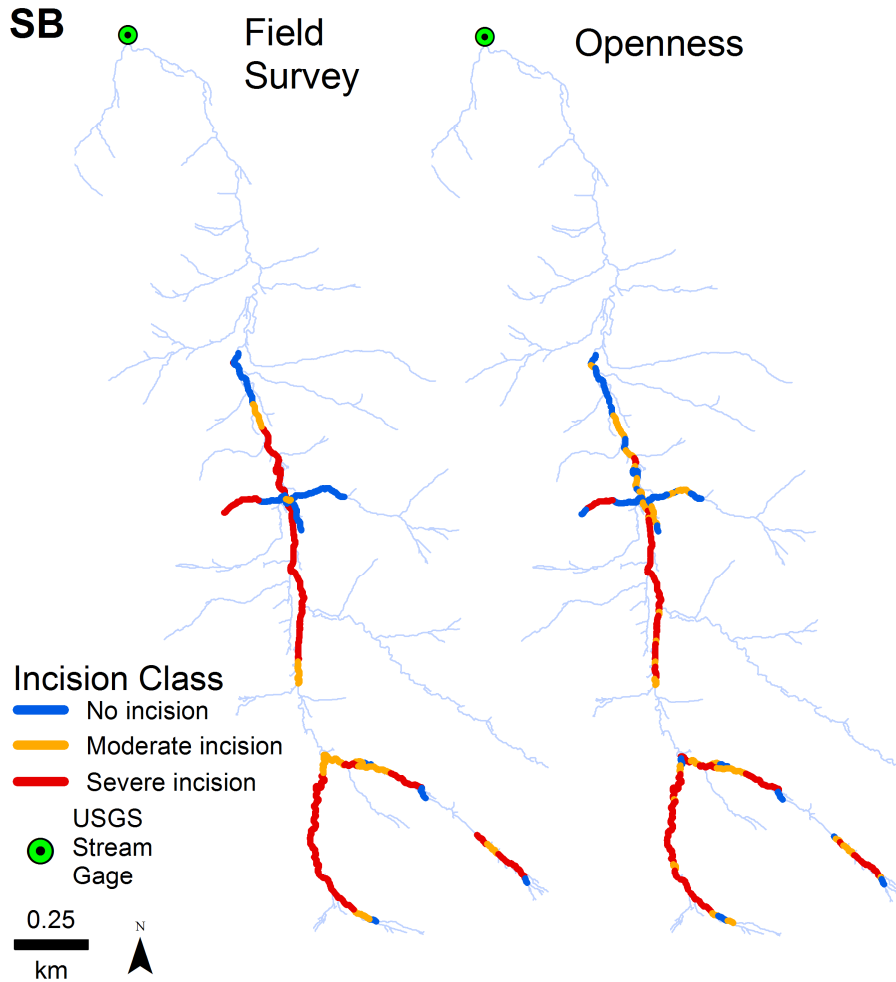


Figure 2.19: Results of the openness model, after smoothing, compared with the field survey for SB.

2.3.3.d. Combined results

Patterns in the combined results were most similar to patterns in the SB results, likely because a majority of pixels in the combined group came from SB, as this watershed had the largest sample size. Precision in group 1 was low, with a score

of 0.537. However, the only watershed that had a precision score greater than this was TR109.

Although each group performed slightly differently in each watershed, there was a general pattern of strong agreement in classes 0 and 2. In both TR104 and TR109, no field-surveyed classes of 0 or 2 were classified as 2 or 0, respectively, meaning the openness method does not mistake a non-incised channel as being severely incised, or vice versa. There were also low counts of non-incised pixels being classified as severe in the SB and combined models. Overall, the model best predicts areas with no incision or severe incision, likely because these classifications only have a one-sided threshold so they can include more outliers than class 1, which is constrained to pixels falling between 81 – 84 (Figure 2.12). Although group 1 tends to score lowest in each metric, these low scores are partly driven by the influence of group 2. There is consistency in each watershed for more pixels surveyed as 2 to be classified as 1, compared with pixels surveyed as 1 and classified as 2, indicating issues with group 1 and 2 in both openness classification method and field surveys. This is further discussed in section 2.4.1.C using an example from SB.

2.4. Discussion

2.4.1. Method errors

Of all the metrics in Table 2.3, the lowest score was precision for class 1 in SB. In group 1, there were 189 TP pixels, 114 FN pixels, and 240 FP pixels. The majority of FPs were pixels surveyed as 2 in the field but classified as 1 even though many surveyed sections of SB were severely incised and very easy to identify in the field. In the furthest upstream section of SB, the model and field results match well (Figure 2.18). The main channel on the downstream end of the field survey was also severely incised in most surveyed sections, but this is where the method failed at correctly identifying severe incision. Figure 2.20 displays this in more detail. The entire extent shown should have been classified as severely incised (Figure 2.20A) but only a small section was correctly classified (Figure 2.20A). This area contained the widest surveyed channel and although the banks were incised, there were depositional bars next to the channel reflecting the degradation and widening stage of the channel evolution model of incised channels described by Simon and Hupp (1986). The method developed here to classify channels into incision levels did not differentiate between these types of incised channels and the narrower and steeper channels more likely to be correctly classified by the openness method. In the more complex incised channel in SB, the openness values used to classify the channel were likely capturing the shallower bank features rather than the steeper banks beyond the depositional features along the lower bank. The location where the polyline version of the stream channel was delineated also poses additional problems since the phi pixels used for each incision classification were those that directly overlapped with the

polyline version of the stream channel network. There are in fact low phi values along SB near steep banks, but the channel pixels are not always overlapping with these phi pixels (Figure 2.20C) and in larger channels in general, the line delineating the channel would not be expected to overlap with pixels representing the banks. There are also more complex in-channel bars within the incised banks that may be influencing the phi values (Figure 2.20D). This highlights an issue with scaling methods developed in smaller channels to larger drainage areas without making any adjustments to the method. TR104 and TR109 have drainage areas around 1 km² and the area where SB is consistently misclassified occurs above a drainage area of 1.5 km². Before applying this method to larger watersheds, methods should be further refined across a broader range of channels with various channel complexities that may result in adjustments to the method or lidar data.

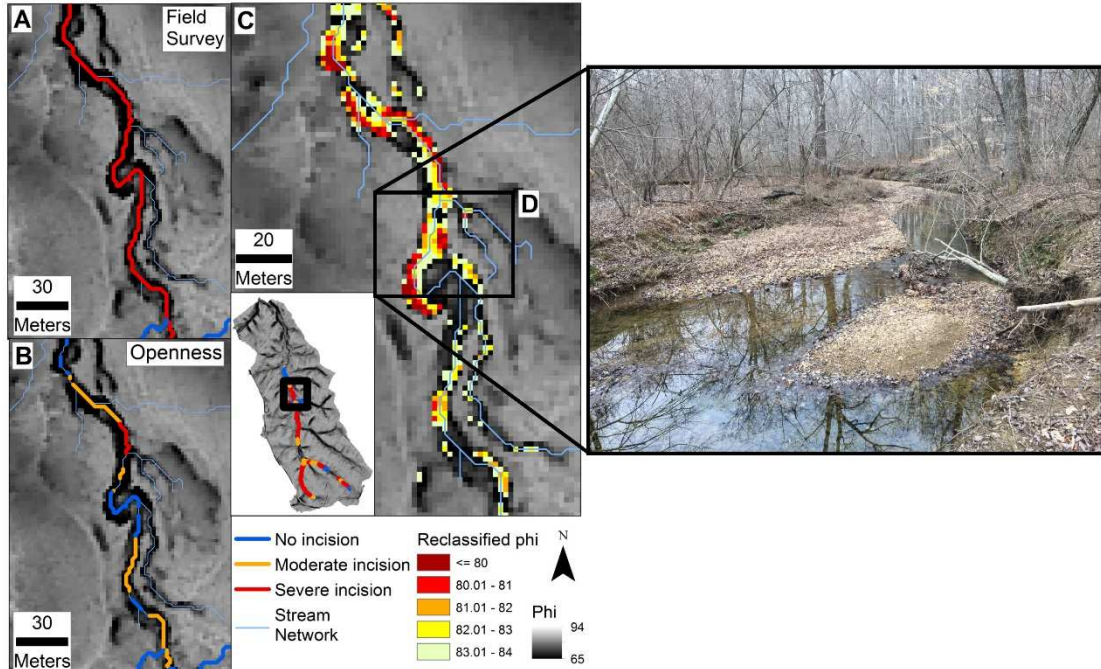


Figure 2.20: Large discrepancies between the field survey (A) and openness model (B) in main channel of SB. Reclassified openness pixels show some areas of the channel with a range of incision but the result of the openness model is based on where within the channel the network is delineated (C). High openness values within the incised channel are likely picking up bars within the channel (D). Here the channel is wider than much of the other survey locations, indicating adjustments may need to be made for higher order channels.

Although expanding field sites was outside the scope of this work, some initial refinements to the method were explored using existing data. The current method uses the polyline delineated for the stream to select the phi pixels used to classify incision. Although this was suitable for smaller channels that were not much wider than the resolution of the DEM where a single pixel represented the channel, the errors observed in the wider reaches in SB illustrate why this method doesn't work well in larger channels. Rather, all phi pixels within the channel need to be considered in the incision classification.

A landform classification tool, Geomorphon (Stepinski & Jasiewicz 2011, Jasiewicz & Stepinski 2013), was explored to isolate all phi pixels within the stream channel. Geomorphon is available within GRASS GIS (GRASS Development Team,

2017) and uses both negative and positive topographic openness (Figure 1.1) to classify and characterize landforms. A ternary code is created for each pixel based on the 8 features within the line-of-sight of the focal pixel being either equal to, above, or below the focal pixel. Ternary patterns are then used to classify pixels into one of 10 common terrain forms (Figure 2.21). Using GRASS Version 7.2.2, landforms were calculated using a 5 pixel (9 m) search radius, and terrain forms classified as valley or pits were used to mask phi pixels calculated from Peters (2015). Phi pixels within the Geomorphon mask were then reclassified into incision groups using the established thresholds (Figure 2.22).

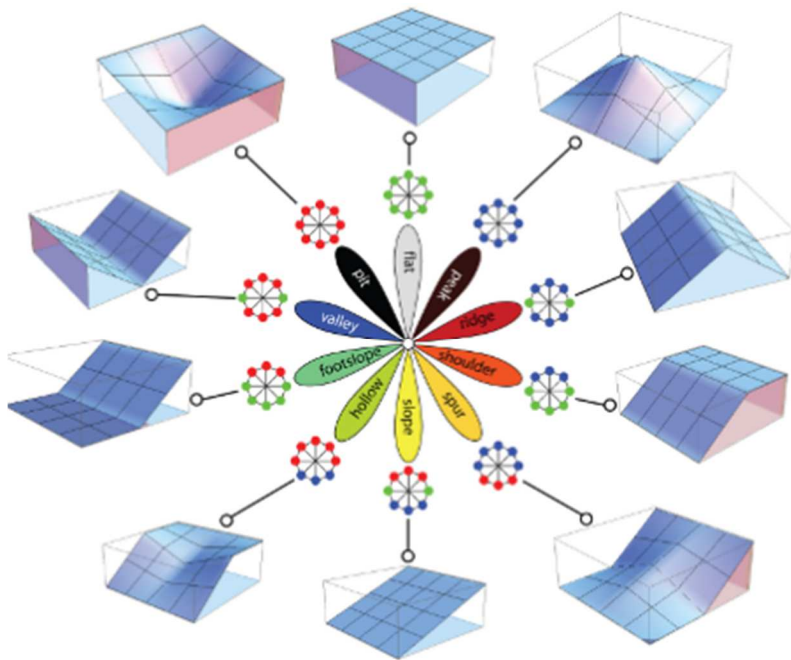


Figure 2.21: The 10 most common landforms classified with Geomorphon and an example of the typical form for each classification. Each of the 8 points surrounding the focal pixel in each form indicate if the point is above (red), below (blue), or equal (green). Adapted from Jasiewicz & Stepinski (2013).

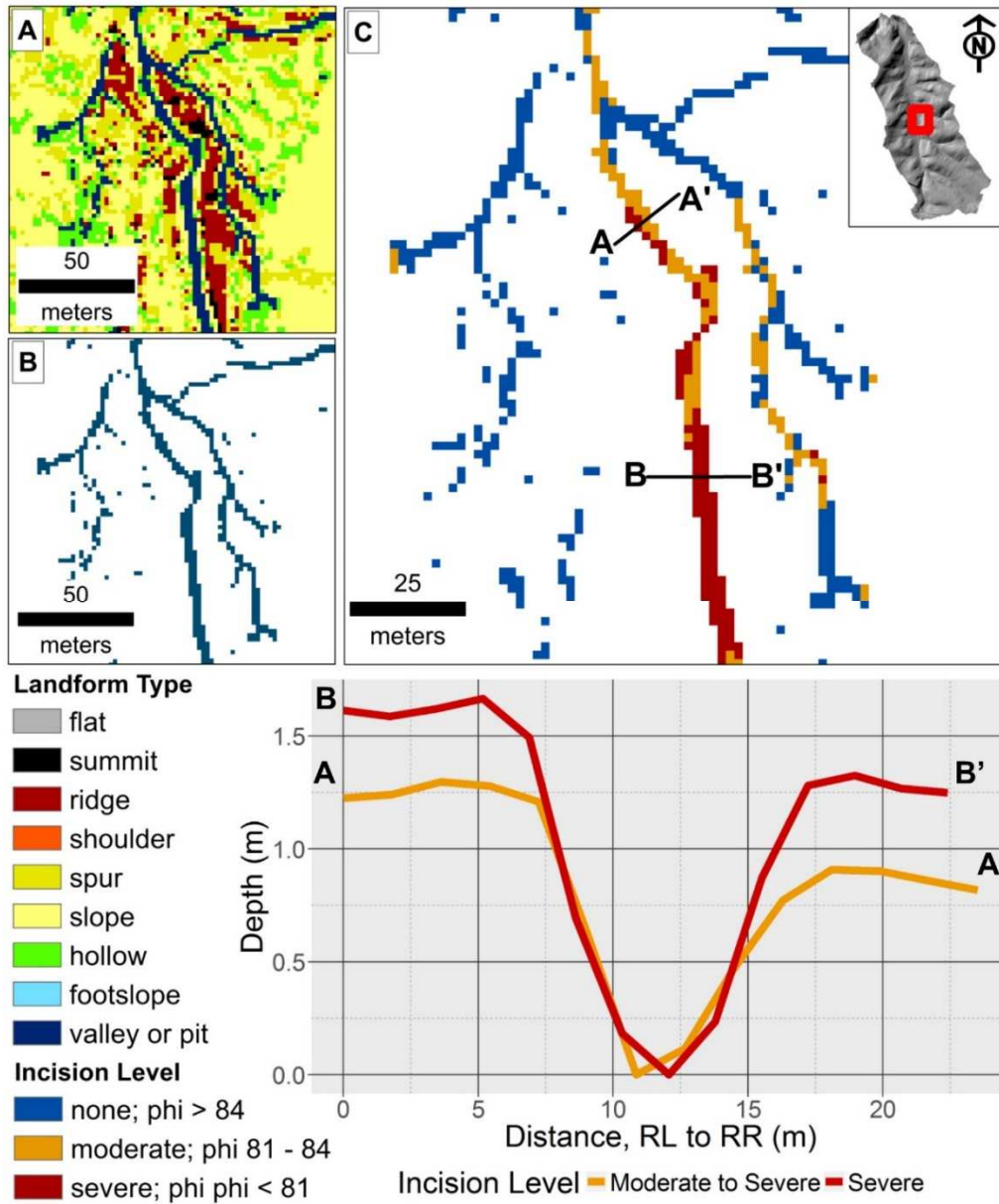
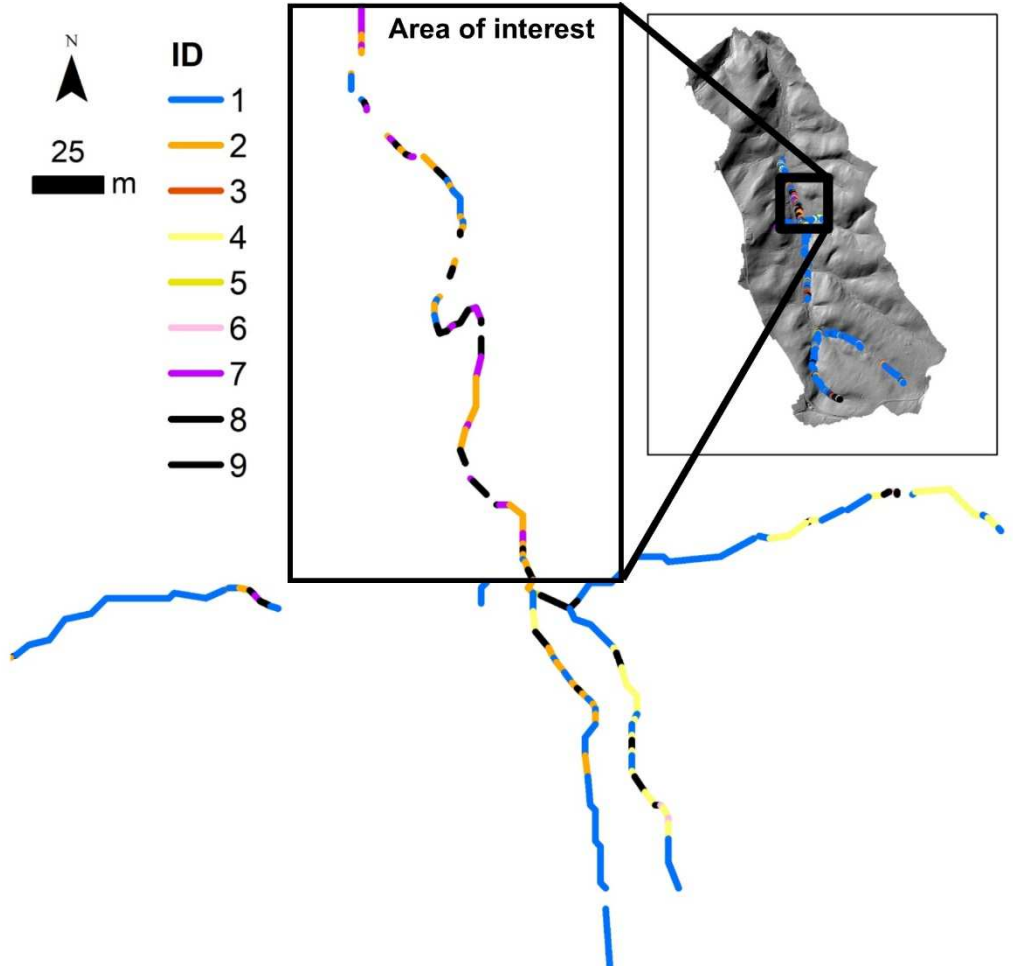


Figure 2.22: Geomorphon is a landform classification tool (A) and was used to isolate pixels classified as valley or pits, indicative of stream channels (B). The valley and pits were used as a mask to isolate and then reclassify openness into incision levels. This method better displays channel complexity in wider channels (C). Cross section A shows how the side of the channel with severe incision corresponds to a steeper bank than the other side showing only moderate incision. Cross section B shows a severely incised channel, which corresponds to the incision classification.

This refinement better highlights channel complexity in wider channels and has potential to better describe incision characteristics not fitting into the original three classes, such as channels that have incised and are now laterally eroding. In Figure 2.22C, the southern end of the main channel near transect B is severely incised and was correctly classified with the original method. The area near transect A is where the channel is misclassified as moderately incised but surveyed as severely incised. To summarize the variability within the channel, a focal range in a 3 x 3 pixel window was calculated to highlight areas of consistent vs. varying incision classes across the channel. The area near transect A in Figure 2.22C resulted in a range of 1 since the incision classes within the window included both moderate (1) and severe (2). The area near transect B resulted in a range of 0 since all pixels within the window were severely incised. The focal range output was combined with the reclassified openness values masked to the Geomorphon-derived channel (see Figure 2.22 C) and the field classified values to identify the ranges associated with areas where the field and openness classifications did not match. Results are shown in Figure 2.23 and highlight the same area of SB shown in Figure 2.20 where the channel has incised and then continued to widen. Areas like this were identified as severely incised in the field, so these types of channels would result in the combination of classes found in ID 2 (Figure 2.23), accounting for 8.9% of the total area surveyed in the field. Although this method helped identify a portion of this reach highlighted in Figure 2.20, there were still other sections where openness was showing no incision or there was a range of all three incision classes within the 3 x 3 window. This reach also contained areas where the range was 0 meaning there was

only one incision class within the 3 x 3 window and it did not match with the field surveyed class. These areas account for 7.6% of the total area surveyed in the field and tend to occur near the transition of different incision classes measured in the field or small patches along long reaches of a continuous incision class. These patches may be representing true shifts in channel characteristics where the transition area identified in the field was slightly off, or small changes in incision were not noted in the field if they were patchy and located within a long reach of a dominant incision type.

The remaining IDs account for areas where there were two different incision classes within the 3 x 3 window and the field surveyed class did not match with the overlapping reclassified phi pixel. These are potentially areas where there is not as clear of a distinction between severe/moderate and moderate/no incision. Although future work is necessary to identify the most effective method for summarizing and classifying reaches that do not fit into the original three classes, this presents a method for isolating the reaches that need further attention.



ID	Match	Range	Openness	Field	Count	% of Total
1	Yes	-	-	-	1038	69.2
2	No	1	Moderate	Severe	133	8.87
3	No	1	Severe	Moderate	57	3.8
4	No	1	Moderate	None	73	4.87
5	No	1	None	Moderate	15	1
6	No	1	Severe	None	12	0.8
7	No	1	None	Severe	33	2.2
8	No	0	-	-	114	7.6
9	No	2	-	-	25	1.67

Figure 2.23: Results from combining the focal range, reclassified openness, and field classification. The channel location is the same area shown in figure 2.20 where the channel has incised and then widened. The box highlights the area where the channel was misclassified and displayed complex incision and widening.

2.4.2. Spatial variation of channel incision across reaches

All three watersheds contain varying lengths of consistent incision with sometimes frequent transitions from one incision class to the next (Figures 2.12 – 2.14). The degree to which a channel will incise or aggrade is primarily driven by shifts in sediment supply (controlled by sediment load and particle size diameter) and transport capacity (controlled by slope of the bed and water discharge) (Lane 1955). Although the openness method cannot detect these variables, the ability for openness to detect shifts in incision levels can help explain various geomorphic processes occurring throughout the network at transitions between shifts in sediment supply and transport capacity. In some instances, shifts in the slope of the bed that were detectable from the lidar correspond to changes in incision level where severe incision occurs with steeper slopes and the severity of incision declines as slope also declines (Figure 2.24). In TR109, a shift from moderate incision to a long continuous reach of no incision corresponded to a broad, flat wetland (Figure 2.17).

A change in the slope of the bed along the shift in incision shown in Figure 2.22 was not detectable from the lidar. Although this type of reach was not as well characterized, the context of surrounding channel conditions can be used to infer channel characteristics in these types of reaches. The incorporation of Geomorphon to classify all pixels within the channel illustrates how the channel is deeply incised near transect B before the channel widens and aggradation occurs, represented by a wider channel width a lower bank height at transect A. Sinuosity also increases downstream from this transition point (Figure 2.20). This point indicates a transition in the dominant geomorphic processes occurring in the channel that causes a shift from

vertical to lateral erosion based on both stream power and longitudinal profile form (Jain et al. 2008). Below this transition, depositional sand and gravel bars were observed in the field (Figure 2.20). The growth of these bars can divert the channel to disproportionately erode one side of the bank, leading to bank failure and channel widening. This process begins at the boundary between a confined valley upstream and a partially confined valley downstream where the confined bank erodes and discontinuous floodplains begin to form on the depositional side (Jain et al. 2008). Moving downstream, erosion and deposition alternate from one side of the channel to the other as the channel meanders. There may also be a bedrock control preventing the channel from downcutting further, as observed in other Piedmont streams (Colosimo & Wilcock 2007, Lyons et al. 2015). Just downstream from transect A are two tributaries entering the main channel and the contribution of sediment from these tributaries may also lead to additional aggradation from the increased sediment supply. The transition between a partially confined and laterally unconfined valley was less distinct, but evidence of an unconfined valley was also observed near the confluence with a larger river. Figure 2.25 shows how topographic openness and Geomorphon can be used to identify all three valley settings described by Jain et al. (2008) within SB.

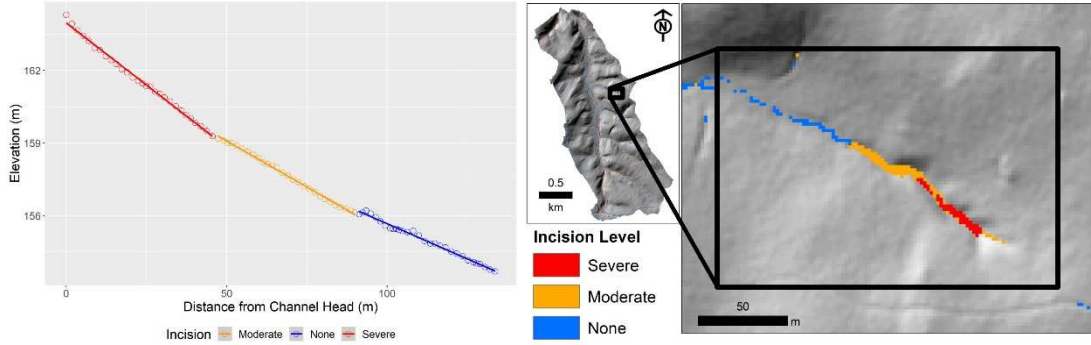


Figure 2.24: Longitudinal profile of a reach within Soper Branch that begins as an incised channel near the head, where the slope is steeper, and gradually transitions to moderately incised, and finally not incised, with slope of the bed becoming more gradual as incision severity declines. Sediment eroded in the steeper reach could also be deposited in the shallower slopes and further contribute to the development of the longitudinal profile and shifts in slope corresponding to shifts in incision level.

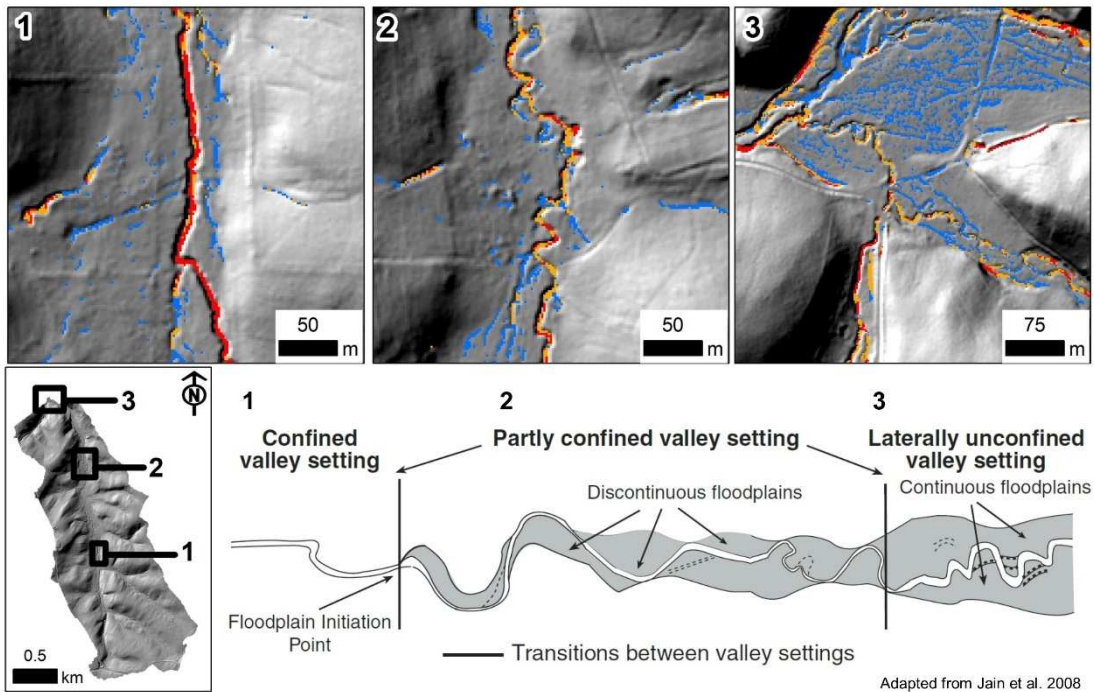


Figure 2.25: Examples of various channel forms in SB extracted from Geomorphon and topographic openness, with the corresponding channel form described by Jain et al. (2008). Example 1 shows the channel in a confined valley setting, characterized by a relatively straight channel with steep banks. Example 2 shows a partially confined valley with evidence of meandering. The red pixels indicate some severe incision or steep slopes along cut banks but the orange pixels indicate more gradual banks throughout most of the channel as a result of channel widening and point bar development that creates discontinuous floodplains. Example 3 shows the lower portion of SB near the confluence with a larger channel within an unconfined valley. The blue pixels indicate small side channels suggesting there is a broad, continuous floodplain.

2.4.3. Influence of DEM source, processing, and resolution

The influence of DEM resolution and processing steps on the results were also explored to further diagnose issues with the method. Although field data was used to calibrate the method, it only requires the input of a DEM. This requires a set of assumptions including adequate lidar accuracy within the channel (Jarnagin 2010), optimal DEM resolution (Thomas et al. 2017) and DEM conditioning. The results show that there are more severely incised pixels being incorrectly classified as 0 or 1 than there are non-incised pixels being incorrectly classified as 1 or 2. A potential reason is that the lidar is more likely to have false flat areas than false depressions due to interpolation errors near gaps in point coverage (Figure 2.6). An effort was made to remove these types of errors using density of bare earth lidar points to remove areas with large gaps from the analysis. However, potential errors associated with incorrect las point classification by the vendor or dense vegetation mistaken for ground may be more subtle and difficult to identify.

To test the influence of DEM resolution on the wider channels found in SB, the original 0.9 m DEM that had been resampled to 1.8 m for the original analysis was instead resampled to 3.7 m, (12 ft). All methods applied to the 1.8 m DEM were replicated for the 3.7 m DEM. The results, summarized in Table 2.4, indicated that DEM resolution had little influence on the accuracy and kappa statistic of the openness method.

DEM Resolution	SB	
	% Accuracy	Kappa
1.8 m (6 ft)	73	0.556
3.7 m (12 ft)	73.6	0.566

Table 2.5: Results of incision model using a coarser DEM. Results did not change significantly between the two resolutions.

To test the sensitivity of the openness method to a DEM with different pre-processing steps, the 1.8 m DEM was processed through a tool intended to remove errors from lidar-derived DEMs. The De-Noise DEM tool within Whitebox GAT 3.4 removes small-scale variation in fine resolution DEMs and smooths DEMs without affecting features important for modelling surface drainage (Lindsay, 2016). After the 1.8 m DEM was processed through this tool, the same methods applied to the 1.8 m DEM were applied to this DEM, and results from the openness method and field results were compared. The smoothed DEM resulted in only a slight improvement of overall accuracy. These tests verify that further refinement of the method will require focusing on how to classify geomorphic characteristics not described in the original decision tree used to classify reaches in the field (Figure 2.11).

Pre-Processing Step	SB		TR104	
	% Accuracy	Kappa	% Accuracy	Kappa
Original	73	0.556	70.7	0.539
Whitebox DeNoise	73.4	0.559	70.3	0.51

Table 2.6: Results of applying the Whitebox GAT De-Noise tool to the input DEM to test the sensitivity of the analysis to varying DEM pre-processing steps, compared with the original results.

2.4.4. Applications and Future work

This method was applied to three small headwater streams within one physiographic province in Maryland. The thresholds selected for each category of incision were based on field surveys and SfM-derived DEMs of stream channels at a resolution of 0.1 m. The method was implemented on 1.8 m lidar-derived DEMs. Future work is needed to determine if and how this method can be adjusted to accurately model channel incision in other physiographic provinces and in higher

order streams, especially with the incorporation of Geomorphon to summarize complex channels. Although the results of SB did not change when using a 1.8 m DEM compared with a 3.7 m DEM, different resolutions should still be tested in watersheds larger than those in this study. Expanding field surveys to higher order channels may help determine optimal DEM resolutions for wider channels. The influence of resolution and DEM pre-processing methods may also change with higher quality lidar and should be considered in future projects.

The actual thresholds defining the levels of incision may also need to be adjusted for different physiographic provinces with differing relief and topographic complexity. Once tested in a diverse set of watersheds, this method will be more reliable for large scale modelling, such as the scale of the entire Chesapeake Bay watershed.

Other models that require field data input may improve accuracy, but a tradeoff is that this model can be applied in areas where field data is not available, or as an exploratory tool to further assess areas of concern and optimize use of limited resources. This model can also be used to characterize channel geometry in DEMs that were collected at a time when field data was not collected. In chapter 3, this model is explored to quantify channel incision in urbanizing watersheds using repeat lidar. The goal of chapter 3 is to use information on the extent and degree of incision over time to help infer links between urban development and channel change.

2.5. Conclusions

A novel GIS-based model was introduced that used aerial lidar-derived DEMs to remotely detect stream channel incision in small headwater streams using

topographic openness. A variety of field-based surveys were applied to calibrate this model, including SfM surveys using a handheld digital camera to develop detailed streambank models.

The model was statistically compared with field data for accuracy and revealed moderate agreement with 70.7 – 75.1% of pixels accurately classified as no incision, moderate incision, or severe incision. Results indicate this method needs further refinement before being applicable across watersheds of differing scale and regions. In its current form, it is able to detect non-incised channels and those with severe incision on both sides in small headwater streams with drainage areas around 1 km².

This is a straightforward method for rapidly characterizing channel characteristics with potential to inform a broad range of watershed management decisions. Knowledge of field conditions can be combined with the incision results to better understand where shifts in geomorphic processes are occurring within the watershed. This information can be crucial for modelling sediment dynamics and developing stream monitoring or restoration plans.

This model was tested in limited watersheds with QL3 lidar. Further work will need to assess the applicability of this method on higher quality DEMs of finer or coarser resolution, in higher order channels, and in channels within different physiographic provinces. Additional criteria will need to be developed to better classify incised channels with more complex erosional features that result from mass wasting and channel widening as incised channels shift from vertical to lateral erosion.

Chapter 3: Measuring changes in channel incision over time

3.1 Background

3.1.1. Geomorphic change

The effects of urbanization on local waterways are well documented. During the construction phase of urbanization, exposed bare earth becomes mobilized and sediment is delivered to surrounding streams at a higher rate (Wolman 1967). Once construction is complete, dense storm drain networks intended to quickly evacuate stormwater from impervious surfaces cause more rapid delivery rates of runoff directly to streams (Leopold 1968, Arnold & Gibbons 1996, Paul & Meyer 2001, Walsh et al. 2005). A combination of erosive flows and decreased sediment supply in a paved landscape leads to channel incision and channel instability (Hammer 1972, Booth 1990, Henshaw & Booth 2000, Colosimo & Wilcock 2007, Miller & Kochel 2010).

Over time, a stream that has experienced a disturbance could eventually reach a new state of equilibrium as stream morphology adjusts to the new flow regime and sediment load (Mackin 1948, Wolman 1967, Knox 1976). However, this post urbanization equilibrium has not been commonly observed. Some streams may reach a new equilibrium, but they might also stay in disequilibrium, depending on the type and extent of urbanization (Wolman 1967, Leopold 1973, Hammer 1972, Colosimo & Wilcock 2007). Henshaw & Booth (2000) studied natural channel re-stabilization in urbanized watersheds and found no universal pattern of channel stability relating to the magnitude or rate of urbanization. Rather, re-stabilization patterns are controlled

by the way in which channels respond to altered sediment loads and flow regimes, based on specific channel-scale and watershed-scale factors (Henshaw & Booth 2000). Difficulty in relating stream stability to urbanization can also stem from the different types of stream adjustments that can occur within the same urbanizing watershed (Wolman 1967, Colosimo & Wilcock 2007) and the variability in the time-frame required for channel re-stabilization (Henshaw & Booth 2000). To better understand stream responses following urbanization, monitoring needs to capture geomorphic characteristics before, during, and following completion of urban development. Monitoring should also cover the entire watershed to understand how upland processes might be related to downstream responses.

3.1.2. Infiltration-focused SWM

To mitigate symptoms of the urban stream syndrome, low impact and green infrastructure practices have been developed in an attempt to restore or preserve pre-development hydrologic conditions by reducing erosive stormflows, protecting water quality, and providing wildlife habitat (Tillinghast et al. 2012, Bhaskar et al. 2016). Compared with conventional SWM that collects stormwater into a centralized location before delivering the collected runoff directly to streams, distributed IF-SWM attempts to infiltrate stormwater runoff closer to the source to mimic a pre-development hydrologic system (Loperfido et al. 2014). This allows for more natural physical, chemical, and biological management of stormwater (Lehner et al. 2001). Another practice of low impact and green infrastructure development can include land conservation, such as preserving forested riparian buffers along streams because they can act as a natural filter of sediment, nutrients, and pollutants, add roughness to

a channel, and protect habitat (Groffman et al. 2003, Pusey & Arthington 2003).

Although these practices are intended to preserve pre-development stream conditions, empirical studies have revealed that they are not always effective in achieving this goal (Tillinghast et al. 2012, Hogan et al. 2014, Loperfido et al. 2014, Vietz et al. 2015, Bhaskar et al. 2016, Hopkins et al. 2017, Li et al. 2017, Jefferson et al. 2017). While the development project in Clarksburg, MD followed proper soil and erosion control BMPs throughout the construction process, Hogan et al. (2014) still observed a pattern of aggradation due to mobilized sediment during construction, followed by degradation as a result of increased runoff, consistent with observations by Wolman (1967).

Another observed result of distributed infiltration-focused SWM is increased baseflow (Loperfido et al. 2014, Bhaskar et al. 2016). Baseflow can also increase as a result of leaking water supply pipes and lawn irrigation (Lerner 2002, Bhaskar et al. 2015). This contrasts with past observations for baseflow to decrease in urbanized streams because impervious surfaces cause reduction of groundwater recharge (Leopold 1968). This suggests that the excess stormwater infiltrated by these SWM facilities is still eventually discharged into the channel as baseflow, likely because vegetation removal reduces the amount of groundwater lost to evapotranspiration (Bhaskar et al. 2016).

3.1.3. Seepage erosion

Even if IF-SWM succeeds at controlling erosive stormflows, erosion from groundwater influx can still occur through bank failure from groundwater seepage (Fox et al. 2007, Wilson et al. 2007, Chu-Agor et al. 2008, Fox & Wilson 2010).

However, seepage erosion is a complex process and can be difficult to differentiate from other fluvial processes leading to streambank erosion (Midgley et al. 2011). It is not clear whether increased baseflow from IF-SWM facilities could contribute to seepage erosion and bank failure. What is clear is that in any watershed that has been substantially altered, there are complex hydrologic responses and advanced SWM is still not mimicking the natural hydrologic conditions. While some studies have observed hydrologic changes associated with various green infrastructure SWM, there is no apparent answer yet on how or if flow-regime management protects or restores channel morphology (Vietz et al. 2015).

Even though evidence of erosion from groundwater seeps is visible, not all active seeps can be detected from simple observation. Thermal infrared (TIR) imagery can be used to detect heat differences between surface water and groundwater seeping into a stream (Deitchman & Loheide, 2009) and identify active groundwater seeps. This information can be compared with locations of infiltration-focused SWM and changes in bank erosion and channel incision to understand relationships between groundwater seepage erosion and landscape changes associated with urban development and infiltration of stormwater.

3.2. Methods

The extent of temporal coverage of lidar in SB, TR104, and TR109 provided an opportunity to document geomorphic change occurring in headwater streams experiencing urban development with IF-SWM. The openness method described in chapter 2 to detect channel incision was applied to lidar collected over the study area prior to 2013 to measure the level of incision before and during urban development,

in an attempt to identify where the most change occurred along the stream network in each watershed. Indications of seepage erosion were also identified to better understand the connection between groundwater seeps, bank characteristics, and the proximity of IF-SWM.

3.2.1. Lidar data processing

Airborne lidar was collected over the study area during leaf-off season in 2002, 2004, 2006, 2007, and 2008, in addition to the 2013 lidar previously described in chapter 2. The instruments, vendors, and reported accuracy were not consistent across years and the details are documented in Table 3.1. The 2013 lidar was available as a las dataset but all prior years were available as ASCII XYZ files. Although the format differed from the 2013 lidar available as las points, the same processing steps used for the 2013 lidar were followed for the lidar from 2002 – 2008. Bare earth points were interpolated into 0.9 m (3 ft) DEMs and then smoothed to 1.8 m (6 ft) using the aggregate tool in ArcGIS 10.3 (ESRI, Redlands, CA). DEMs were hydrologically conditioned manually to create continuous downslope elevation along the stream network in areas where raw lidar does not automatically detect underground features that route water through SWM outlets and culverts.

Year	Month	Vendor	Instrument	Mean lidar raw		Horizontal accuracy	Max vertical distance	Max horizontal distance
				point spacing	Vertical accuracy			
2002	December	Airborne 1	Optech ALTM-2025	sub 0.8 m	0.07 m avg. vertical distance	0.04 m avg. horizontal distance	0.12 m	0.07 m
2004	March	Lazer Mapping Specialists Inc.	Optech ALTM-2033	sub 0.8 m	0.05 m RMSE	< 0.03 m avg. horizontal distance	0.08 m	not reported
2006	March	Canaan Valley Institute (CVI)	Optech ALTM-3100	sub 0.1 m	0.04 m RMSE	0.13 m avg. horizontal distance	0.08 m	not reported
2007	March	Canaan Valley Institute (CVI)	Optech ALTM-3100	sub 0.15 m	0.03 m RMSE	0.05 m avg. horizontal distance	not reported	not reported
2008	March	Sanborn	Leica ALS-50	1.4 m	0.15 m RMSE	1.00 m RMSE	not reported	not reported
2013	December	Kucera Internatinoal Inc.	Leica ALS-60	1.1 m	0.12 m RMSE	0.25 m RMSE	not reported	not reported

Table 3.1: Information on instruments and accuracy for each year of lidar data, reported by the vendor.

A stream network for each year was delineated using field surveyed channel head locations to initiate channel delineations (Metes et al. *in preparation*). Although some of the channel heads surveyed in 2014 may not have been at the same location during the year of each lidar flight, this provided for a consistent way to compare a similar stream network for each year. Lidar-derived stream channels do not always overlap from year to year because of possible lidar errors and channel migration (Jarnagin 2010). Flatter wetland areas may contain anastomosing channels that are not well delineated from elevation data using the common flow accumulation method that delineates a single continuous network. In areas where channels did not overlap, aerial imagery was used to confirm that channels with high variance of migration were not natural or did not follow the dominant channel (Figure 3.1). To account for some variation in channel form throughout the 11-year period, a 2.7 m (9 ft) buffer was created around the stream network for each year. This was equivalent to 1 extra pixel as a buffer on either side of the raster version of the channel. When assessing year to year change, only the areas where 2.7 m buffers overlapped were considered.

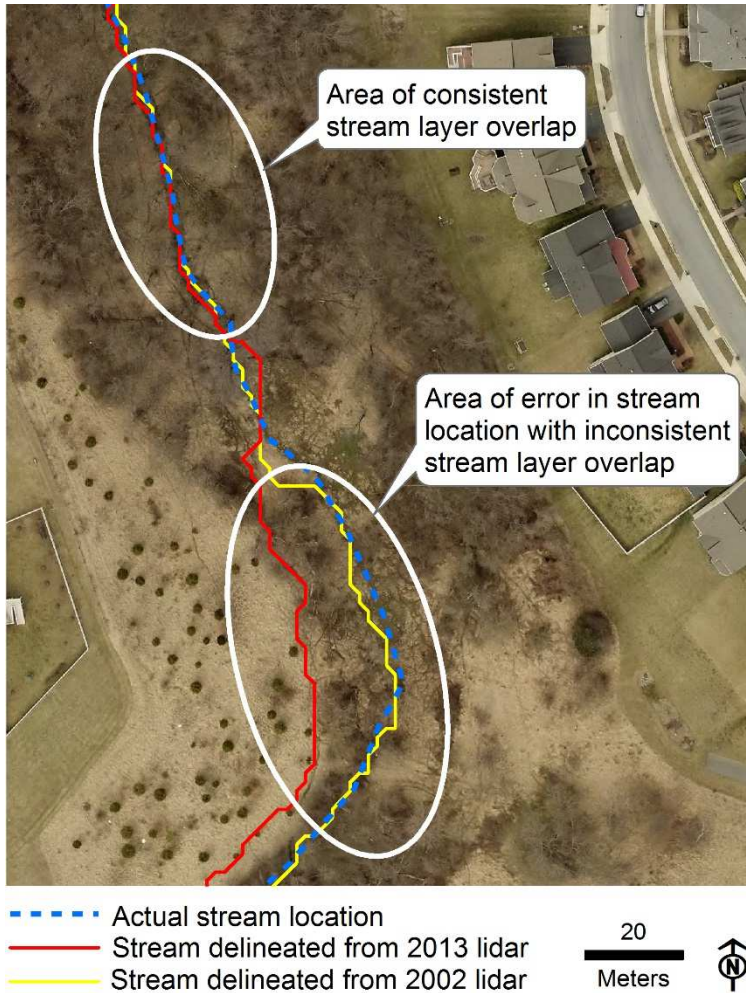


Figure 3.1: Example of the stream network deviating from the dominant channel location in 2013. (Aerial imagery is from 2012.) This was in a non-incised wetland section that quickly transitions to severe incision. Although the 2013 stream network appears to follow a less dominant channel in the wetland, the network does not overlap with the severely incised section until about 100 m downstream. The 2013 stream layer deviates outside the main channel and was removed from the analysis. Further upstream, the 2002 and 2013 stream layers accurately match the actual stream location.

3.2.2. *Classifying channel incision from 2002 to 2013*

Positive topographic openness grids (hereafter referred to as phi) were calculated from the raw, unconditioned 1.8 m DEMs for 2002, 2004, 2006, 2007, and 2008 using the same 36.6 m (120 ft) search radius that was used to calculate the 2013 phi grid for each watershed. Openness values that overlapped with the delineated

stream networks for each year were reclassified into 0 if values were less than 81, 1 if values were between 81 and 84, and 2 if values were greater than 84. A no data mask was applied to the reclassified openness grid following similar methods described in section 2.2.3.a. This method had to be adjusted for lidar from 2002 – 2008 because the las point statistics tool was unavailable for the ASCII datasets. Therefore, the pixels containing no bare earth points were identified using the focal median and applied as a no data mask. The final reclassified phi values along the delineated stream networks were then smoothed based on methods and values described in sections 2.2.3.b. and 2.3.3. In SB and TR109, any contiguous pixels of the same incision class less than 4 pixels long were smoothed and in TR104 any pixels less than 5 were smoothed over.

After areas of the stream network falling outside the 2.7 m (9 ft) buffered overlapping stream layers for each year were removed, the percent of the remaining stream network within each level of incision was calculated for each year to assess any trends of change over time. The length of channel containing no incision, moderate incision, and severe incision was calculated as a percentage of the total stream length. Areas with consistent incision classifications over time were also identified.

3.2.3. Comparing raw changes in phi

Comparing shifts in the raw values of phi can also indicate if areas are incising, especially if they are already incised in 2002 and continue to erode. Raw changes in phi values also indicate the relative magnitude of incision. Results from

SB in chapter 2 illustrated how single values of incision within a complex channel may not capture true channel form. To avoid additional errors associated with summarizing multiple pixels to a single line, all phi values within the channel were assessed for pixel by pixel change. Rather than use the buffered stream networks described above to capture phi values within the channel, Geomorphon (Stepinski & Jasiewicz 2011, Jasiewicz & Stepinski 2013) was used to identify pixels most indicative of a stream channel. Geomorphon was calculated on the raw, 1.8 m DEM derived from lidar for every year lidar was available using a 5 pixel (9.1 m) search radius using GRASS 7.2.2 and pixels classified as valley and pit were isolated. Finally, only valley and pit forms within a 4.6 m (15 ft) buffer around the true stream network layer were considered. This resulted in grids identifying likely stream pixels for each year lidar was available and in each of the three study watersheds. These grids were used to isolate and assess only phi values falling within a likely stream channel.

For each temporal comparison, the two valley/pit grids for the years being compared were combined so all phi values within those two masks were compared. This allowed for comparison to detect drastic change such as implementation of SWM outlets where a valley/pit may not form until after an outfall is built. To remove areas with possible interpolation errors that might be classified as change, the no data masks described in section 3.2.1 were applied to the valley/pit layer for each respective year. T1 was then subtracted from T2. Any resulting negative value meant the phi value decreased from T1 to T2 and an area became more enclosed,

representative of channel incision. Any resulting positive value meant the phi value was becoming more open and may represent either aggradation or channel widening.

To first assess the spatial pattern of change, the 2002 (T1) phi values were subtracted from 2013 (T2) for any pixel classified as valley/pit in either year. To confirm both change and stability resulting from the difference in phi over time, cross sections were extracted across the channel using the lidar for all available years. Aerial imagery from 2012 was used to verify cross sections were extracted perpendicular to the channel. Channel changes were also verified using information from the field surveyed cross sections collected by Montgomery County (Appendix A.) The GPS locations for the cross sections were not accurate enough to compare directly with the lidar, so the information from the field cross sections was used to verify whether the phi differences followed the same general pattern of measured geomorphic change within the area.

To compare overall change across the entire watershed throughout the course of development, each time increment (i.e. 2002 (T1) and 2004 (T2), 2004 (T1) and 2006 (T2), etc.) was also compared based on phi differences for any pixel classified as valley or pit in the two time periods in question. The degree of channel change was compared across watersheds by comparing the distribution of differenced phi values.

3.2.4. Groundwater seep survey

The banks were surveyed in the field to locate areas of potential concentrated groundwater flux by locating active and potentially inactive groundwater seep locations. Active seeps were identified by active, concentrated flow discharging from

the banks, often within cavities or small holes that form in the banks (Wilson et al. 2007). Inactive seeps were identified if they resembled features indicative of concentrated groundwater influx along stream banks such as cavities, pipes, and oxidized groundwater containing iron (Figure 3.3). The location of each seep was surveyed using a Trimble Juno 5 series with 2 – 4 m accuracy, a photo was collected, and notes were taken to describe the feature. This coincided with the incision survey described in section 2.2.1.

The pattern of geomorphic change and stability detected from the changes in phi over time was then compared to the spatial distributions of groundwater seeps.

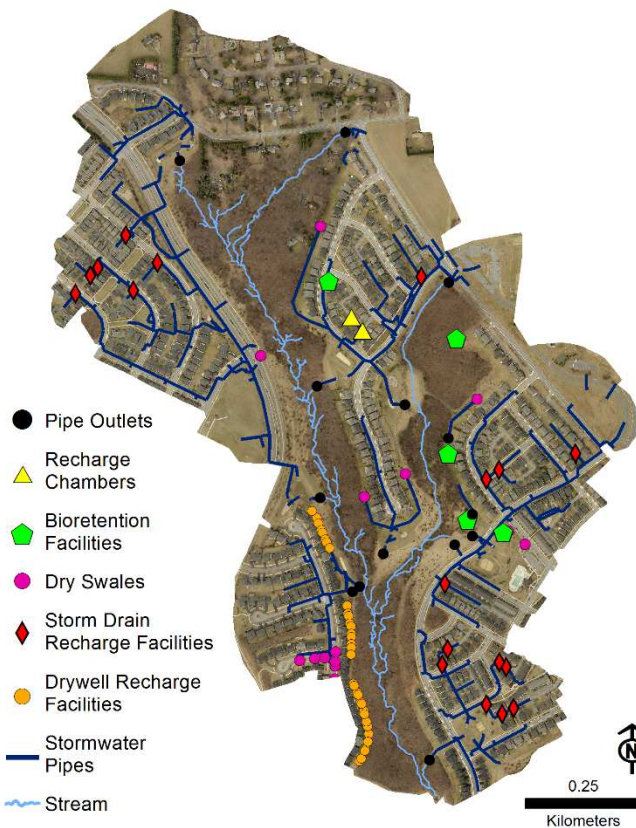


Figure 3.2: Locations of IF-SWM facilities in TR104. The drywell recharge facilities on the lower west side of the watershed show an area where seeps would be expected to occur more frequently on the west side of the stream bank if these facilities are enhancing groundwater discharge.



Figure 3.3. Indications of groundwater seeps in stream banks. The picture on the left shows iron in groundwater reacting with oxygen to form the rust color when seeping out. The picture in the middle shows water actively seeping from the bank. The picture on right does not have any indication of groundwater seepage other than the features formed in the bank.

3.2.5. Thermal Infrared Camera Survey

Once locations with evidence of groundwater seeps were identified, a subset of locations were selected to resurvey and more thoroughly describe active groundwater discharge to the stream. A FLIR i7 handheld TIR camera was used to identify active groundwater seeps by detecting thermal differences between surface water and groundwater. This method cannot quantify the change in discharge from groundwater flux, but it can detect and characterize active groundwater seepage by differentiating between diffuse and focused groundwater discharge (Deitchman & Loheide, 2009) and left versus right bank seepage. Images were collected in December 2016 when groundwater was warmer than surface water. GPS points were also collected at sites of active groundwater seeps to map the spatial distribution of groundwater influx. A YSI multi-parameter sonde was used to collect temperature and conductivity at the site of and just upstream from each groundwater seep to better characterize seeps.

3.3. Results

3.3.1. Change in incision class over time

The year 2002 contained the highest percentage of channels classified as not incised in all three watersheds, and the percentage dropped by about 20% in all three watersheds from 2002 to 2004 (Figure 3.4). There was no consistent pattern to changes in incision class over time but the direction of change was similar in all three watersheds, with TR104 exhibiting the highest magnitude of change from 2004 to 2008 with an overall increase in moderate incision (Figure 3.4). This may be a result of regional weather patterns affecting streamflow in all three watersheds and regional geomorphic adjustments from previous land use, combined with disturbance from urban development in TR104, which has been urbanized for longer than TR109. The similarity in patterns across time may also reflect systematic errors in the lidar datasets from year to year. Gardina (2008) analyzed the same 2002 and 2006 lidar datasets used in this study for errors and found lidar system errors accounted for 70% of the total error in the 2006 lidar. In this study, the percentage of non-incised reaches dropped by about 20% in all three watersheds between 2002 and 2004 despite land use change occurring only in TR104, while land use in SB and TR109 remained stable, and could be a reflection of systematic errors described by Gardina (2008).

The spatial pattern of incision levels across each watershed also revealed interesting patterns of consistency (Figure 3.5). When considering a pixel to be consistent if at least five of the six years contained the same incision classification, 72% of SB, 65% of TR104, and 81% of TR109 remained the same. Many areas that were classified as severely incised in 2013 have been classified as incised for all dates

since at least 2002 (Appendix B). This is consistent with the field-surveyed cross sections documenting change at discrete locations since 2003 (Appendix A). All three watersheds have an agricultural land use history, so this result may reveal the influence of past land use. Additionally, many first order channels in TR104 and TR109 resisted incision throughout the course of urban development. However, the only areas included in this part of the analysis were locations where all stream layers overlapped in every year. This resulted in gaps in the analysis, such as in newly developed channels at the outlet of SWM facilities. At these locations incision would be typical, but was not identified in all stream delineations (Figure 3.6). If a stream network in any of the years deviated from the channel as shown in Figure 3.1, the entire reach was removed from the analysis. These removed sections were still included when directly comparing the change in phi values within all valley/pit pixels, unless within the no data mask. In areas without consistent incision classes, no clear trend of increasing or decreasing incision over time was evident. Areas that did display this trend were only isolated pixels that were not likely representing true channel trends over time. However, the raw changes in phi values provided a more detailed analysis of incising areas and it was not necessary to remove as much of the network to conduct the analysis.

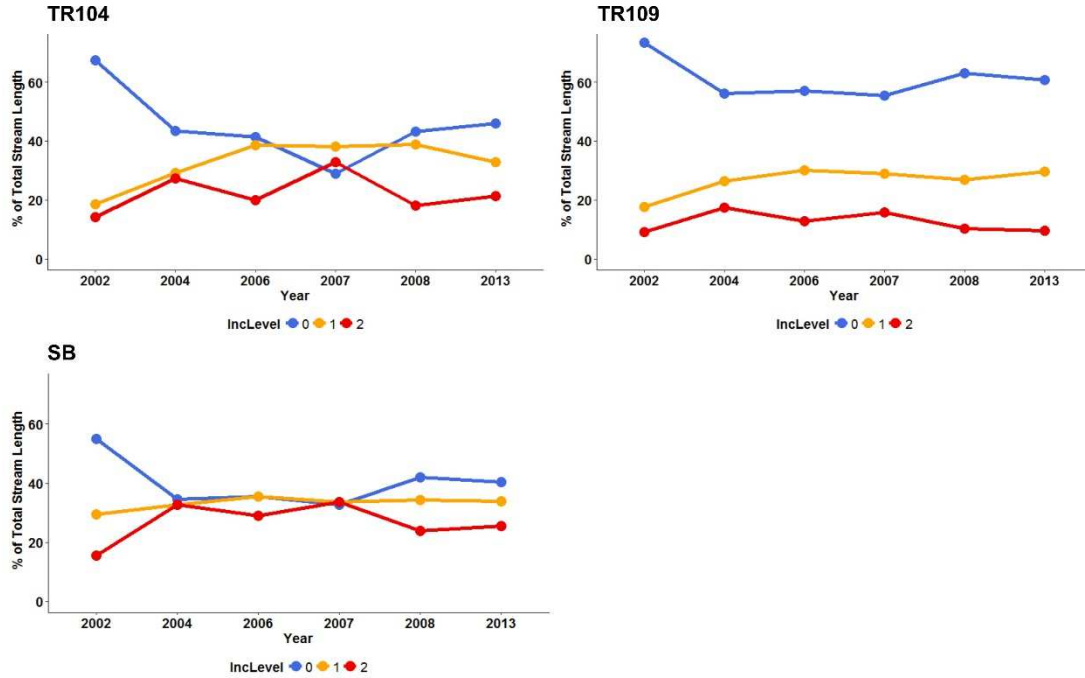


Figure 3.4.: The percent of the stream network classified as not incised (0), moderately incised (1), and severely incised (2). Only areas of the stream network that overlap within a 2.7 m (9 ft) buffer in every year are considered.

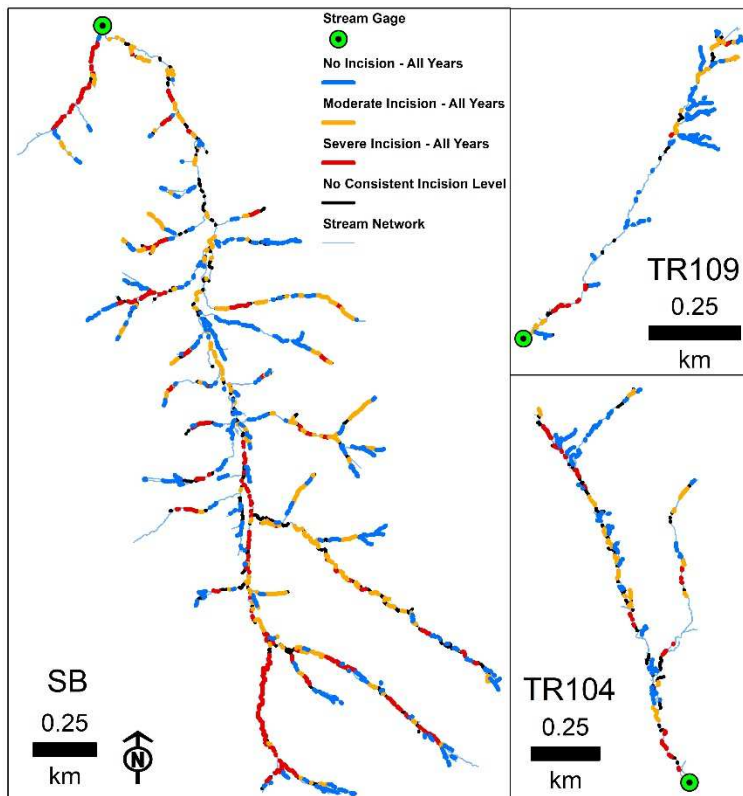


Figure 3.5.: Areas of each network where the incision level has remained consistent in at least five of the six years. Gaps are areas where the stream network did not overlap within a 2.7 m buffer in every year.

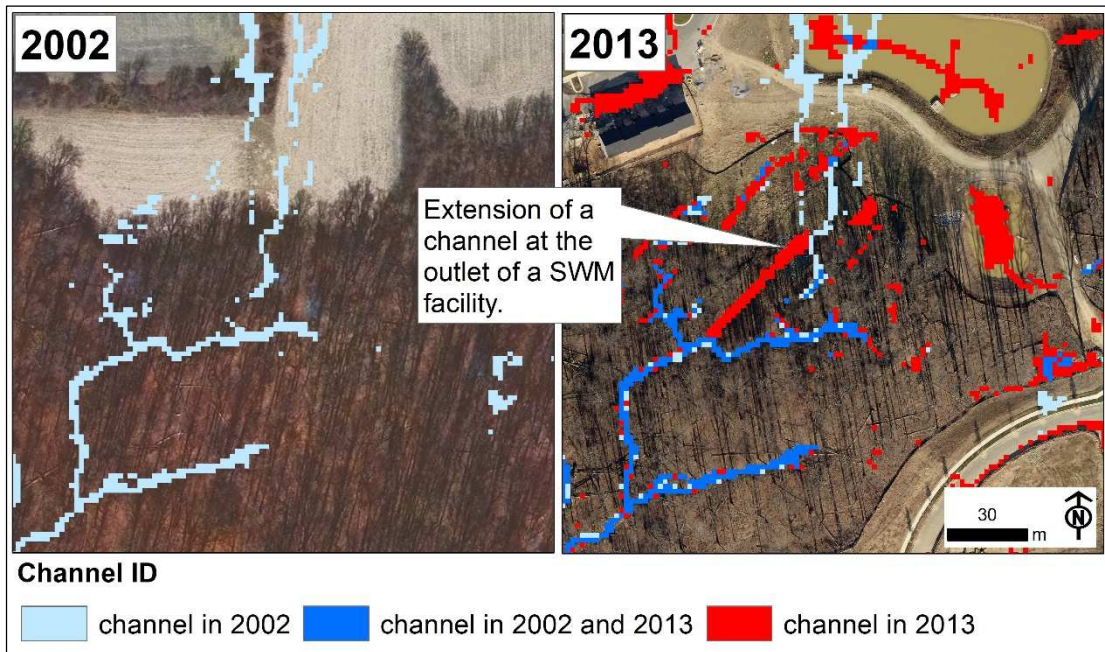


Figure 3.6: Example of channels in TR109, represented by valleys and pits extracted from Geomorphon. The darker blue shows areas that were mapped as channels in both 2002 and 2013. The red shows areas mapped as channels in 2013 but not in 2002, and a prominent feature is the artificial channel at the outlet of a SWM pond that was added to the stream network as a direct result of urban development. The light blue pixels in the panel on the right show channels that were filled in as a result of urban development. These types of areas were excluded from the portion of the analysis assessing overlapping stream networks but were included when incorporating Geomorphon to delineate the channel extent.

3.3.2. Groundwater seeps

Active seeps accounted for 11 of 48 surveyed groundwater seep features in TR104, 4 of 26 in TR109, and 3 of 20 surveyed in SB (Table 3.2, Figure 3.7). Of all surveyed seep locations (active and inactive), 7.4% occurred in banks with no channel incision, 54.3% occurred in moderately incised channels, and 38.3% occurred in severely incised channels (Table 3.2). In TR104, where seeps could be compared to the location of IF-SWM facilities, there was no apparent pattern of increased seepage near the southwest corner of the watershed where there is a high concentration of IF-SWM facilities adjacent to the west side of the channel (Figures 3.7 – 3.8). Active

seeps occurred on both sides of the channel and in areas with and without IF-SWM upslope from the location of the seep (Figure 3.8), suggesting no direct connection between IF-SWM and the location of groundwater seeps.

Incision Level	TR104		TR109		SB	
	# GW Seep Features	# Active	# GW Seep Features	# Active	# GW Seep Features	# Active
None (0)	3	1	0	0	4	0
Moderate (1)	25	5	23	3	3	0
Severe (2)	20	5	3	1	13	3

Table 3.2: The number of active and inactive groundwater seeps surveyed within each watershed, grouped by incision classification based on the field survey.

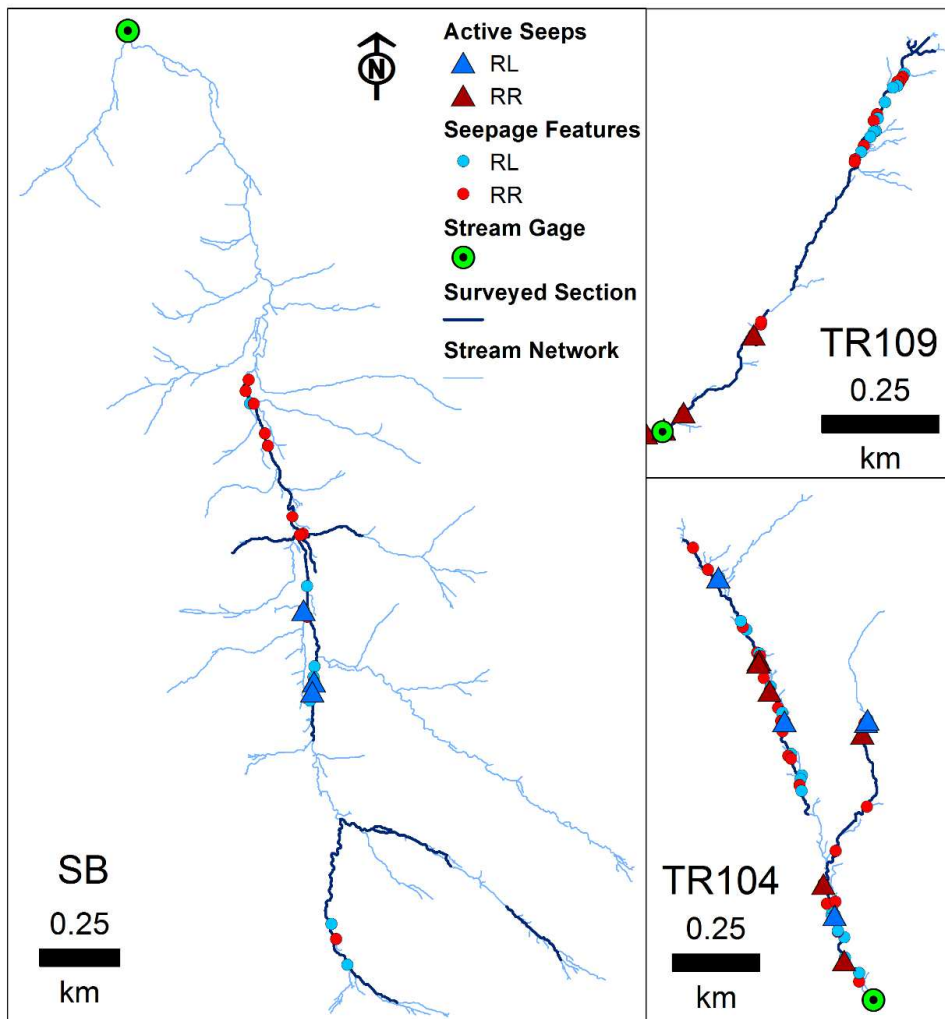


Figure 3.7: Results of the groundwater seep survey. Triangles indicate seeps were active. Circles indicate seeps were inactive but resembled characteristics of known groundwater seeps. Blue indicates the feature was on the left bank and red indicates the feature was on the right bank.

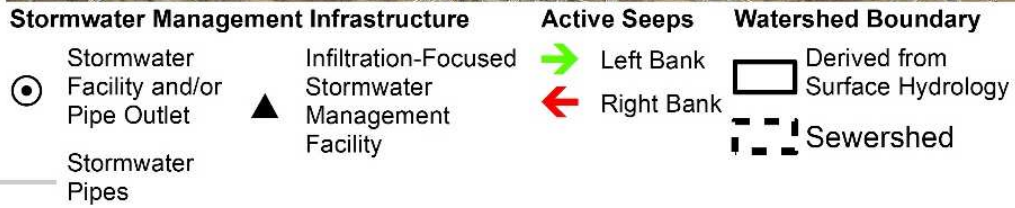
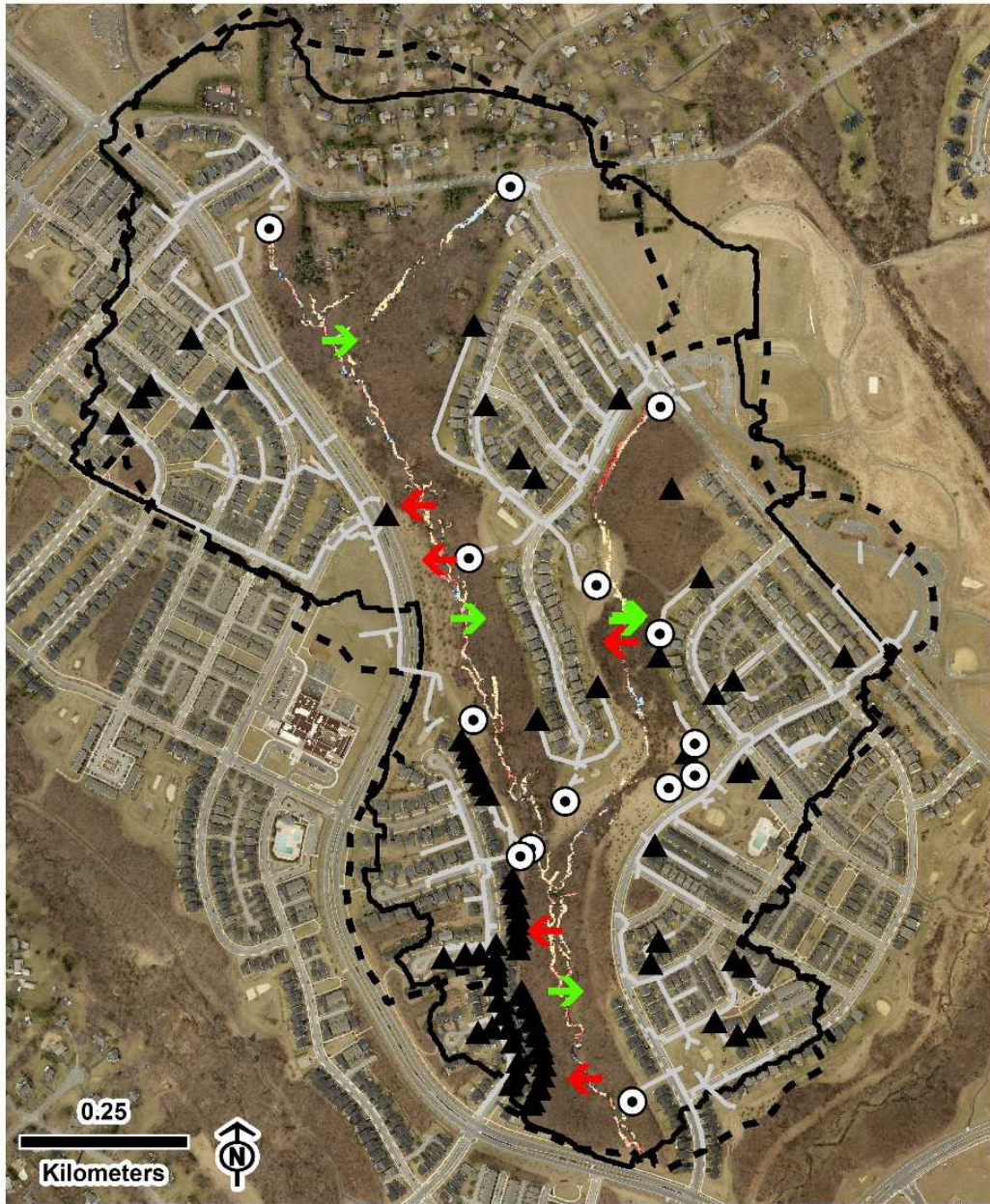


Figure 3.8: The location of active seeps in TR104 in relation to IF-SWM facilities.

Since there is no clear connection between the locations of IF-SWM facilities and the locations of groundwater seeps, the occurrence of active seeps could also be a result of natural groundwater discharge that existed prior to urban development. To test for this, the topographic wetness index (TWI) was calculated for both 2013 and 2002 using the lidar data. TWI is the natural log of the ratio of specific catchment area to slope and is used to assess the extent of soil saturation and runoff generation potential (Beven & Kirkby 1979). In TR104, areas with active groundwater seeps surveyed in the field coincided with high TWI values in 2002. Some of these locations even had higher TWI values in 2002 than in 2013. In Figure 3.9, the two top panels show a location in TR104 where a channel was buried during urban development (see also Figure 1.5) (Jones 2013). The TWI is able to detect this channel in 2002 and although it is not present in 2013, this is still a location of active groundwater discharge. Other sites of active groundwater discharge have high TWI values in both 2002 and 2013, which is also an indication that discharge in these areas is due to natural processes that existed prior to urban development. It is unclear whether IF-SWM could cause the rate and magnitude of groundwater discharge to increase at these locations and future research would be needed to test this. In SB, TWI indicates that the left side of the floodplain is more likely to be saturated, which could explain why all the active seeps were also located along the left bank.

A majority of the surveyed features that are assumed to have formed from groundwater were not active at the time they were inspected in the field. Although these features resembled characteristics of active seeps observed elsewhere within the watershed, there are other processes that could form pipes and cavities in stream

banks such as crayfish and other animal burrowing (M. Cashman, personal communication, November 2017). Crayfish burrows have arched chambers and tend to occur in patches along steep banks with minimal vegetation (Faller et al. 2016). The majority of pipes and cavities surveyed in this study were similar in shape and occurred in patches along banks with similar conditions. Crayfish (unknown sp.) have also been observed in TR104. Since crayfish burrows can cause significant bank erosion (Faller et al. 2016), this is an area of potential research.

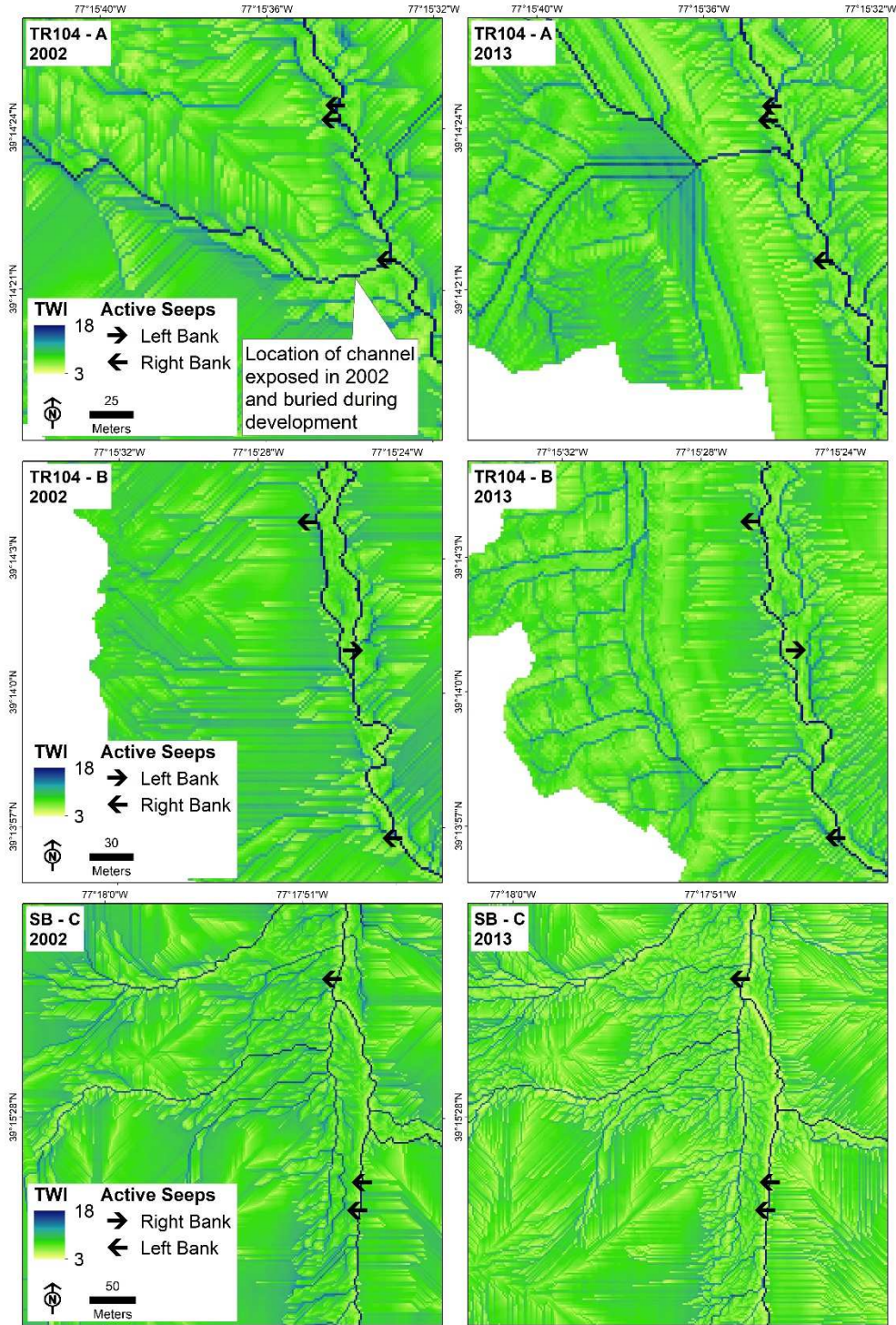


Figure 3.9: TWI for two different locations in TR104 and one location in SB. Higher values of TWI, represented as linear features in dark blue, indicate likely sites of groundwater discharge. The left panels show each location derived from 2002 lidar and the right panels show the same location derived from 2013 lidar. Changes in both drainage network and watershed boundaries for TR104 and TR109 are a direct result of the development process.

3.3.3. *Raw phi differences and changes relative to IF-SWM and groundwater influx*

Although many areas in each watershed had consistent incision levels through the study period, this did not indicate how areas were changing within those incision levels, especially in severe incision and no incision where the threshold of phi is only limited on one end. The comparison between raw phi values was able to assess change within consistent incision levels and the relative magnitude of change. It is assumed that a higher magnitude of negative values of the phi difference correspond to a higher magnitude of incision. Higher magnitudes of positive values of phi differences could indicate either channel widening or aggradation. Within areas that were consistently incised in at least five of the six years, the most change occurred within the severely incised reaches in all three watersheds (Figure 3.10). In TR109 and SB, most of the change included negative phi difference values suggesting continued incision.

The degree of change was also measured at the locations of each groundwater seep feature by calculating the mean of all phi difference pixels within a 4 m buffer of each groundwater seep feature in the banks. Overall phi decreased in these locations but showed similar pattern across all three watersheds (Figure 3.11). This suggests similar seepage-induced erosion patterns are occurring in the urban and forested watersheds. However, the overall number of seep features is twice as high in TR104, the urban watershed that has been urbanized for a longer period of time, and the median value of phi differences near these seeps is the most negative of the three watersheds. This shows that the most geomorphic activity related to seepage erosion is occurring in TR104. Data on stream bank characteristics with a higher spatial and

temporal resolution would help to better compare seepage-induced erosion across the three watersheds and understand how IF-SWM may influence erosion rates.

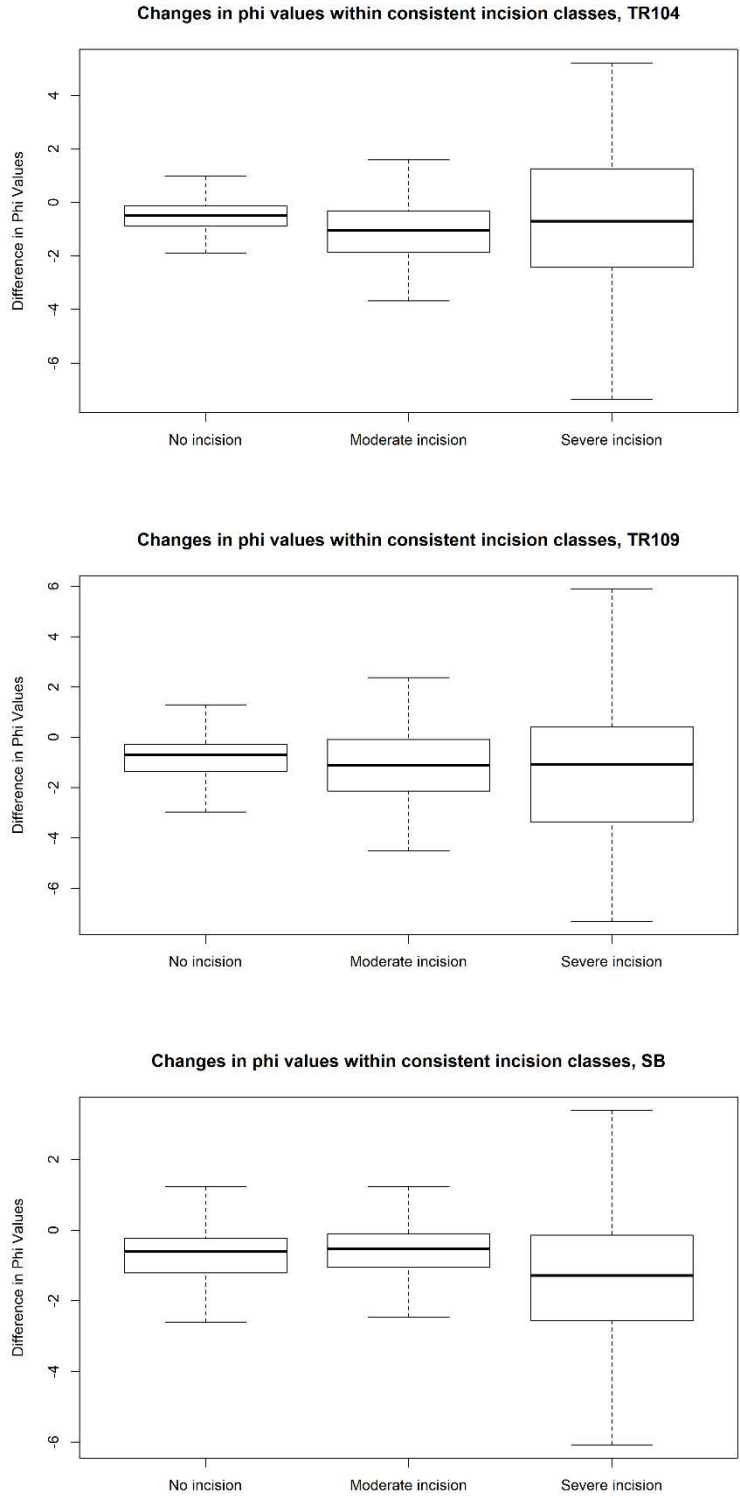


Figure 3.10: The range of phi value differences between 2002 and 2013 only within areas of consistent incision classes.

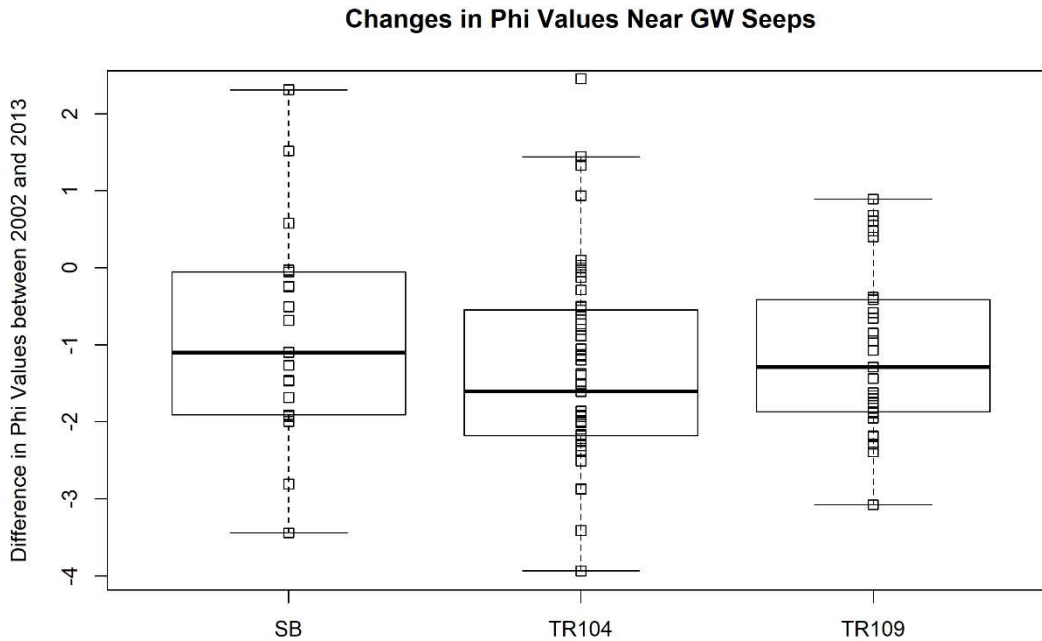


Figure 3.11: The range of changes in phi between 2002 and 2013 near sites of active and potentially inactive groundwater seep locations. Similarities across all three watersheds indicate similar erosion patterns in the forested and urban watersheds with respect to groundwater seepage.

In both urban watersheds, all areas at the outlet of SWM facilities became more incised, likely from a combination of excavation to install the outlets and through concentrated flow discharging at these locations. Aerial imagery shows most of the change detected within the riprap installed at the outlet, with incision extending a few meters downslope at some outlets. However, the incision did not extend all the way to the main channel at these outlets. (Figure 3.12).

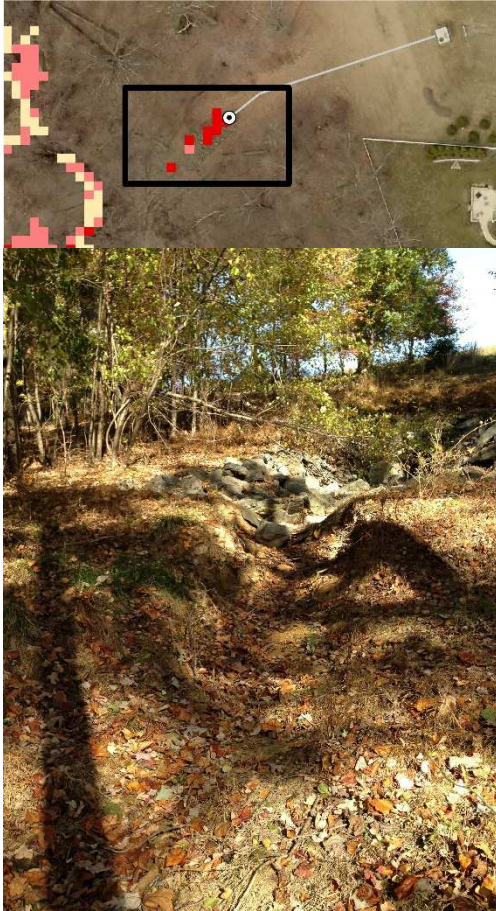


Figure 3.12: The outlet of a SWM facility in TR104 where the phi difference is showing incision directly downstream from the outlet (top) and evidence of erosion observed in the field (bottom). Incision tapers to a small, non-incised channel in the floodplain.

The following series of figures (3.13 – 3.18) shows a variety of changes observed from the phi difference values, along with cross sections extracted from the lidar to show more detailed change between 2002 and 2013 using all available lidar at 2004, 2006, 2007, and 2008 time steps. Changes from phi differences tended to agree with change measured from the field cross sections but no direct comparisons were made between the two datasets to quantify absolute change using phi differences. The field cross sections were used to determine if there was agreement in channel stability between the two datasets. Near cross sections with minimal change, phi differences also showed minimal change. The cross sections that showed the most change in

TR104 (Area 3, Appendix A) corresponded with a location that showed more phi changes (Figure 3.13). Both sets of cross sections show channel instability with a trend of downcutting and left-bank retreat. The dominant change in this area shows phi differences between -2 to -4. This figure also shows little change at the SWM outlets in the southern portion of the map, but incision at the outlet in the northwest corner. Aside from incision directly at SWM outlets, there were no clear connections between channel changes and proximity to IF-SWM. The areas along the channel closest to and down gradient from IF-SWM had varying degrees of change. This may be related to the amount of runoff flowing into each SWM facility. Modelling channel change using detailed information about each SWM facility is an area of future research.

Figure 3.14 shows headcut erosion in an area that has been incised since 2002 but is continuing to incise. There is a SWM outlet about 50 meters upstream but the change is not detectable until just downstream from active groundwater seeps, which are likely contributing to rapid erosion. TWI derived from the 2002 lidar shows this area likely being a natural groundwater discharge site, but it's unknown if the nearby IF-SWM has influenced the rate and magnitude of groundwater discharged here.

In TR109, there is a long contiguous reach that has not been incised since at least 2002 (Figure 2.17). A positive phi difference indicates the area was becoming even flatter (Figure 3.15). Transect 1 and 2 shows aggradation occurring between 2007 and 2008, around the time when development began in this watershed. This is an area that has consistently remained relatively flat (Appendix B) so any sediment

mobilized during development could likely be deposited in this reach if there's a natural change in gradient.

Downstream from the bridge in TR109, transect 1 (Figure 3.16) shows a small tributary that has resisted change. Transect 2 shows an area that was classified as moderately incised in 2002 and severely incised in 2013. The reach between the bridge and transect 2 was severely incised in both 2002 and 2013 and underwent little change in this time period.

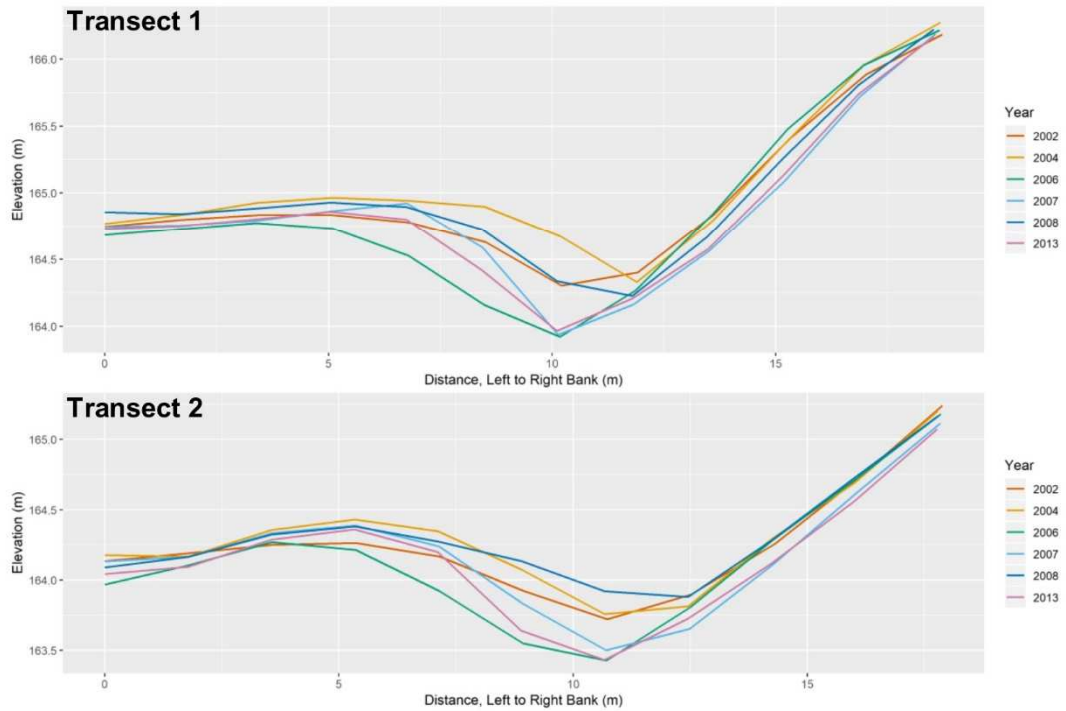
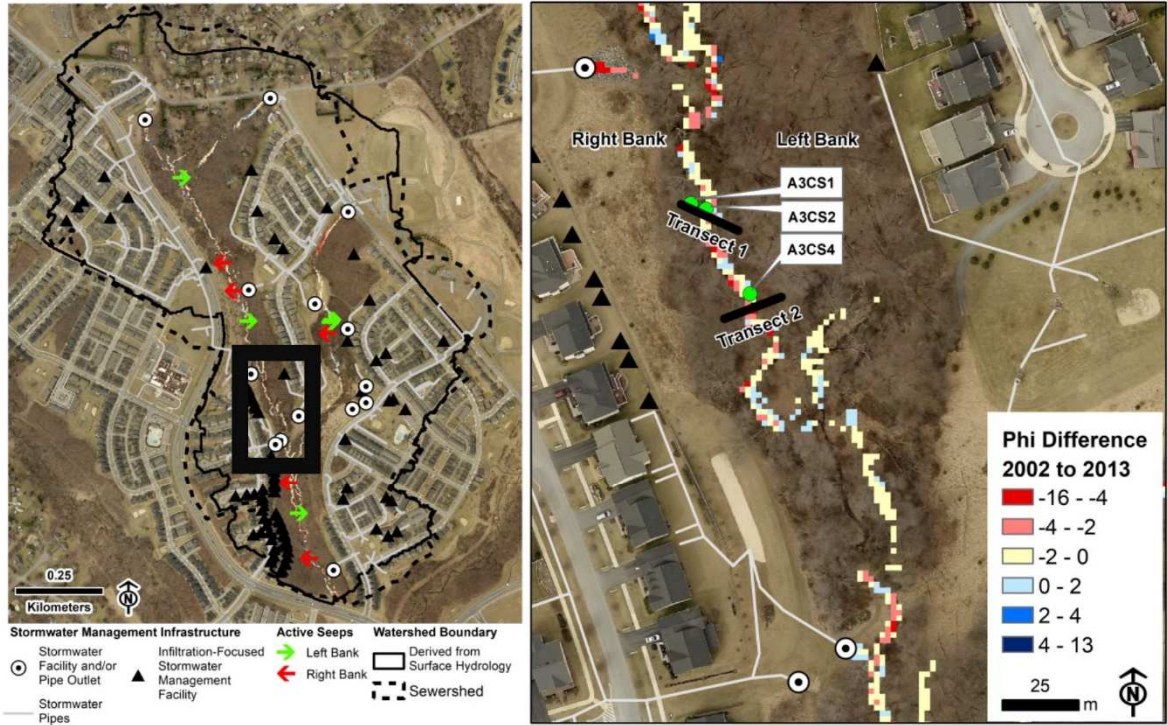


Figure 3.13: Transects 1 and 2 show channel instability and the pattern of bank retreat and downcutting resemble the patterns of change from the field surveyed cross sections in this area of TR104.

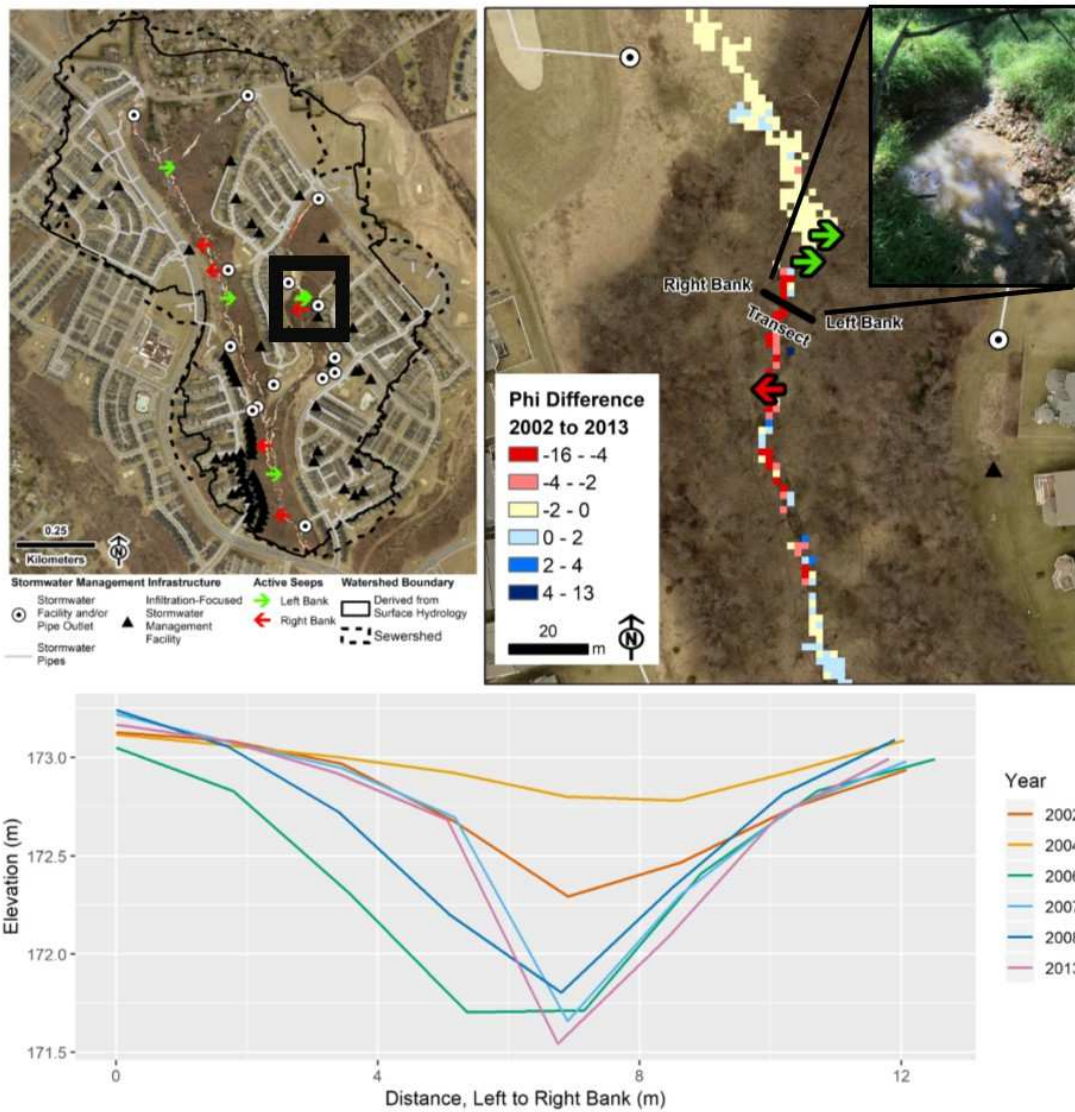


Figure 3.14: This transect shows an area of headcut erosion at the beginning of a severely incised reach in TR104. There is also groundwater actively seeping from the banks just upstream from the headcut. The image in the upper right corner shows the area near the headcut.

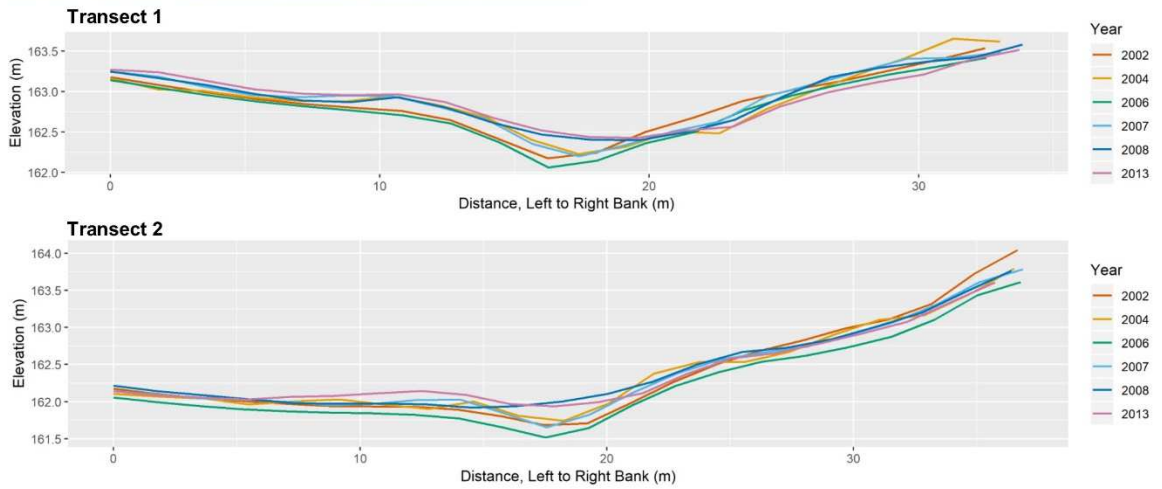
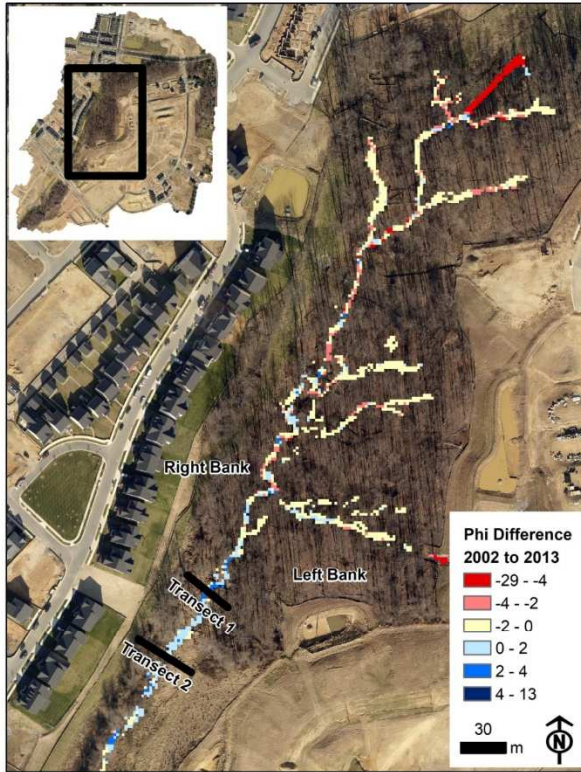


Figure 3.15: Transect 1 and 2 both show areas that have never been moderately or severely incised during the study period, but appear to be flattening in TR109. This could potentially be a hot spot for sediment deposition.

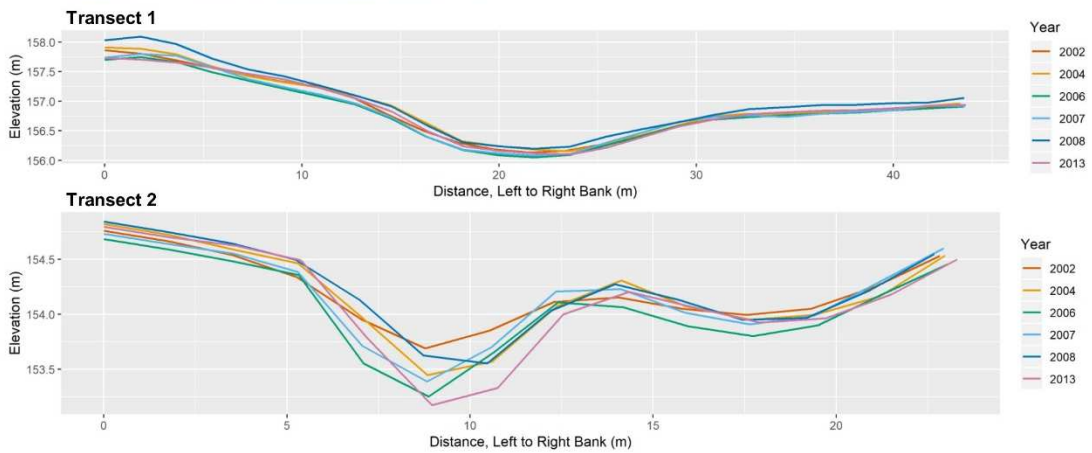
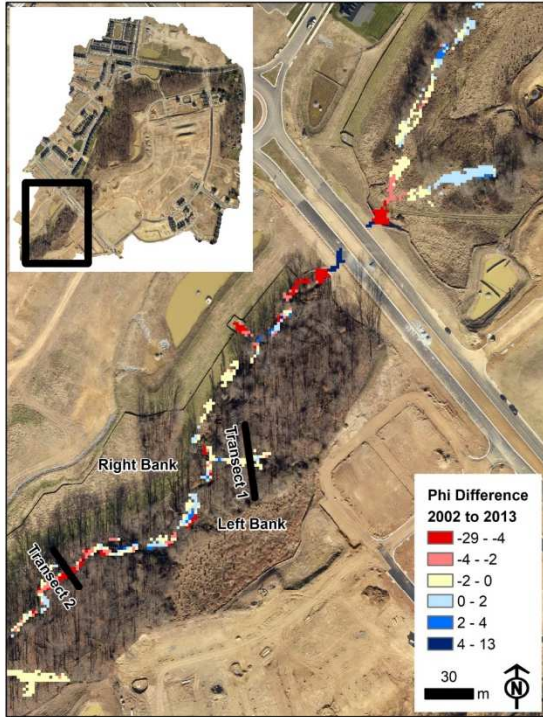


Figure 3.16: Transect 1 shows an area of stability in TR109 which is also reflected in the phi difference. Transect 2 is an area in TR109 that was already severely incised and continued to incise through 2013.

Although SB is a forested watershed, there are many areas of instability, especially in reaches already incised in 2002 (Figures 3.10 and 3.17). Further downstream in SB where the channel becomes wider and more complex, the phi difference shows patterns of erosion and of deposition or widening (Figure 3.18). Across the watershed scale, phi differences at each time increment showed similar patterns in all three watersheds, despite TR104 and TR109 being urbanized while SB remained forested (Figure 3.19). This may be a result of systematic error associated with the lidar (Gardina 2008) that is driving similar patterns of change in Figure 3.4. This could also be a reflection of the influence of prior agricultural land use contributing to the incision of all three watersheds or storm events that generate erosive flows in all three watersheds. Although runoff in SB is significantly lower than TR104 during large precipitation events (3 – 7 cm), sediment export is highest in SB (Hopkins et al. 2017, Figure 3.20). Sediment is easily exported from the already incised banks in SB, where most of the geomorphic change is occurring (Figure 3.10), though specific areas of accelerated erosion could be controlled by local factors such as soil composition along exposed banks, local gradient, and groundwater seeps. The field-surveyed cross sections also show significant fluctuations in channel conditions in SB (Appendix A).

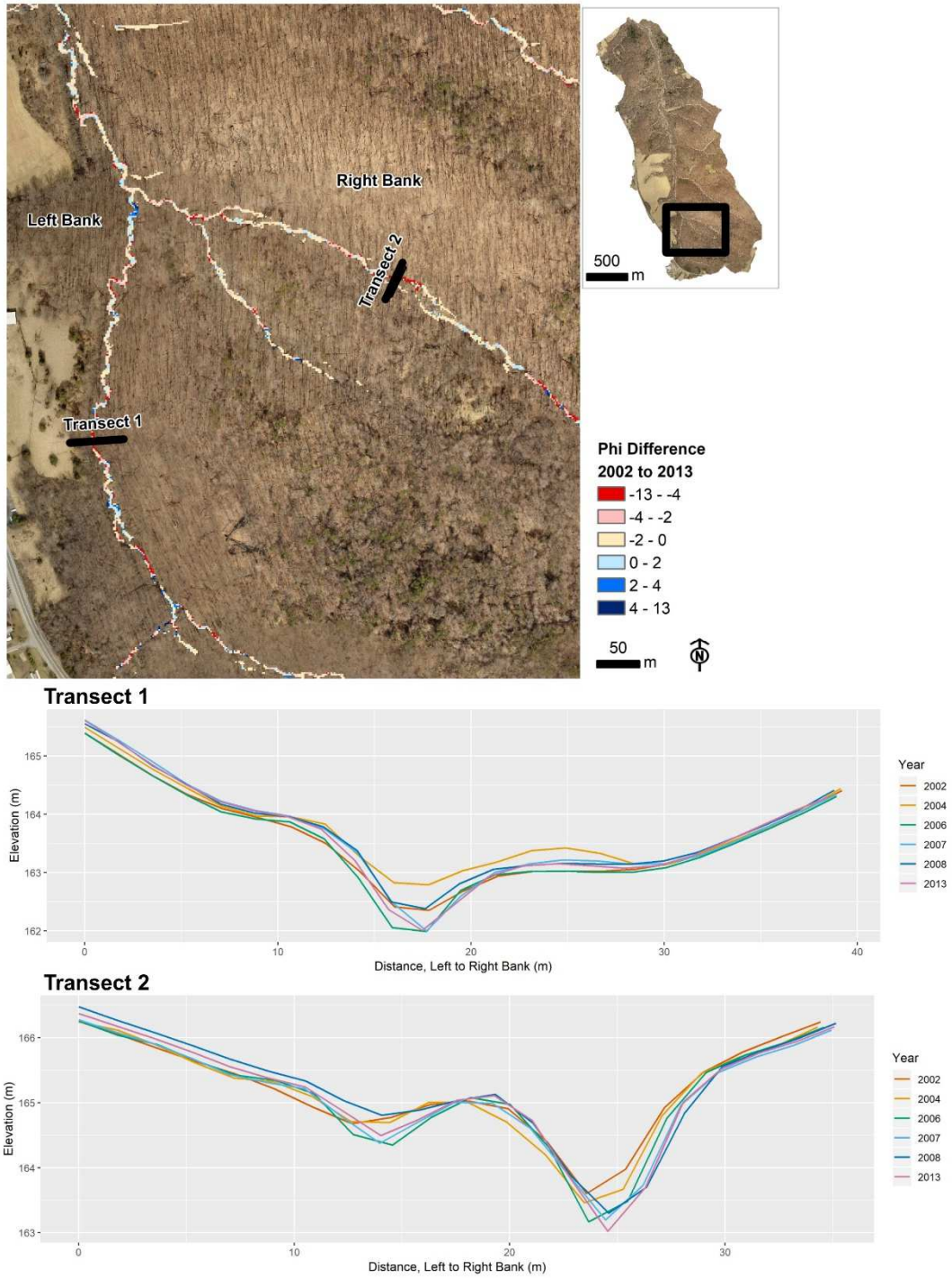


Figure 3.17: Transects 1 shows an area that transitioned from moderately to severely incised in SB. Transect 2 is an area that was already incised in 2002 and continued to incise through 2013.

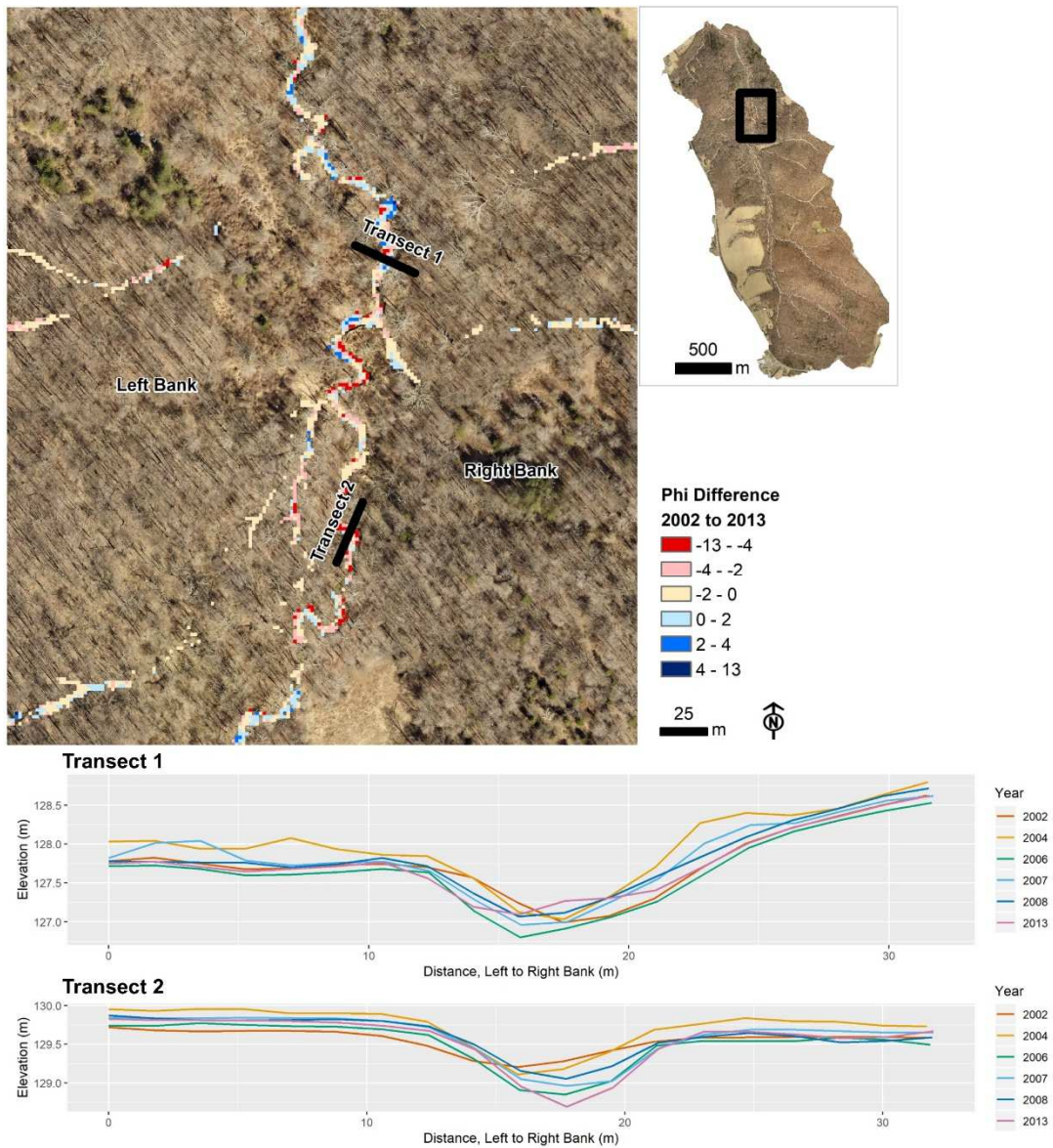


Figure 3.18: Two transects showing change over time in SB. Transect 1 shows an area where the channel has widened and has positive values of phi differences because the channel became more open. Transect 2 shows an area that has been eroding and becoming more enclosed.

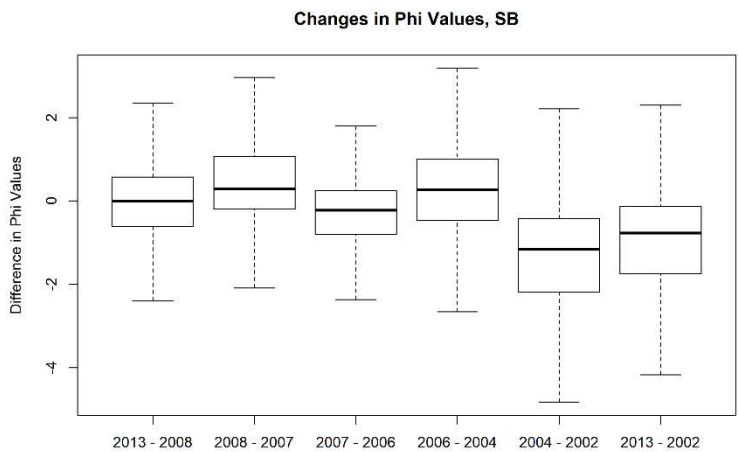
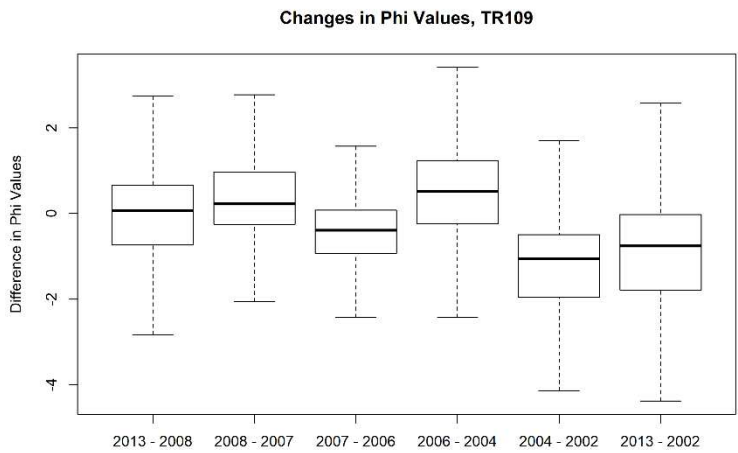
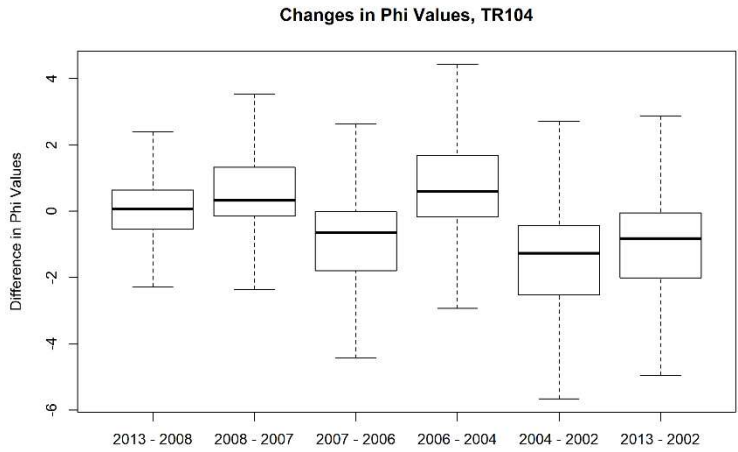


Figure 3.19. Boxplots showing the difference in raw phi values for incremental time steps in each watershed. Negative values indicate areas becoming more enclosed, indicative of incision, and positive values indicate areas becoming more open, either through deposition or channel widening. Outliers have been removed from the plots.

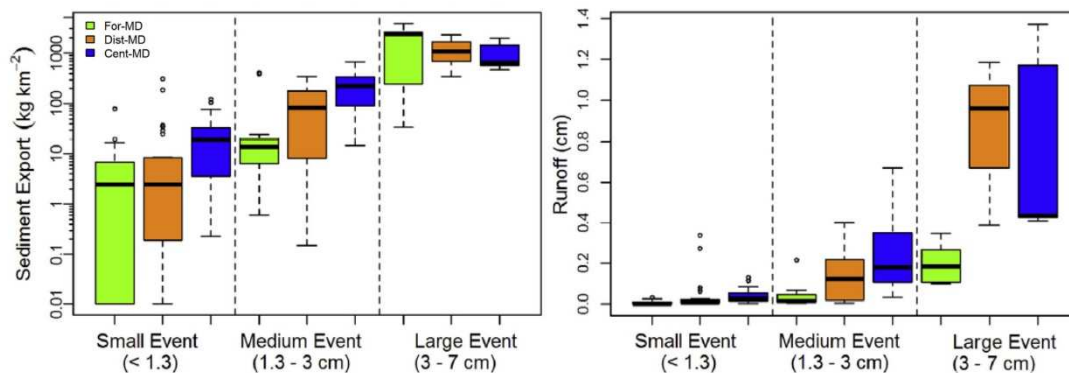


Figure 3.20: Boxplots showing sediment export and runoff for SB (green plots) and TR104 (orange plots), along with a nearby watershed developed using older, centralized SWM (blue plots). Adapted from Hopkins et al. (2017).

3.3.4. Characterizing active seeps with a TIR camera

Active seeps were difficult to identify and characterize using a TIR camera to detect thermal differences between ground and surface water. One seep was visibly active and had a conductivity difference of about 300 $\mu\text{S}/\text{cm}$ between ground and surface water but little difference in temperature. However, another visibly active seep had a greater difference in temperature but little difference in conductivity (Table 3.3). Although the groundwater was warmer than the surface water at the time of data collection, there may not have been a strong enough difference at this time of the year or time of day (late afternoon). A better time to collect this type of data may be during late summer when the difference between surface and groundwater is greater or earlier in the morning before sunlight can warm the cooler surface.

This was an inefficient method to identify and characterize seep locations. Although the TIR camera successfully located concentrated flow in certain locations, diffuse flow and very slow seeps like the example in SB (Table 3.3) were not easily detected. Although the magnitude of erosion near seeps was similar in all three watersheds, the

greater number of seeps observed in TR104 compared with the other watersheds opens further questions about the influence of development patterns on groundwater seeps. To further understand whether IF-SWM accelerated seepage and resulting bank erosion, temperature sensors could be deployed at sites of groundwater seep locations identified in the urban and forested watersheds to compare patterns over time and responses to storm events. Although sediment export in TR04 is similar to SB during small precipitation events, the sediment export in TR104 is significantly higher than SB during medium precipitation events, which fall within the range of rainfall quantities that the SWM facilities were designed to manage (Hopkins et al. 2017). However, contributions from seepage-induced bank erosion are unknown and documenting this process would be a valuable contributing to the literature on urban stormwater management and erosional processes.

Watershed	Temperature (°C)		Conductivity (µS/cm)		Notes	TIR (left) and true color (right) images	
	Near Seep	In Stream	Near Seep	In Stream			
TR104	4.07	4.05	450	751	Water is actively flowing in. There is a small difference in stream temperature but conductivity of groundwater was 300 µS/cm lower than the surface water just upstream of the seep location.		
TR104	4.4	3.94	521	552	Water is actively flowing in. There is a slight difference in conductivity between the ground and surface water.		
TR104	4.3	4.3	900	788	There is no visible evidence of groundwater seeps from the banks but the TIR camera is showing warmer water flowing in and there is visible bank erosion.		
TR104	4.06	3.98	NA	NA	There is no visible evidence of groundwater seeps from the banks but the TIR camera is showing warmer water flowing in from the undercut bank.		
SB	2.6	2.6	375	375	The bank is represented by green, yellow, red, and orange, with the area in red areas being the warmest. This warmer section of the bank was soggy, indicating groundwater seepage. This had no influence on stream temperature or conductivity near the bank compared with the stream just upstream of the seep location.		

Table 3.3: Description and images for active groundwater seeps in TR104 and SB. In the TIR image, the warmest temperatures are shown in red and white. Temperatures in the images are relative. Temperatures reported in the table were collected with the YSI multi-parameter sonde.

3.4. Discussion

3.4.1. Incision changes and management implications

The use of multitemporal lidar to document channel conditions prior to development revealed a number of interesting patterns. Many of the areas in the urban watersheds that were presently incised were already severely incised before development began. There were also a number of severely incised reaches in the forested reference watershed. Differences in phi values in the reaches that remained within the same incision classification across the study period showed how the most unstable reaches were those already severely incised. This has important implications for sediment dynamics in streams across the Piedmont and mid-Atlantic where incised channels may still be adjusting from agricultural land use (Jacobson & Coleman 1986) even if these watersheds have since been reforested or urbanized. On the other hand, severe incision that typically follows urbanization in older development projects lacking SWM intended to control erosive flows (Hammer 1972, Booth 1990, Arnold & Gibbons 1996) was not observed in TR104 or TR109. This suggests that the IF-SWM has been more effective than previous forms of SWM for controlling erosive stormflows that cause severe incision. Although the three watersheds showed similar temporal patterns of erosion, TR104 experienced a slightly higher degree of change over the course of the study period and could reflect change associated with runoff from storm events that exceed the threshold of runoff that can be mitigated by the SWM facilities (Loperfido et al. 2014, Hopkins et al. 2017).

Maps derived in this study showing areas of severe incision and change over time can be used to predict erosional hot-spots within watersheds and help implement practices to mitigate sediment and phosphorous contamination to nearby waterways. Although studies have reported a wide range of suspended sediment loads in streams originating from stream banks (7 – 92%) (Fox et al. 2016), studies unique to the Chesapeake Bay region have demonstrated that stream banks can be a significant source of sediment, especially within mixed urban/agricultural/forested land use (Gellis et al. 2009, Cashman et al. 2018). Identifying incision over time using only lidar data can have broad applications in river and watershed management by helping to identify potentially degraded stream habitats, hot spots for sediment and pollutant inputs to streams, or disconnected floodplains. Since floodplains are also sediment sinks (Gellis et al. 2008, Hupp et al. 2013), this method could also identify potential sediment sinks. Knowing the locations for potential hot spots of erosion (incised banks) and deposition (non-incised banks) could also help determine where sediment mobilized from incised banks may be more likely to be redeposited on downstream floodplains (Bigelow et al. 2016) since even watersheds with incised eroding banks can be a net depositional system if there are functioning floodplains (Hupp et al. 2013). This type of information can help prioritize restoration projects with limited resources to most efficiently control excess sediment and nutrients. More detailed physical streambank characteristics could also be incorporated into water quality models such as SWAT and SPARROW to better inform water quality estimates. Although the phi thresholds used in this study to group reaches into incision levels may need to be adjusted in areas with different size channels and with different

resolution DEMs, the direct phi differencing to measure change over time with the incorporation of Geomorphon to isolate channel pixels is a method that could easily be applied to any watershed with the understanding that lidar quality and resolution will limit accurate change detection in smaller channels, especially those that are heavily vegetated.

3.4.2. Future work and data collection in the study area

This study has shown that generating photogrammetric models of stream banks using a hand held camera is a relatively quick and easy method to detect small changes along stream banks and quantify bank erosion. Groundwater seeps and possible crayfish burrows have been observed along banks in the study sites and these features are known to erode banks (Midgley et al. 2011, Faller et al. 2016). Sediment erosion could be easily studied at these sites using repeat SfM surveys to quantify the amount of sediment eroded in areas with and without groundwater seeps and/or animal burrowing. SfM surveys can also detect finer scale changes that may not be captured from lidar, such as mass wasting and bank failure from undermined banks (Figure 3.21). This type of comparison may help clarify how seepage-induced erosion may or may not differ in the urban versus forested watersheds.



Figure 3.21: An area with features formed from groundwater seeps and/or animal burrowing in November 2016 was observed with recent bank erosion two months later. These features create unstable banks that eventually leads to bank failure.

In the watersheds where advanced SWM was implemented, the channels have not severely downcut further once the area was converted from agriculture to urban, and incision did not extend more than a few meters downstream from SWM outlets. However, this study only documented change between 2002 and 2013 with QL 3 lidar. Montgomery County and the USGS collected QL 2 lidar with better accuracy and smaller distances between bare earth points in winter 2018. Once this dataset is available, change that occurred between 2013 and 2018 can be assessed, perhaps at finer scales using higher accuracy data. Comparisons can also be made between the QL 2 lidar and newer data by generating DEMs from images collected either aerially or from the ground using SfM.

3.5. Conclusions

Topographic openness was derived from multitemporal lidar to measure channel incision over time in two urbanizing watersheds and a forested reference watershed that underwent little change. Results show that all three watersheds contained severely incised banks prior to development, where most of the geomorphic

change occurred. The urban watersheds contained SWM intended to mimic pre-development conditions but pre-development conditions included channels that were already incised from a prior agricultural land use history and these incised banks are where most of the geomorphic change has occurred. Although minor incision occurred at SWM outlets, changes in the urban watersheds were similar to the forested watershed. Although TR104 exhibited more change than the forested watershed and TR109, which has been urbanized for less time, it is still unclear what are dominant controls on geomorphic change in these watersheds and if the timeframe of the study (2002 – 2013) allowed for enough time to measure geomorphic change that may be a result of recent urban development. Systematic lidar errors may also obscure fine scale changes since the vendor, instrumentation, accuracy, and post-processing standards varied across each time step, limiting the extent to which change can be accurately measured with multitemporal lidar.

Groundwater seeps were also located in each of the watersheds. The data used for this study was insufficient to understand whether seepage-induced erosion is connected to the development of IF-SWM, but the data show that most of the seeps occurred in moderately and severely incised banks and could be contributing to bank erosion. TR104 also contained more seeps than the other watersheds and bank erosion from seep locations was evident in the field. To better understand the dynamics of groundwater seeps and bank erosion within the vicinity of seeps, temperature sensors could be deployed to track activity of seeps and repeat SfM surveys could quantify differences between bank erosion in areas with and without groundwater seeps for a more robust comparison between the urban and forested watersheds.

Chapter 4: Conclusions

The research presented here resulted in a method using lidar to calculate landscape metrics using topographic openness and Geomorphon, along with field and SfM surveys to characterize the degree and spatial patterns of incision in headwater streams. This method was then applied to multitemporal lidar to better understand the spatial-temporal component of geomorphic change related to urbanization and whether there were unintended consequences of IF-SWM contributing to channel erosion. The following research questions were explored:

- 1) Can topographic openness remotely detect channel incision? If so, are there limitations to the scale at which incision can be characterized?
- 2) What does topographic openness reveal about the spatial pattern of incision at the watershed scale?
- 3) To what extent can incision over time be measured using topographic openness with multitemporal lidar; are there observed differences in the magnitude of change between the forested and urban watersheds?

Headwater streams with drainage areas less than about 1.5 km² and channel widths less than 5 m can successfully be classified as severely, moderately, or not incised with 70 – 75 % accuracy. Incision was accurately detected in drainage areas as small as 2.3 x 10⁻³ km², suggesting that the method can be applied to most headwater streams that are detectable from lidar and not obscured by thick vegetation. The approach used field surveys and photogrammetric models of stream banks to

validate the method but can be applied using only a DEM as input data and the calculation of topographic openness. However, the method was only validated in three watersheds and poor results from the larger watershed suggest further work is needed to refine the method for broader applications. As drainage area and channel width increased, another significant erosional characteristic of channel widening following incision was observed in the field but not well characterized or able to be accurately mapped with the original method described in section 2.2. Additional methods were explored with promising results incorporating Geomorphon to isolate all openness pixels within the channel rather than summarize values along a single pixel wide linear stream network that is less representative of the channel. This method provides more details about channel characteristics and can differentiate incised, confined channels from those with more complexity that contain steep, eroding cut banks on one side of the channel and point bars on the opposite side. The ability to map these channel characteristics across an entire watershed helps to infer dominant geomorphic processes that are crucial to understanding channel dynamics and clarifying relationships between upstream processes and downstream responses. Improving methods to characterize these types of reaches is an important consideration for future work.

Topographic openness was then applied to lidar data collected in 2002, 2004, 2006, 2007, and 2008 documenting two urban watersheds before, during, and after urban development, and a nearby forested control, to assess whether multitemporal lidar could be used to detect changes in the pattern of channel incision over time. Changes in the urban watersheds were compared with changes over the same time

interval in the forested control watershed. Similar patterns of change across all watersheds suggest either regional weather controls on channel adjustment, systematic lidar errors, or a combination of the two. The temporal analysis also revealed interesting patterns of consistency in incision over time. Although the urban watersheds contained reaches with severe incision, this analysis revealed that many of these areas were already incised prior to urbanization as a result of previous erosion under agricultural land use. Areas that incised the most during the study period were already heavily eroded prior to urbanization and may also be contributing to the similarity in patterns of change occurring in all three watersheds.

The urban watersheds displayed a slight increase in erosion relative to the non-urbanized watershed, especially downslope from SWM outfalls, but did not result in drastic incision that has typically been observed in other urban streams with little to no stormwater management control. But of the two urban watersheds, the one that has been urbanized for a longer portion of the study period, TR104, showed the most change over time, suggesting that urbanization may have contributed to some additional incision despite the use of IF-SWM to limit urban stormwater runoff.

There was no apparent direct connection between the locations of groundwater seepage and IF-SWM, but urban watersheds contained a greater number of seeps than the forested watershed and more geomorphic change occurred around the seep features in TR104 than the other watersheds. Areas of active seepage may be a result of groundwater naturally discharging to specific areas, but further research is necessary to better understand if IF-SWM is accelerating seepage erosion in these areas. This is an important future consideration because evidence of bank erosion at

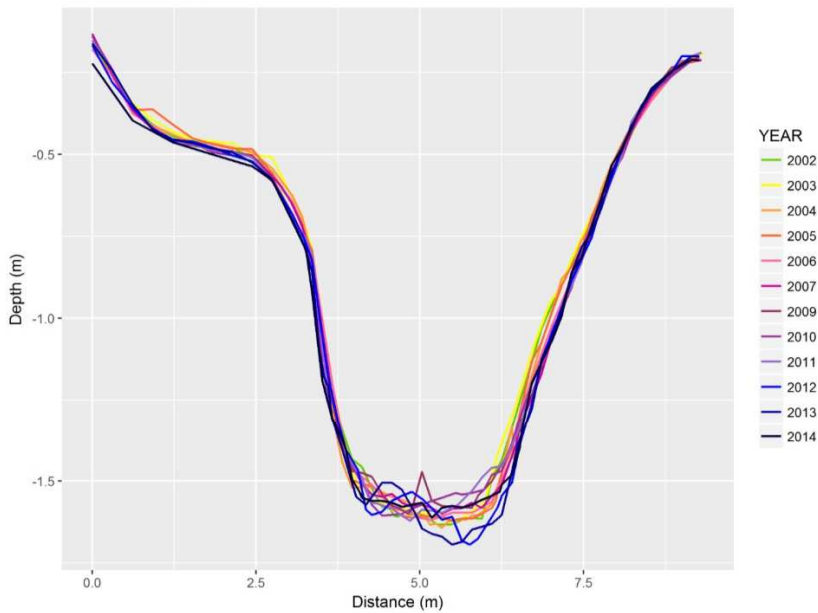
the location of seeps was observed in the field and has been documented in other studies as a significant source of suspended sediment in streams. The amount of sediment could not be accurately quantified using aerial lidar data but could be easily measured in high temporal resolution using repeat photogrammetric models.

Appendices

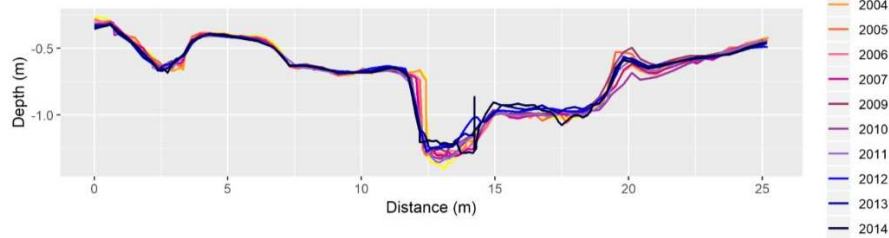
Appendix A. Montgomery County field-surveyed annual cross section data in TR104, TR109, and SB.

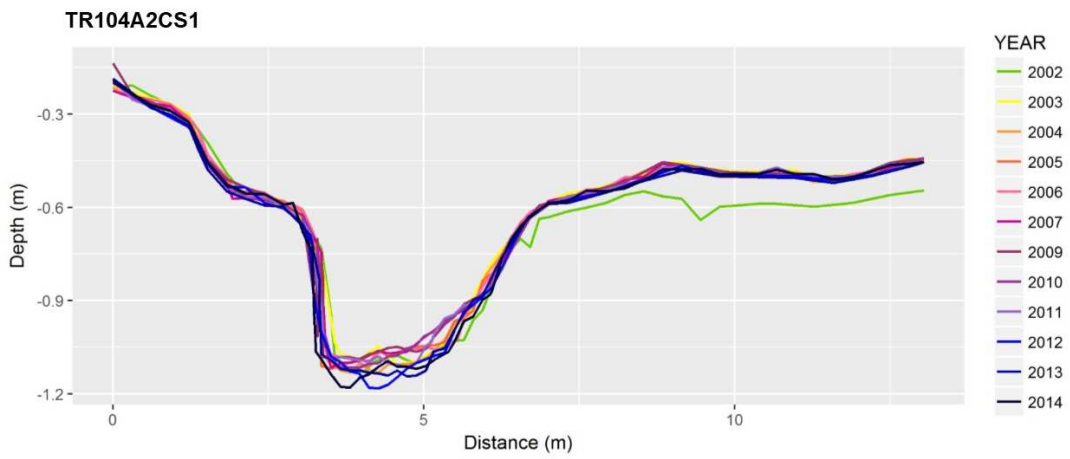
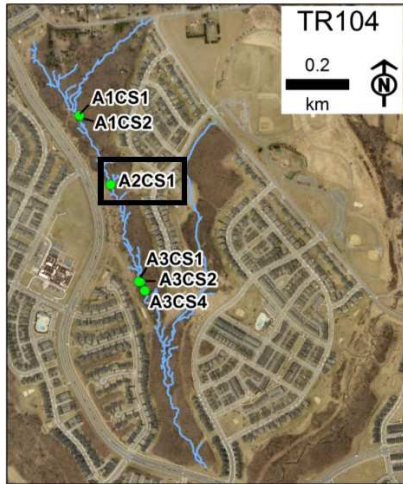


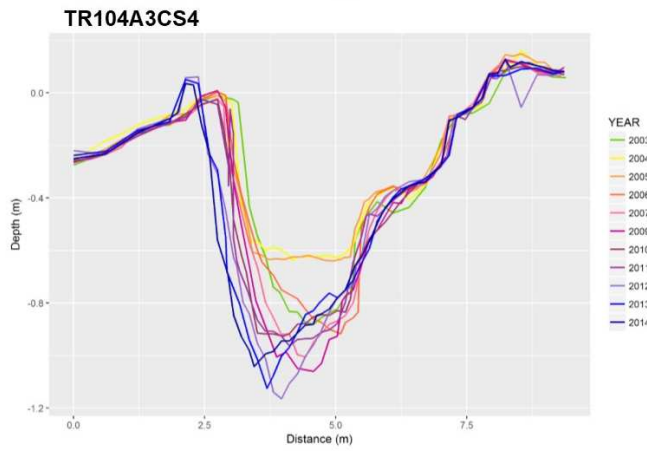
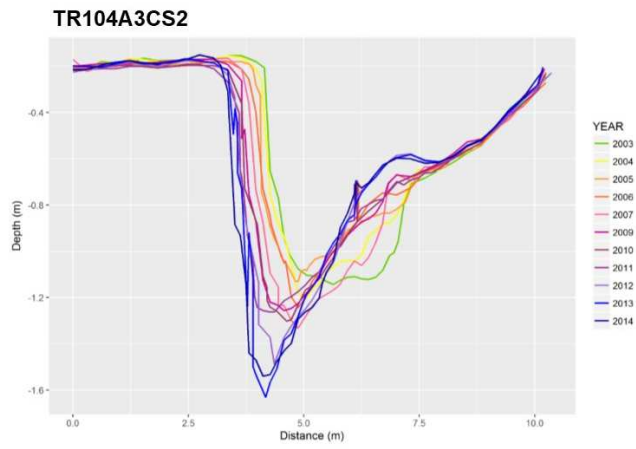
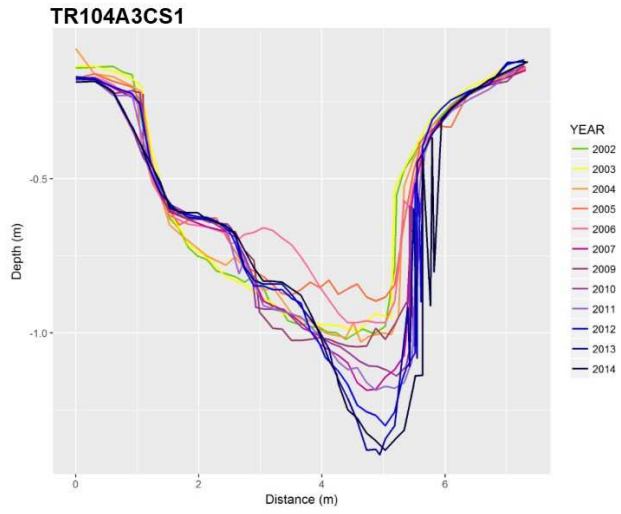
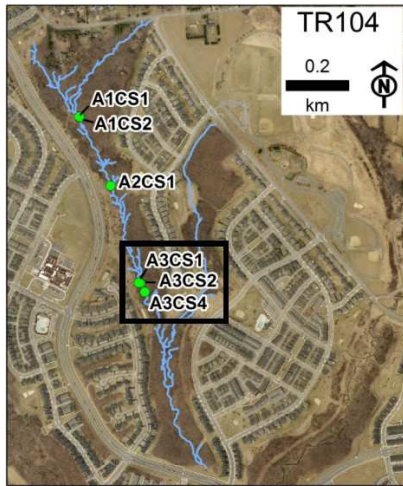
TR104A1CS1

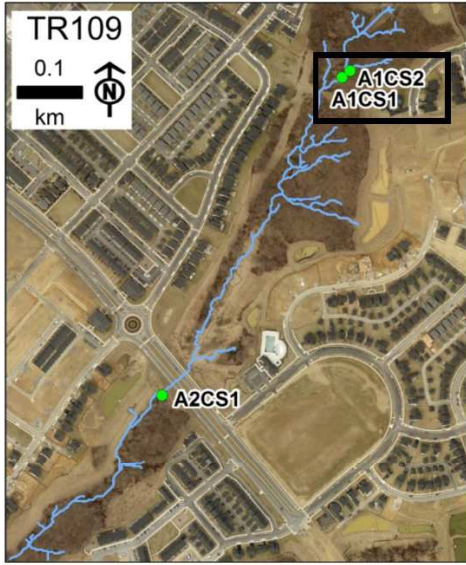


TR104A1CS2

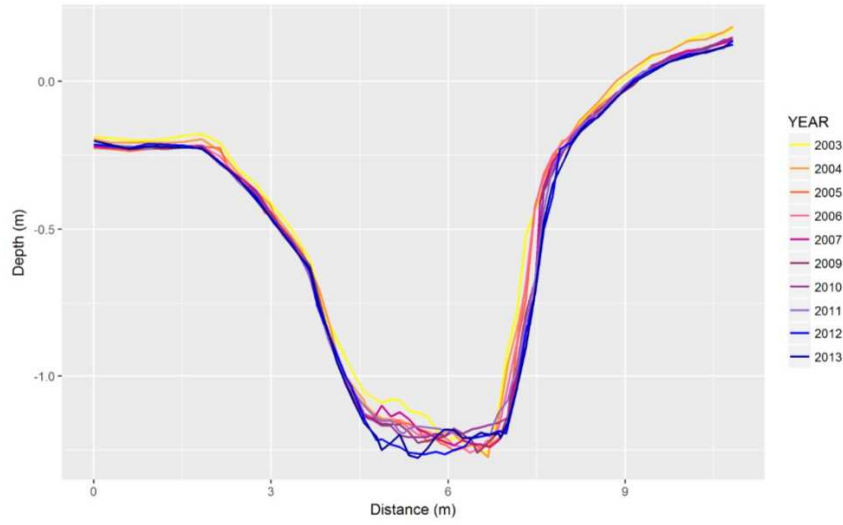




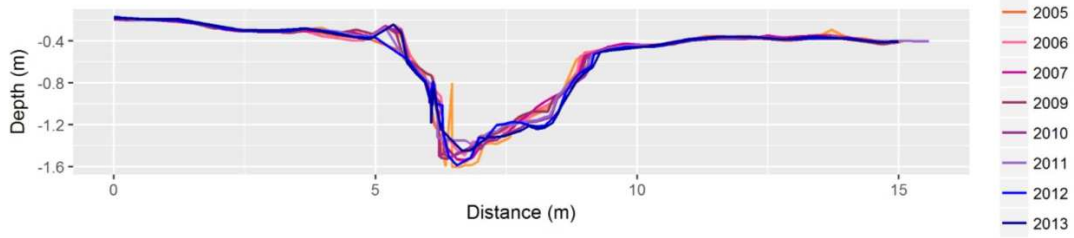


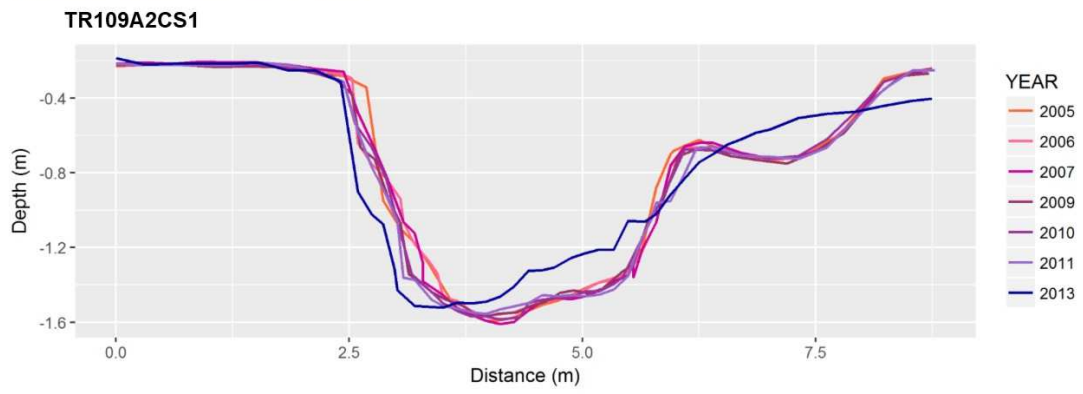


TR109A1CS1



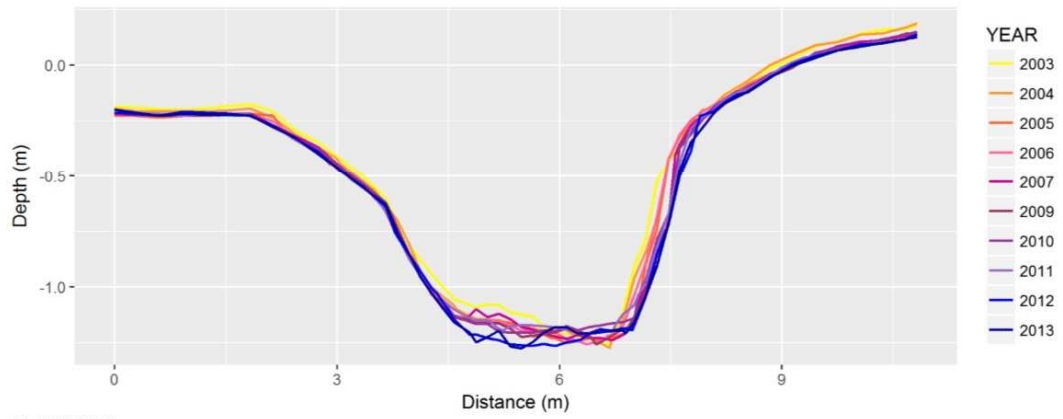
TR109A1CS2



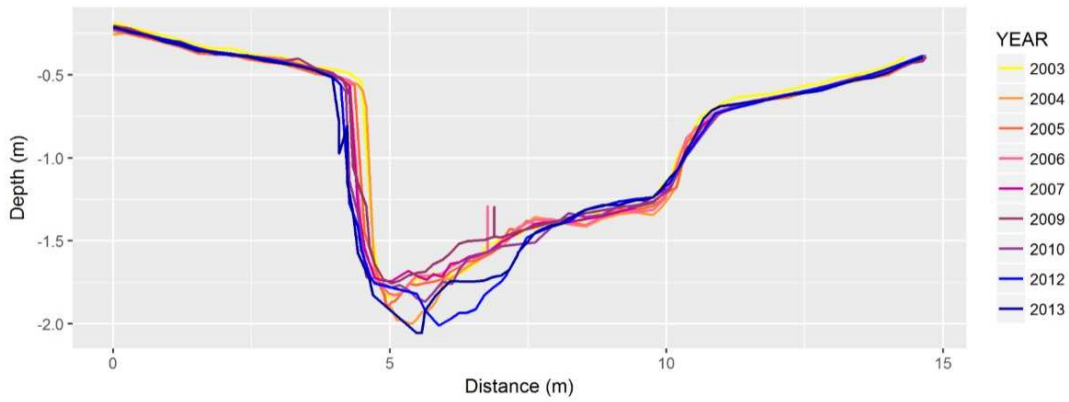


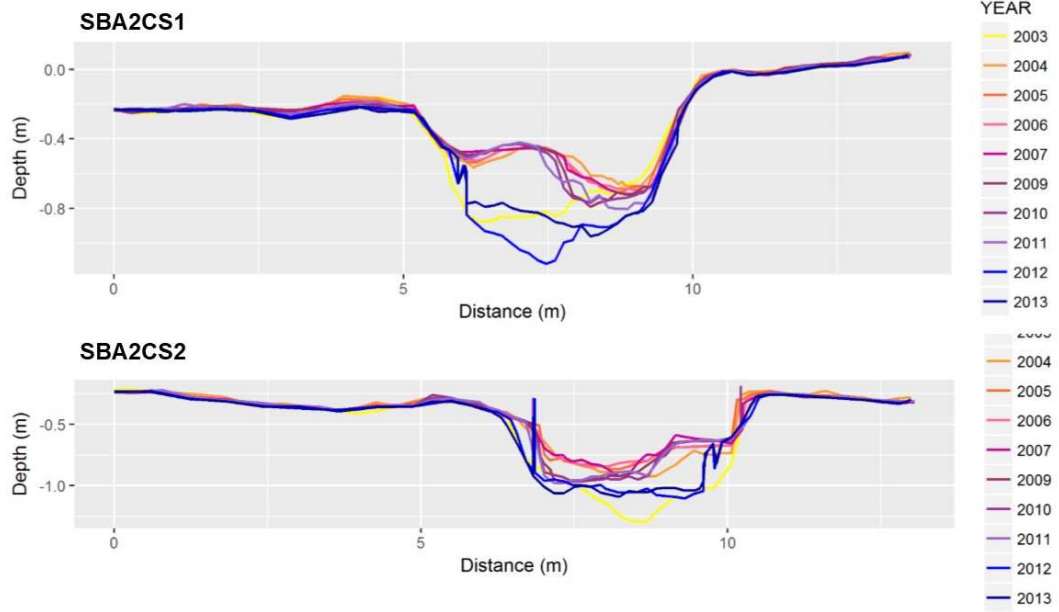


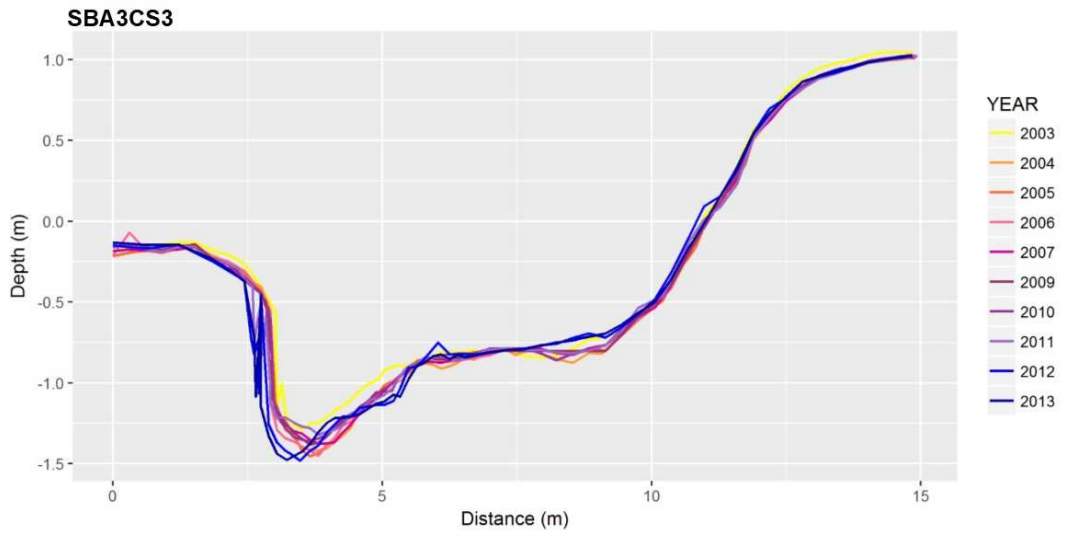
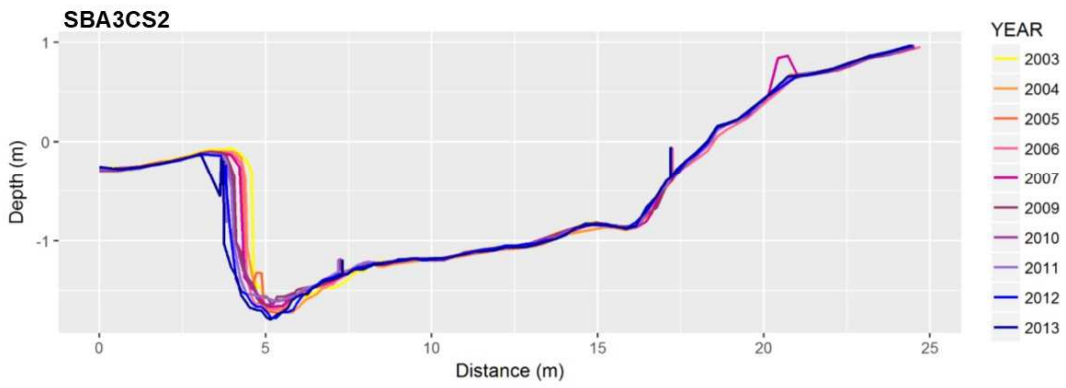
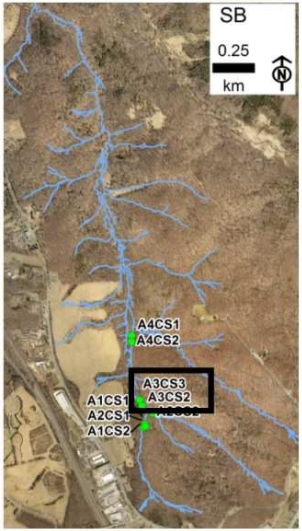
SBA1CS1



SBA1CS2

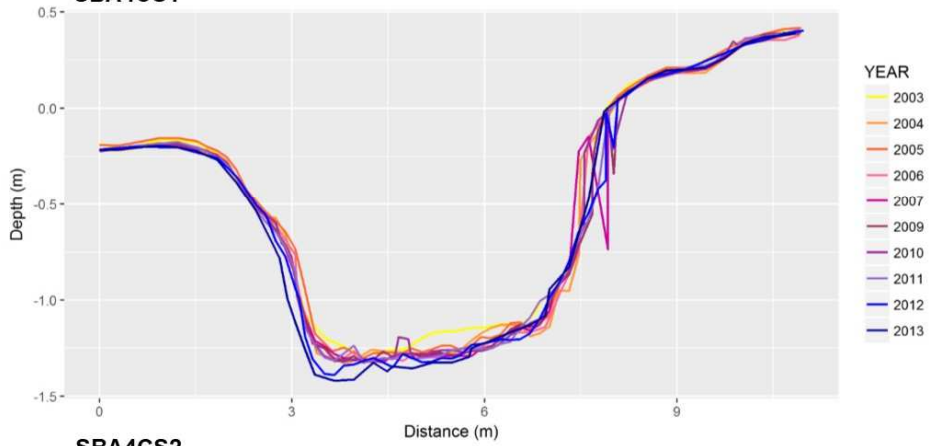




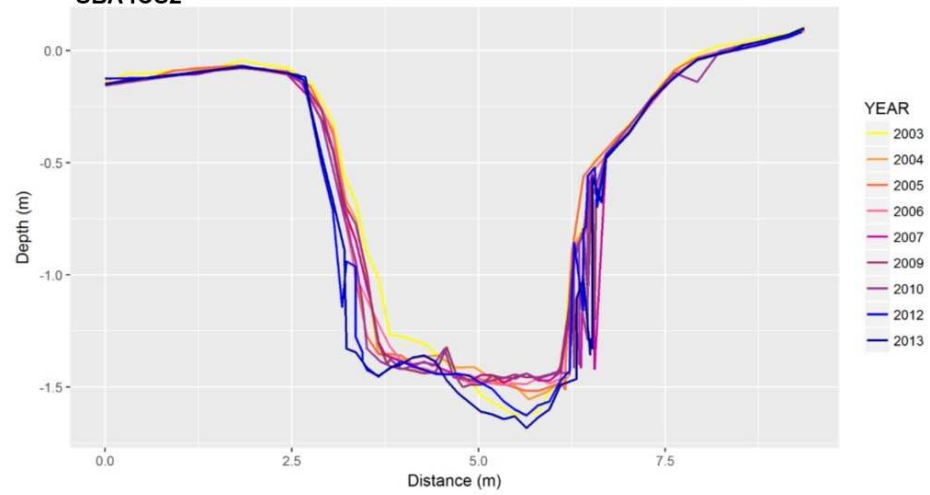




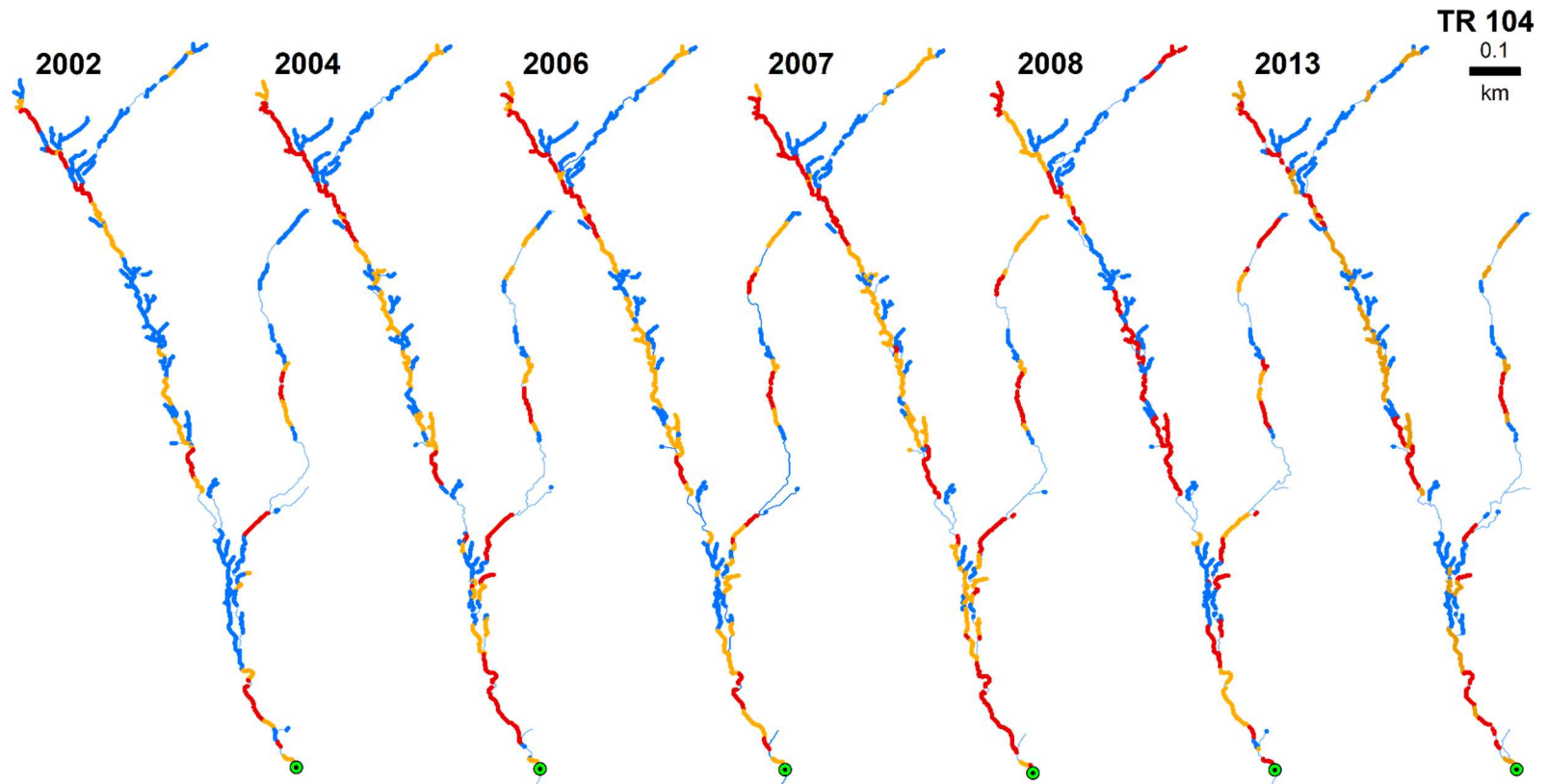
SBA4CS1

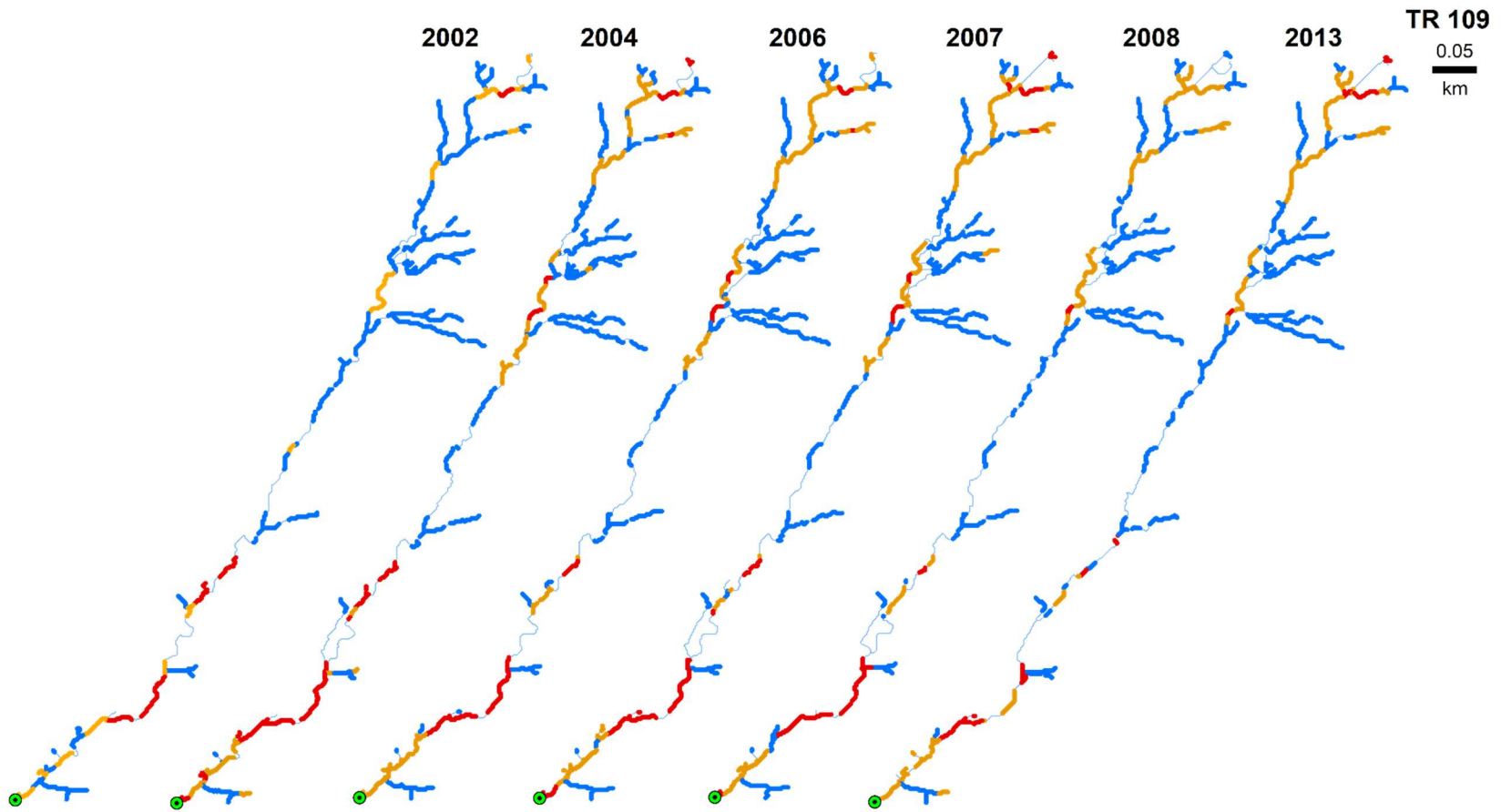


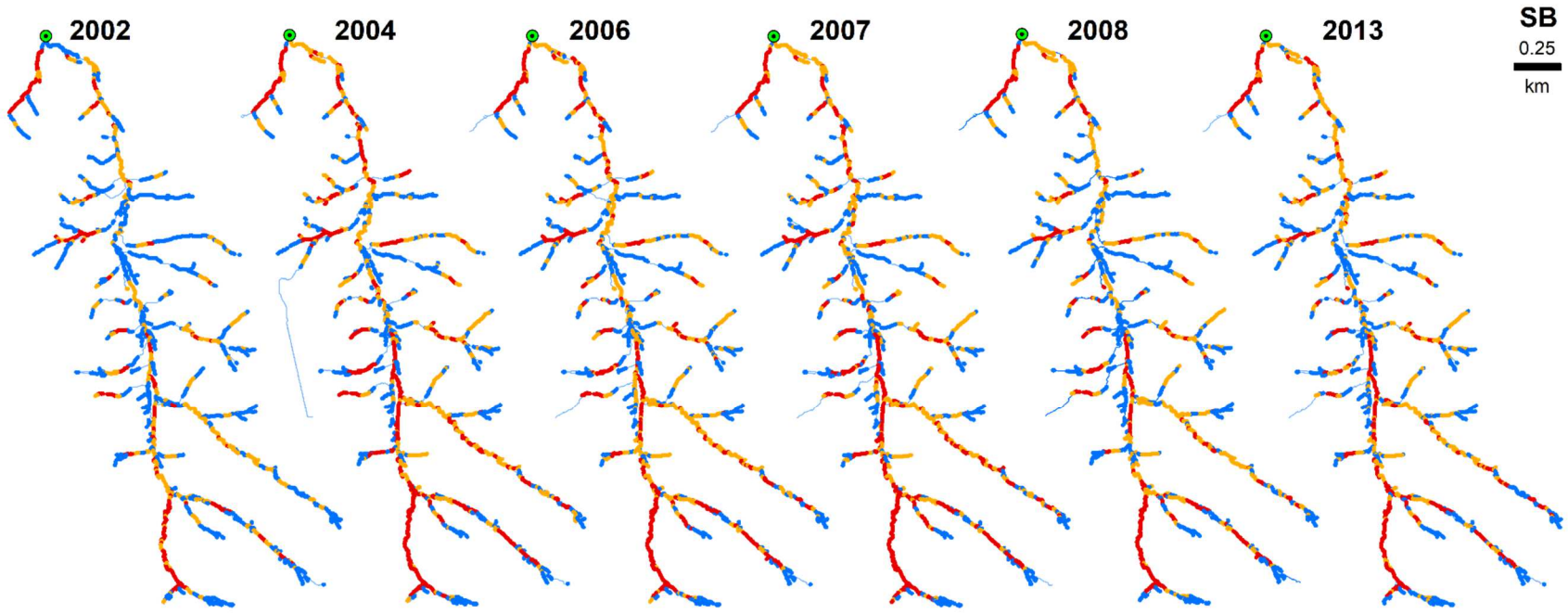
SBA4CS2



Appendix B. Incision classifications for each year in each watershed.







Bibliography

- Alexander, R. B., Boyer, E. W., Smith, R. A., Schwarz, G. E., & Moore, R. B. (2007). The Role of Headwater Streams in Downstream Water Quality. *JAWRA Journal of the American Water Resources Association*, 43(1), 41-59.
- Allen, J. D. (2004). Landscapes and riverscapes: The influence of land use on stream ecosystems. *Annual Review of Ecology and Systematics*, 35, 257-284.
- Altman, D. G., & Bland, J. M. (1994). Diagnostic tests. 1: Sensitivity and specificity. *BMJ: British Medical Journal*, 308(6943), 1552.
- Agisoft LLC (2017). Agisoft PhotoScan User Manual: Professional Edition; Version 1.3; Agisoft: St. Petersburg, Russia, 105.
- Arnold, C. L., Jr, and Gibbons, C. J. (1996). Impervious surface coverage. *Journal of the American Planning Association*, 62(2).
- Beven, K. J., & Kirkby, M. J. (1979). A physically based, variable contributing area model of basin hydrology. *Hydrological Sciences Journal*, 24(1), 43-69.
- Bhaskar, A. S., Welty, C., Maxwell, R. M., & Miller, A. J. (2015). Untangling the effects of urban development on subsurface storage in Baltimore. *Water Resources Research*, 51(2), 1158-1181.
- Bhaskar, A. S., Hogan, D. M., and Archfield, S. A. (2016). Urban base flow with low impact development. *Hydrological Processes*, 30(18), 3156-3171.
- Bigelow, P., Benda, L., & Pearce, S. (2016). Delineating incised stream sediment sources within a San Francisco Bay tributary basin. *Earth Surface Dynamics*, 4(3).
- Booth, D. B. (1990). Stream channel incision following drainage basin urbanization. *Journal of the American Water Resources Association*, 26(3), 407-417.
- Booth, D. B., Hartley, D., & Jackson, R. (2002). Forest cover, impervious-surface area, and the mitigation of stormwater impacts. *Journal of the American Water Resources Association*, 38(3), 835-845.
- Cartwright, J. M., & Diehl, T. H. (2017). *Automated identification of stream-channel geomorphic features from high-resolution digital elevation models in West Tennessee watersheds* (No. 2016-5141). US Geological Survey.
- Cashman, M. J., Gellis, A., Sanisaca, L. G., Noe, G. B., Cogliandro, V., & Baker, A. (2018). Bank-derived material dominates fluvial sediment in a suburban Chesapeake Bay watershed. *River Research and Applications*.
- Chu-Agor, M. L., Fox, G. A., Cancienne, R. M., and Wilson, G. V. (2008). Seepage caused tension failures and erosion undercutting of hillslopes. *Journal of hydrology*, 359(3), 247-259.
- Cohen, J. (1960). A coefficient of agreement for nominal scales. *Educational and psychological measurement*, 20(1), 37-46.
- Cole, J. N., Miller, A. J., Stapleton, E., & Welty, C. (2016). Quantifying Spatial Patterns of Channel Geometry and Stream Incision in Urban Drainage Network. *Journal of Hydrologic Engineering*, 22(2), 06016017.
- Colosimo, M. F., and Wilcock, P. R. (2007). Alluvial sedimentation and erosion in an urbanizing watershed, Gwynns Falls, Maryland. *Journal of the American Water Resources Association*, 43(2), 499-521.

- Costa, J. E. (1975). Effects of agriculture on erosion and sedimentation in the Piedmont Province, Maryland. *Geological Society of America Bulletin*, 86(9), 1281-1286.
- Deitchman, R. S., and Loheide, S. P. (2009). Ground-based thermal imaging of groundwater flow processes at the seepage face. *Geophysical Research Letters*, 36(14).
- Dunne, T., & Leopold, L. B. (1978). *Water in environmental planning*. Macmillan.
- Elmore, A. J., & Kaushal, S. S. (2008). Disappearing headwaters: patterns of stream burial due to urbanization. *Frontiers in Ecology and the Environment*, 6(6), 308-312.
- Emerson, C. H., Welty, C., & Traver, R. G. (2005). Watershed-scale evaluation of a system of storm water detention basins. *Journal of Hydrologic Engineering*, 10(3), 237-242.
- Faller, M., Harvey, G. L., Henshaw, A. J., Bertoldi, W., Bruno, M. C., & England, J. (2016). River bank burrowing by invasive crayfish: Spatial distribution, biophysical controls and biogeomorphic significance. *Science of the Total Environment*, 569, 1190-1200.
- Fanelli, R., Prestegard, K., & Palmer, M. (2017). Evaluation of infiltration-based stormwater management to restore hydrological processes in urban headwater streams. *Hydrological Processes*, 31(19), 3306-3319.
- Fletcher, T.D., Shuster, W., Hunt, W.F., Ashley, R., Butler, D., Arthur, S., Trowsdale, S., Barraud, S., Semadeni-Davies, A., Bertrand-Krajewski, J.L. and Mikkelsen, P.S. (2015). SUDS, LID, BMPs, WSUD and more—The evolution and application of terminology surrounding urban drainage. *Urban Water Journal*, 12(7), 525-542.
- Fox, G. A., Wilson, G. V., Simon, A., Langendoen, E. J., Akay, O., and Fuchs, J. W. (2007). Measuring streambank erosion due to ground water seepage: correlation to bank pore water pressure, precipitation and stream stage. *Earth Surface Processes and Landforms*, 32(10), 1558-1573.
- Fox, G. A., and Wilson, G. V. (2010). The role of subsurface flow in hillslope and stream bank erosion: a review. *Soil Science Society of America Journal*, 74(3), 717-733.
- Fox, G. A., Purvis, R. A., & Penn, C. J. (2016). Streambanks: A net source of sediment and phosphorus to streams and rivers. *Journal of environmental management*, 181, 602-614.
- Freeman, M. C., Pringle, C. M., & Jackson, C. R. (2007). Hydrologic connectivity and the contribution of stream headwaters to ecological integrity at regional scales. *Journal of the American Water Resources Association*, 43(1), 5-14.
- Galay, V. J. (1983). Causes of river bed degradation. *Water resources research*, 19(5), 1057-1090.
- Gardina, V. J. (2008). *Analysis of Lidar data for fluvial geomorphic change detection at a small Maryland stream*. (Unpublished master's thesis). University of Maryland, College Park, MD.
- Gellis, A.C., Hupp, C.R., Pavich, M.J., Landwehr, J.M., Banks, W.S., Hubbard, B.E., Langland, M.J., Ritchie, J.C. and Reuter, J.M. (2009). *Sources, transport, and storage of sediment at selected sites in the Chesapeake Bay Watershed*. U. S. Geological Survey.
- Gomi, T., Sidle, R. C., & Richardson, J. S. (2002). Understanding processes and downstream linkages of headwater systems: headwaters differ from downstream reaches by their close coupling to hillslope processes, more temporal and spatial variation, and their need for different means of protection from land use. *AIBS Bulletin*, 52(10), 905-916.

- GRASS Development Team (2017). Geographic Resources Analysis Support System (GRASS) Software, Version 7.2. Open Source Geospatial Foundation. Electronic document: <http://grass.osgeo.org>
- Groffman, P. M., Bain, D. J., Band, L. E., Belt, K. T., Brush, G. S., Grove, J. M., Pouyat, R. V., Yesilonis, I. C., and Zipperer, W. C. (2003). Down by the riverside: Urban riparian ecology. *Frontiers in Ecology and the Environment*, 1(6), 315-321.
- Hammer, T. R. (1972). Stream channel enlargement due to urbanization. *Water Resources Research*, 8(6), 1530-1540.
- Heine, R. A., & Lant, C. L. (2009). Spatial and temporal patterns of stream channel incision in the loess region of the Missouri River. *Annals of the Association of American Geographers*, 99(2), 231-253.
- Henshaw, P. C., and Booth, D. B. (2000). Natural restabilization of stream channels in urban watersheds. *Journal of the American Water Resources Association*, 36(6), 1219-1236.
- Historical Image Viewer. (n.d.). Retrieved August 31, 2017, from http://gis3.montgomerycountymd.gov/historical_images/
- Hodgson, M. E., Jensen, J., Raber, G., Tullis, J., Davis, B. A., Thompson, G., & Schuckman, K. (2005). An evaluation of lidar-derived elevation and terrain slope in leaf-off conditions. *Photogrammetric Engineering & Remote Sensing*, 71(7), 817-823.
- Hogan, D. H., Jarnagin, S. T., Loperfido, J. V., and Van Ness, K. (2014). Mitigating the effects of landscape development on streams in urbanizing watersheds. *Journal of the American Water Resources Association*, 50(1), 163-178.
- Hopkins, K. G., Loperfido, J. V., Craig, L. S., Noe, G. B., & Hogan, D. M. (2017). Comparison of sediment and nutrient export and runoff characteristics from watersheds with centralized versus distributed stormwater management. *Journal of environmental management*, 203, 286-298.
- Hupp, C. R., Noe, G. B., Schenk, E. R., & Benthem, A. J. (2013). Recent and historic sediment dynamics along Difficult Run, a suburban Virginia Piedmont stream. *Geomorphology*, 180, 156-169.
- Jacobson, R. B., & Coleman, D. J. (1986). Stratigraphy and recent evolution of Maryland Piedmont flood plains. *American Journal of Science*, 286(8), 617-637.
- Jain, V., Fryirs, K., & Brierley, G. (2008). Where do floodplains begin? The role of total stream power and longitudinal profile form on floodplain initiation processes. *Geological Society of America Bulletin*, 120(1-2), 127-141.
- James, L. A., Watson, D. G., and Hansen, W. F. (2007). Using LiDAR data to map gullies and headwater streams under forest canopy: South Carolina, USA. *Catena*, 71(1), 132-144.
- Jarnagin, S.T., 2010. Using repeated LIDAR to characterize topographic changes in riparian areas and stream channel morphology in areas undergoing urban development: an accuracy assessment guide for local watershed managers. U.S. Environmental Protection Agency, Washington, D.C. p. 167
- Jasiewicz, J., & Stepinski, T. F. (2013). Geomorphons—a pattern recognition approach to classification and mapping of landforms. *Geomorphology*, 182, 147-156.
- Jefferson, A. J., Bhaskar, A. S., Hopkins, K. G., Fanelli, R., Avellaneda, P. M., & McMillan, S. K. (2017). Stormwater management network effectiveness and implications for urban watershed function: A critical review. *Hydrological Processes*, 31(23), 4056-4080.

- Jones, D. K. (2013). *Examining development-induced geomorphic change using multi-temporal lidar-derived digital elevation models* (Unpublished master's thesis). The University of Maryland, Baltimore County, Baltimore, MD.
- Jones, D. K., Baker, M. E., Miller, A. J., Jarnagin, S. T., and Hogan, D. M. (2014). Tracking geomorphic signatures of watershed suburbanization with multitemporal Lidar. *Geomorphology*, 219, 42-52.
- Kasai, M., Ikeda, M., Asahina, T., and Fujisawa, K. (2009). LiDAR-derived DEM evaluation of deep-seated landslides in a steep and rocky region of Japan. *Geomorphology*, 113(1), 57-69.
- Kaushal, S.S., Likens, G.E., Jaworski, N.A., Pace, M.L., Sides, A.M., Seekell, D., Belt, K.T., Secor, D.H. and Wingate, R.L. (2010). Rising stream and river temperatures in the United States. *Frontiers in Ecology and the Environment*, 8(9), 461-466.
- Knox, J. C. (1976). Concept of the graded stream. In W. N. Melhorn and R. C. Flemel (Eds.), *Theories of landform development* (pp. 169-198). Binghamton, NY: Publications in Geomorphology, State University of New York at Binghamton.
- Kuhn, M. (2008). Caret package. *Journal of statistical software*, 28(5), 1-26.
- Landis, J. R., & Koch, G. G. (1977). The measurement of observer agreement for categorical data. *Biometrics*, 159-174.
- Lane, E. W. (1955). Importance of fluvial morphology in hydraulic engineering. *Proceedings (American Society of Civil Engineers)*; v. 81, paper no. 745.
- Lehner, P. H., Aponte Clarke, G. P., Cameron, D. M., and Frank, A. G. (2001). Low impact development. In Natural Resources Defense Council (Comp.), *Stormwater strategies: Community responses to runoff pollution*.
- Le Mauff, B., Juigner, M., Ba, A., Robin, M., Launeau, P., & Fattal, P. (2018). Coastal monitoring solutions of the geomorphological response of beach-dune systems using multi-temporal LiDAR datasets (Vendée coast, France). *Geomorphology*, 304, 121-140.
- Leopold, L. B. (1968). Hydrology for urban land planning - A guidebook on the hydrologic effects of urban land use. USGS Circular 554.
- Leopold, L. B. (1973). River channel change with time: an example. *Geological Society of America Bulletin*, 84, 1845-1860.
- Lerner, D. N. (2002). Identifying and quantifying urban recharge: a review. *Hydrogeology journal*, 10(1), 143-152.
- Li, C., Fletcher, T. D., Duncan, H. P., & Burns, M. J. (2017). Can stormwater control measures restore altered urban flow regimes at the catchment scale?. *Journal of Hydrology*, 549, 631-653.
- Lindsay, J. B. (2016). Whitebox GAT: A case study in geomorphometric analysis. *Computers & Geosciences*, 95, 75-84.
- Loperfido, J. V., Noe, G. B., Jarnagin, S. T., and Hogan, D. M. (2014). Effects of distributed and centralized stormwater best management practices and land cover on urban stream hydrology at the catchment scale. *Journal of Hydrology*, 519, 2584-2595.
- Lyons, N. J., Starek, M. J., Wegmann, K. W., & Mitasova, H. (2015). Bank erosion of legacy sediment at the transition from vertical to lateral stream incision. *Earth Surface Processes and Landforms*, 40(13), 1764-1778.
- Mackin, J. H. (1948). The concept of the graded river. *Geological Society of America Bulletin*, 59, 463-512.

- MCDEP (Montgomery County Department of Environmental Protection) (2011). Special Protection Area Program Annual Report. Prepared by the Montgomery County Department of Environmental Protection in Cooperation with the Department of Permitting Services and the Maryland-National Capital Park and Planning Commission, Rockville, Maryland. Retrieved March 31, 2015, from http://www.montgomerycountymd.gov/DEP/Resources/Files/downloads/water-reports/spa/2011_SPA_Report_Final_4_11_13.pdf
- Metes, M. J., Jones, D.K., Baker, M. E., Miller, A.J., Hogan, D. M., and Loperfido, J. V. (*in preparation*). Considerations for the extraction of drainage networks from high-resolution topographic data across variable land uses.
- Meyer, J. L., Paul, M. J., and Taulbee, W. K. (2005). Stream ecosystem function in urbanizing landscapes. *Journal of the North American Benthological Society*, 24(3), 602-612.
- Meyer, J. L., Strayer, D. L., Wallace, J. B., Eggert, S. L., Helfman, G. S., & Leonard, N. E. (2007). The contribution of headwater streams to biodiversity in river networks1. *JAWRA Journal of the American Water Resources Association*, 43(1), 86-103.
- Meyer, J. L., & Wallace, J. B. (2001). Lost linkages and lotic ecology: rediscovering small streams. *Ecology: Achievement and challenge*, 295317.
- Midgley, T. L., Fox, G. A., Wilson, G. V., Heeren, D. M., Simon, A., and Langendoen, E. J. (2011). Streambank Erosion and Instability Induced by Groundwater Seepage. In *2011 Louisville, Kentucky, August 7-10, 2011* (p. 1). American Society of Agricultural and Biological Engineers.
- Miller, J. R., & Kochel, R. C. (2010). Assessment of channel dynamics, in-stream structures and post-project channel adjustments in North Carolina and its implications to effective stream restoration. *Environmental Earth Sciences*, 59(8), 1681-1692.
- Mora, O. E., Lenzano, M. G., Toth, C. K., Grejner-Brzezinska, D. A., & Fayne, J. V. (2018). Landslide Change Detection Based on Multi-Temporal Airborne LiDAR-Derived DEMs. *Geosciences*, 8(1), 23.
- Muthukrishnan, S., Madge, B., Selvakumar, A., Field, R., & Sullivan, D. (2004). The use of best management practices (BMPs) in urban watersheds. *Cincinnati, OH, USEPA, Office of Research and Development, National Risk Management Research Laboratory*.
- Napieralski, J., Keeling, R., Dziekan, M., Rhodes, C., Kelly, A., & Kobberstad, K. (2015). Urban stream deserts as a consequence of excess stream burial in urban watersheds. *Annals of the Association of American Geographers*, 105(4), 649-664.
- Nobre, A.D., Cuartas, L.A., Hodnett, M., Rennó, C.D., Rodrigues, G., Silveira, A., Waterloo, M. and Saleska, S. (2011). Height Above the Nearest Drainage—a hydrologically relevant new terrain model. *Journal of Hydrology*, 404(1-2), 13-29.
- Obu, J., Lantuit, H., Grosse, G., Günther, F., Sachs, T., Helm, V., & Fritz, M. (2017). Coastal erosion and mass wasting along the Canadian Beaufort Sea based on annual airborne LiDAR elevation data. *Geomorphology*, 293, 331-346.
- Paul, M. J., and Meyer, J. L. (2001). Streams in the urban landscape. *Annual Review of Ecology and Systematics*, 32, 333-365.
- Peters, M. (2015). Variable Terrestrial GPS Telemetry Detection Rates: Part 7—Openness Python Script version 2.0: U.S. Geological Survey software release,

<https://doi.org/10.5066/F7PG1PT2>.

- Peterson, B.J., Wollheim, W.M., Mulholland, P.J., Webster, J.R., Meyer, J.L., Tank, J.L., Martí, E., Bowden, W.B., Valett, H.M., Hershey, A.E. and McDowell, W.H. (2001). Control of nitrogen export from watersheds by headwater streams. *Science*, 292(5514), 86-90.
- Pickett, S. T. A. (1989). Space-for-time substitution as an alternative to long-term studies. In G. E. Likens (Ed.), *Long-term studies in ecology*.
- Pusey, B. J., and Arthington, A. H. (2003). Importance of the riparian zone to the conservation and management of freshwater fish: a review. *Marine and Freshwater Research*, 54, 1-16.
- Rosgen, D. L. (1994). A classification of natural rivers. *Catena*, 22(3), 169-199.
- Roy, A. H., Freeman, M. C., Freeman, B. J., Wenger, S. J., Meyer, J. L., and Ensign, W. E. (2006). Importance of riparian forests in urban catchments contingent on sediment and hydrologic regimes. *Environmental Management*, 37(4), 523-539.
- Schumm, S. A., Harvey, M. D., & Watson, C. C. (1984). *Incised channels: morphology, dynamics, and control*. Water Resources Publications.
- Shields, F. D., Knight, S. S., & Cooper, C. M. (1994). Effects of channel incision on base flow stream habitats and fishes. *Environmental Management*, 18(1), 43-57.
- Shields Jr, F. D., Lizotte Jr, R. E., Knight, S. S., Cooper, C. M., & Wilcox, D. (2010). The stream channel incision syndrome and water quality. *Ecological Engineering*, 36(1), 78-90.
- Sibson, R., & Barnett, V. (1981). Interpreting multivariate data. *A brief description of natural neighbor interpolation*, 21-36.
- Simon, A. (1989). The discharge of sediment in channelized alluvial streams. *JAWRA Journal of the American Water Resources Association*, 25(6), 1177-1188.
- Simon, A., & Hupp, C. R. (1986). Channel evolution in modified Tennessee channels. In *Proceedings of the Fourth Federal Interagency Sedimentation Conference March 24-27, 1986, Las Vegas, Nevada*. (Vol. 2).
- Stepinski, T. F., & Jasiewicz, J. (2011). Geomorphons-a new approach to classification of landforms. *Proceedings of Geomorphometry, 2011*, 109-112.
- Sugarbaker, L., Constance, E. W., Heidemann, H. K., Jason, A. L., Lucas, V., Saghy, D., & Stoker, J. M. (2014). *The 3D Elevation Program initiative: a call for action*. US Geological Survey.
- Thomas, I. A., Jordan, P., Shine, O., Fenton, O., Mellander, P. E., Dunlop, P., & Murphy, P. N. C. (2017). Defining optimal DEM resolutions and point densities for modelling hydrologically sensitive areas in agricultural catchments dominated by microtopography. *International Journal of Applied Earth Observation and Geoinformation*, 54, 38-52.
- Tillinghast, E. D., Hunt, W. F., Jennings, G. D., & D'Arconte, P. (2012). Increasing stream geomorphic stability using storm water control measures in a densely urbanized watershed. *Journal of Hydrologic Engineering*, 17(12), 1381-1388.
- Van Stralen, K. J., Stel, V. S., Reitsma, J. B., Dekker, F. W., Zoccali, C., & Jager, K. J. (2009). Diagnostic methods I: sensitivity, specificity, and other measures of accuracy. *Kidney international*, 75(12), 1257-1263.
- Viera, A. J., & Garrett, J. M. (2005). Understanding interobserver agreement: the kappa statistic. *Fam Med*, 37(5), 360-363.

- Vietz, G. J., Walsh, C. J., and Fletcher, T. D. (2015). Urban hydrogeomorphology and the urban stream syndrome: Treating the symptoms and causes of geomorphic change. *Progress in Physical Geography*, 40(3), 480-492.
- Walsh, C.J., Booth, D.B., Burns, M.J., Fletcher, T.D., Hale, R.L., Hoang, L.N., Livingston, G., Rippey, M.A., Roy, A.H., Scoggins, M. and Wallace, A. (2016). Principles for urban stormwater management to protect stream ecosystems. *Freshwater Science*, 35(1), 398-411.
- Walsh, C. J., Roy, A. H., Feminella, J. W., Cottingham, P. D., Groffman, P. M., and Morgan, R. P., II. (2005). The urban stream syndrome: current knowledge and the search for a cure. *Journal of the North American Benthological Society*, 24(3), 706-723.
- Walter, R. C., & Merritts, D. J. (2008). Natural streams and the legacy of water-powered mills. *Science*, 319(5861), 299-304.
- Westoby, M. J., Brasington, J., Glasser, N. F., Hambrey, M. J., and Reynolds, J. M. (2012). 'Structure-from-Motion' photogrammetry: A low-cost, effective tool for geoscience applications. *Geomorphology*, 179, 300-314.
- Wilson, G. V., Periketi, R. K., Fox, G. A., Dabney, S. M., Shields, F. D., and Cullum, R. F. (2007). Soil properties controlling seepage erosion contributions to streambank failure. *Earth Surface Processes and Landforms*, 32(3), 447-459.
- Wolman, M. G. (1967). A cycle of sedimentation and erosion in urban river channels. *Essays in Geomorphology*, 29(2-4), 385-395.
- Wolman, M. G., & Miller, J. P. (1960). Magnitude and frequency of forces in geomorphic processes. *The Journal of Geology*, 68(1), 54-74.
- Yokoyama, R., Shirasawa, M., and Pike, R. J. (2002). Visualizing topography by openness: a new application of image processing to digital elevation models. *Photogrammetric engineering and remote sensing*, 68(3), 257-266.

